Progress in Aerospace Sciences 114 (2020) 100597

Contents lists available at ScienceDirect

Progress in Aerospace Sciences

journal homepage: http://www.elsevier.com/locate/paerosci

A review of hybrid RANS-LES methods for turbulent flows: Concepts and applications

Stefan Heinz

University of Wyoming, Mathematics Department, Laramie, WY, 82071, USA

ARTICLE INFO

Keywords:
Computational methods for turbulent flow simulations
Hybridization of RANS and LES methods
Review of concepts and applications to separated turbulent flows

ABSTRACT

The hybridization of Reynolds-averaged Navier-Stokes (RANS) and large eddy simulation (LES) methods is seen to be the most promising way to efficiently deal with separated turbulent flow simulations relevant to aerospace and wind energy applications. Characteristic conceptual features of popular hybrid RANS-LES and their applications to hill-type and airfoil flow including flow separation are described. Conceptual questions on existing hybrid RANS-LES are pointed out and ways to overcome these problems are presented. Further analyses show that corresponding novel hybrid RANS-LES methods generalize and improve existing methods. The discussions reveal, in particular, the great value of physical and mathematical realizability constraints for the substantial improvement of simulation methods.

1. Introduction

Direct numerical simulation (DNS) of turbulent flows of practical relevance, which are usually characterized by very high Reynolds numbers, is prohibitively expensive [1,2]. The way to address this issue is to reduce the computational cost of simulations via the inclusion of modeling in turbulence equations, leading to the design of Reynolds-averaged Navier-Stokes (RANS) [1,3–5] and large eddy simulation (LES) equations [1,6–9].

RANS and LES equations have the same structure [10], the only difference is that RANS length or time scales are much larger than the typical scales of LES. This difference has significant implications illustrated in Fig. 1, which was presented by von Terzi et al. [11]. We see results of turbulent channel flow simulations including hills at the bottom at a Reynolds number $Re = 10,595$ based on the bulk velocity. This flow configuration includes a variety of relevant flow features such as separation, recirculation, and natural reattachment: see the blue recirculation bubble behind the hills. Corresponding flows were considered in many experimental and numerical studies of the performance of turbulence models for a wide range of Re [12–30]. Zone 2 versus zone 3 simulations reveal the difference of LES and RANS with respect to the instantaneous and mean streamwise velocity. The comparison of instantaneous velocities shows a significant difference: LES is capable of resolving turbulence, it can simulate fluctuating turbulence structures. The latter structures cannot be described by a model, they are output of appropriate equations if an adequate grid and simulation time step are used. Hence, LES can provide very valuable new insight that we cannot get from RANS: RANS simulations provide smooth variations of turbulence characteristics as implied by the turbulence model considered. The comparison of mean velocities shows another apparent difference between LES and RANS. As a consequence of the lack of resolved motions, RANS simulations often cannot correctly describe main characteristics of separated flows, as given for the case considered by the recirculation region behind hills (e.g., RANS predicts negative mean velocities over extended flow regions in contrast to LES).

The differences between RANS and LES indicate that the use of LES has to be preferred to enable accurate flow simulations. The problem is that LES, in particular for wall-bounded turbulent flows that appear in the majority of applications, can become computationally extremely expensive (almost as expensive as DNS) [31–34]. It needs, therefore, a balancing of the accuracy of physical modeling and related computational cost, in particular for wall bounded flows [34–37]. A reasonable approach to deal with this problem is to design hybrid RANS-LES methods. Given that RANS and LES do only differ by the way in which length or time scale information for modeled turbulent motions is provided, it is surprising to see how difficult it is to develop fully convincing hybrid RANS-LES methods applied by everybody [6,38–43]. The problem is the fundamental inconsistency of RANS and LES equations: LES equations are supposed to produce fluctuations (and usually require fluctuations at boundaries), whereas RANS equations are not designed to deal with fluctuations (and usually suffer from the appearance of fluctuations). This mismatch of physics is not an academic problem, it is

E-mail address: heinz@uwyo.edu.

https://doi.org/10.1016/j.paerosci.2019.100597
Received 31 October 2019; Received in revised form 22 December 2019; Accepted 30 December 2019
Available online 19 March 2020

known to be the reason for an incorrect reflection of wall physics (the logarithmic law of the wall cannot be obtained [44–48]) and other relevant physics (like flow separation [2,49–56]). Empirical approaches for adding fluctuations in RANS-LES transition regions have been suggested, but such methods introduce other inconsistencies [57–59]. A consistent match of RANS and LES equations (based on adding additional source rates to corresponding equations) was suggested recently [60–63]. However, the latter approach results in computational cost that are higher than the cost of LES. To overcome this problem, a variety of approaches for combining RANS and LES equations were suggested so far, for example, wall-modeled LES (WM-LES) [6,32,33,64–76], detached eddy simulation (DES) applied in conjunction with several equations [2,42,43,49–56,77], lattice Boltzmann (LB) methods [78–84], Reynolds-stress-constrained LES (RSC-LES) [85–96], unified RANS-LES (UNI-LES) [10,29,30,97–107], partially averaged Navier-Stokes (PANS) [108–118], partially integrated transport modeling (PITM) [25–27,119–126], and scale adaptive simulation (SAS) methods [42,127–132].

An illustration of the development of hybrid RANS-LES methods is given in terms of Fig. 2. In particular, this figure shows the number of published articles according to a Google Scholar search for "hybrid RANS-LES" (one may argue whether the way of looking at this question is perfect, but it provides a reasonable indication of ongoing developments). The presentation of results applies 1995 as reference year: we use $n = N - 1995$, where N refers to the year considered. Fig. 2a shows the addition of papers per year: P_n is the cumulative number of papers published before and in year n. An indication of when approximately some of the above mentioned hybrid RANS-LES were introduced is also given. This figure also provides support for the modeling of $(P_{n+1} - P_n)^{1/2}$ for the last two decades by $a(n+1)$, where $a = 1.29$. The solution to the implied difference equation $P_{n+1} - P_n = a^2(n+1)^2$, which is given by $P_n = P_0 + a^2 n(n+1)(2n+1)/6$ where $P_0 = 48$ [133], is shown in Fig. 2b. Accordingly, there will be a total of $9.2K$ papers in 2020, and this number can be expected to increase to $25K$ papers in 2030. It is obvious how difficult it is for students and researchers to become familiar and to process this amount of material.

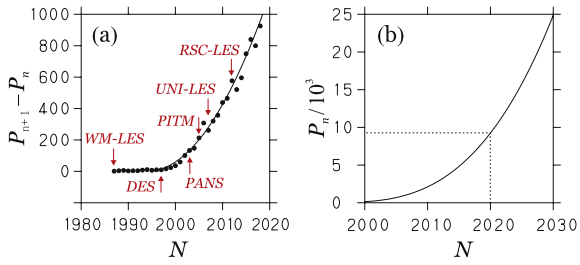

Fig. 2. The number of new papers per year $P_{n+1} - P_n$ at year N is shown in (a). The black line shows $P_{n+1} - P_n = a^2(n+1)^2$, where $n = N - 1995$. The red acronyms refer to the introduction of some hybrid methods. The cumulative number of papers P_n is shown in (b). The dashed line shows the current state. (For interpretation of the references to colour in this figure legend, the reader is referred to the Web version of this article.)

The predominant approach to address the RANS-LES hybridization is the combination of different equation types without explicitly paying attention to the resolved and modeled motion produced in this way. Implied imbalances of modeled and resolved motions can be the reason for significant shortcomings seen in simulations [2,44–48,50–56]. To overcome these issues, the balance of resolved and modeled motions needs to be explicitly addressed. Particular questions in this regard, which are illustrated in Fig. 3, are the following ones:

- How is it possible to explicitly control the balance of resolved and modeled motions, in particular under significant grid and Reynolds number changes?
- Is it possible to implement such a mode-balance control in many turbulence models?

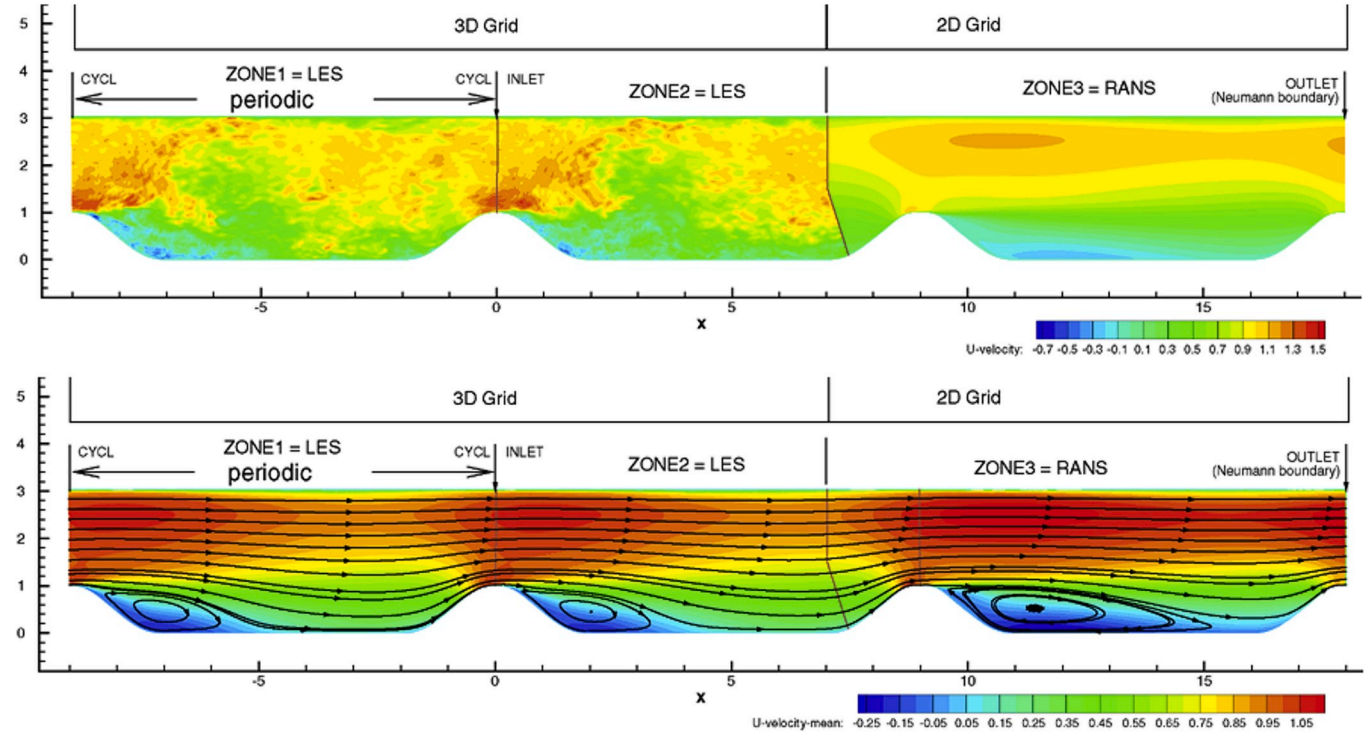

Fig. 1. Periodic hill flow simulations at $Re = 10,595$: illustration of LES and RANS differences [from Ref. [11] with permission]. The instantaneous streamwise velocity is shown on top, the mean streamwise velocity is shown at the bottom. The LES-RANS interface is at $x/h \approx 7$ [11]. LES was performed using $200 \times 64 \times 92$ (= 1.2 million) grid points in downstream, wall-normal and lateral directions, respectively. RANS simulations apply a two-dimensional grid with only one cell in the spanwise direction, i.e., $200 \times 64 \times 1$ (= 12,800) grid points.

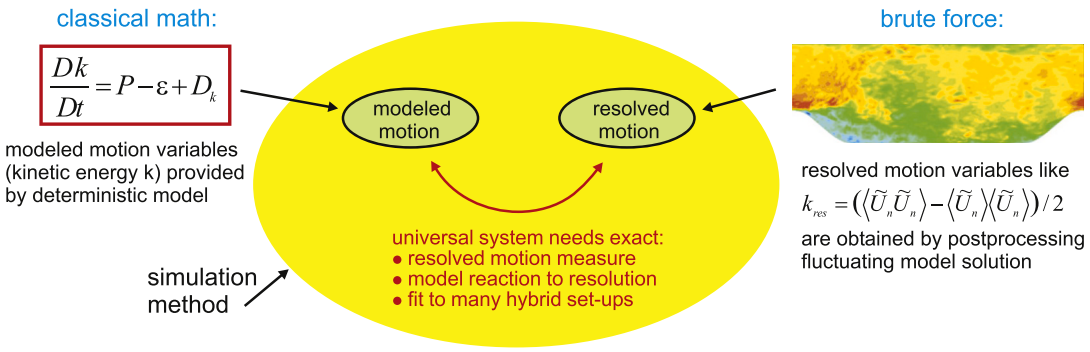

Fig. 3. An illustration of interacting modeled and resolved motions in a hybrid RANS-LES simulation.

- What determines the interaction of resolved and modeled motions (is resolved motion controlled by the grid, and the modeled motion has to adjust to the given resolved motion)?

The goal of this paper is to summarize essential recent developments of hybrid RANS-LES methods by paying attention to the bullet point questions raised in the preceding paragraph.

2. RANS and LES methods

We begin with an introduction to basic concepts in order to prepare discussions in the following. First, this will be done by taking reference to an important principle of turbulence modeling: realizability, which applies to both RANS and LES. Then, common and different characteristics of RANS, LES and their relationships are discussed in following subsections. LB methods are briefly presented in Appx. A: depending on the modeled viscosity assumption, such methods can represent RANS, LES, or hybrid RANS-LES methods.

2.1. Realizability

Realizability is an important guiding principle for turbulence modeling [10,134–141]. Realizability expresses the expectation that a sound turbulence model should be in consistency with physical-mathematical constraints: a realizable model describes processes that can occur in reality. There are different notions of realizability.

Physical realizability is based on the fact that the Reynolds stress D_{ij} in RANS [the subgrid-scale (SGS) stress in LES] represents the variance of the probability density function (PDF) [the variance of the filter density function (FDF) in LES] of turbulent velocities. In particular, knowledge of the velocity PDF $f(\mathbf{w},\mathbf{x},t)$ [FDF] allows to calculate all moments considered in RANS and LES, including the i^{th} component of the mean velocity [filtered velocity] $\tilde{U}_i$. These two variables, $\tilde{U}_i$ and D_{ij}, are defined by

$$\tilde{U}_i = \int w_i f(\mathbf{w},\mathbf{x},t)\, d\mathbf{w}, \qquad D_{ij} = \widetilde{u_i u_j} = \int (w_i - \tilde{U}_i)(w_j - \tilde{U}_j) f(\mathbf{w},\mathbf{x},t)\, d\mathbf{w}. \tag{1}$$

Here, $\mathbf{w} = (w_1, w_2, w_3)$ refers to the sample space velocity. The difference between RANS and LES variables is the different definition of the PDF or FDF: see the details given in Appx. B. Given that RANS and LES equations have the same structure (see Sect. 2.2), we use the same notation for RANS and LES variables keeping in mind that they are defined by different averages. In particular, physical realizability (or PDF-realizability) means the following. We would not like to work with a stress model that cannot describe the variance of a realizable stochastic process, which would be unphysical. This can be accomplished by doing the following (see the illustration in Fig. 4). We consider a physically realizable stochastic model for turbulent velocities [10,30,101,137–140], which implies a transport equation for the PDF of turbulent velocities. The latter equation can be used for the derivation of transport equations for the stress tensor and the derivation of simpler algebraic stress models [1,4,97]. Such algebraic stress models are demonstrated to represent models for the variance of a physical meaningful stochastic process. Basically the same approach can be applied in the context of LES equations [97,99,142–147]. In addition to corresponding RANS results, a corresponding realizability-ensuring approach at the test filter level can be applied to dynamically calculate LES stress model parameters, which is highly beneficial [29,30,100,101,104].

Mathematical realizability (considered with respect to the stress here) means the following. By definition, the exact Reynolds stress tensor in averaged Navier-Stokes equations is positive semi-definite. This property implies that the Reynolds stress has non-negative diagonal components (energies), off-diagonal components that satisfy the Schwarz inequality, and a non-negative determinant (which implies an additional condition on cross-correlations). In correspondence to the properties of the exact Reynolds stress, the realizability constraint proposed by Schumann requires that the modeled Reynolds stress also has to be positive semi-definite [134]. Over the last decades, Schumann's realizability constraint has served as theoretical basis for several refined realizability concepts [137–140,148,149]. The Schumann realizability constraint also can be applied to the development of realizable SGS stress tensor models [10,30,101,150–152] if the filter function is positive [152].

The use of realizability concepts was found to be relevant to the design of RANS and LES equations [152–156]. In particular, the use of these concepts is relevant to avoid numerical instabilities [29,30,100,101,104,141]. Dynamic LES, for example, represents a very convenient approach to overcome serious issues related to the use of constant-coefficient LES methods for wall-bounded turbulent flows or transitional flows. Dynamic LES concepts that do not honor realizability constraints (the dynamic Smagorinsky model [157–159]) are often found to be computationally unstable. This problem can be overcome by working with averaged dynamic model parameters (which often introduces additional problems [30,104]) or by introducing additional clipping parameters (which have to be found empirically and reduce the backscatter ability of LES). In contrast to that, fully realizable dynamic LES ensures computationally stable dynamic LES without having to deal with shortcomings of non-realizable dynamic LES [30].

2.2. Common transport equations

RANS concepts (which also apply to LES) for incompressible velocity fields [1,3–5,40,97,160,161] will be presented now by taking reference to realizability concepts. The PDF $f(\mathbf{w},\mathbf{x},t)$ of turbulent velocities is supposed to be governed by the Fokker-Planck equation

$$\frac{\partial f}{\partial t} + \frac{\partial w_k f}{\partial x_k} = \frac{\partial}{\partial w_k}\left[\frac{1}{\rho}\frac{\partial \tilde{p}}{\partial x_i} - 2\nu\frac{\partial \tilde{S}_{ik}}{\partial x_k} + \frac{w_k - \tilde{U}_k}{\tau_L} + \frac{2kc_0}{3\tau_L}\frac{\partial}{\partial w_k}\right] f. \tag{2}$$

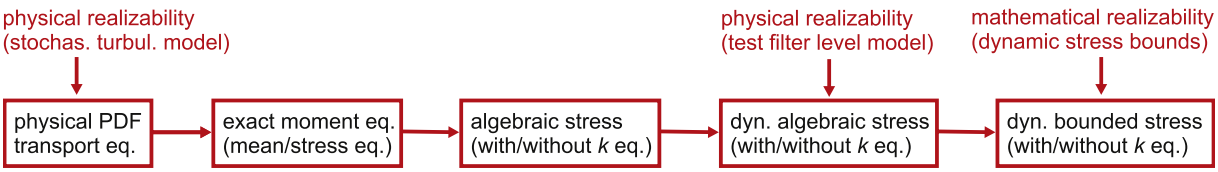

Fig. 4. An illustration of the use of different realizability concepts.

The sum convention is used throughout this paper. The first two terms on the right-hand side (RHS) ensure the correct transport of mean velocities. We have here the mean pressure $\tilde{p}$, ρ is the constant mean mass density, ν is the constant kinematic viscosity, and $\tilde{S}_{ij} = (\partial\tilde{U}_i/\partial x_j + \partial\tilde{U}_j/\partial x_i)/2$ is the rate-of-strain tensor. The last two terms involve modeling: an isotropic PDF diffusion is assumed (controlled by the model parameter c_0, $0 \le c_0 \le 1$, $k = \widetilde{u_i u_i}/2 = D_{nn}/2$ is the modeled kinetic energy), and an isotropic PDF relaxation toward an equilibrium state takes place over the characteristic relaxation time τ_L. This relatively simple model, which is sufficient to recover popular RANS concepts, is applied for simplicity. The multiplication of Eq. (2) with appropriate variables and integration [1,10,97,133] allows to derive the continuity equation $\partial\tilde{U}_i/\partial x_i = 0$ and momentum equation

$$\frac{D\tilde{U}_i}{Dt} + \frac{\partial D_{ik}}{\partial x_k} = -\frac{1}{\rho}\frac{\partial\tilde{p}}{\partial x_i} + 2\nu\frac{\partial\tilde{S}_{ik}}{\partial x_k}. \tag{3}$$

Here, $D/Dt = \partial/\partial t + \tilde{U}_k\partial/\partial x_k$ denotes the mean Lagrangian time derivative.

The advantage of Eq. (2) is that it implies transport equations for all other moments, like D_{ij}, which appears as an unknown in Eq. (3). The latter can be split into isotropic and deviatoric components, $D_{ij} = 2k(\delta_{ij}/3 + d_{ij})$, where $d_{ij} = (D_{ij} - 2k\delta_{ij}/3)/(2k)$ refers to the standardized anisotropy tensor. The equations for k and d_{ij} implied by Eq. (2) read [10,97]

$$\frac{Dk}{Dt} + \frac{1}{2}\frac{\partial T_{knn}}{\partial x_k} + 2kd_{kn}\frac{\partial\tilde{U}_n}{\partial x_k} = -\frac{2(1-c_o)k}{\tau_L}, \tag{4}$$

$$\frac{Dd_{ij}}{Dt} + \frac{1}{2k}\frac{\partial\left(T_{kij} - T_{knn}\delta_{ij}/3\right)}{\partial x_k} + \frac{d_{ij}}{k}\frac{Dk}{Dt} + d_{ik}\frac{\partial\tilde{U}_j}{\partial x_k} + d_{jk}\frac{\partial\tilde{U}_i}{\partial x_k} - \frac{2}{3}d_{kn}\frac{\partial\tilde{U}_n}{\partial x_k}\delta_{ij} = -\frac{2d_{ij}}{\tau_L} - \frac{2S_{ij}}{3}. \tag{5}$$

Here, T_{knn} refers to the triple correlation tensor. The RHS of the k equation identifies the dissipation rate ε of modeled kinetic energy, which is related to the dissipation time scale τ via $\varepsilon = k/\tau$. Correspondingly, we have $\tau_L = 2(1-c_o)\tau$. The equation for d_{ij} can be used for the derivation of a systematic hierarchy of algebraic expressions for d_{ij}. The simplest expression (given by the balance $d_{ij} = -\tau_L S_{ij}/3$ of terms on the RHS of Eq. (5)) implies for D_{ij} the relation $D_{ij} = 2k\delta_{ij}/3 - 2\nu_t\tilde{S}_{ij}$, where the modeled viscosity is given by $\nu_t = k\tau_L/3 = C_\mu k\tau$ with $C_\mu = 2(1-c_o)/3$. Combined with the continuity equation $\partial\tilde{U}_i/\partial x_i = 0$, the momentum equation then reads

$$\frac{D\tilde{U}_i}{Dt} = -\frac{\partial(\tilde{p}/\rho + 2k/3)}{\partial x_i} + 2\frac{\partial(\nu+\nu_t)\tilde{S}_{ik}}{\partial x_k}. \tag{6}$$

By involving the usual model $D_k = \partial[(\nu+\nu_t)\,\partial k/\partial x_j]/\partial x_j$ for the gradient of triple correlations, the k equation can be written

$$\frac{Dk}{Dt} = P - \varepsilon + D_k. \tag{7}$$

$P = \nu_t S^2$ is the production of k, and $S = (2\tilde{S}_{mn}\tilde{S}_{nm})^{1/2}$ is the characteristic shear rate.

2.3. Different scale information

The closure of Eqs. (6) and (7) requires scale information needed to explain the modeled viscosity $\nu_t = C_\mu k\tau = C_\mu k^2/\varepsilon$ and $\varepsilon = k/\tau$. This can be provided, for example, in terms of an equation for the dissipation rate ε, or for the turbulence frequency $\omega = \tau^{-1}$, or for the characteristic length scale $L = k^{1/2}\tau = k^{3/2}/\varepsilon$ of turbulence.

One usual way to provide such length scale information in RANS is to consider the $k-\varepsilon$ model, which involves for ε the equation

$$\frac{D\varepsilon}{Dt} = C_{\varepsilon_1}\frac{\varepsilon^2}{k}\left(\frac{P}{\varepsilon} - \alpha\right) + D_\varepsilon, \quad D_\varepsilon = \frac{\partial}{\partial x_j}\left[\left(\nu + \frac{\nu_t}{\sigma_\varepsilon}\right)\frac{\partial\varepsilon}{\partial x_j}\right]. \tag{8}$$

The settings $C_{\varepsilon_1} = 1.44$, $C_{\varepsilon_2} = 1.92$ [3] imply $\alpha = C_{\varepsilon_2}/C_{\varepsilon_1} = 1.33$, and we have $\sigma_\varepsilon = 1.3$. The ε equation is applicable to the logarithmic flow region if $\kappa^2 = C_\mu^{1/2}\sigma_\varepsilon(C_{\varepsilon_2} - C_{\varepsilon_1})$. This condition can be obtained by disregarding the left-hand side (LHS) of Eq. (8), setting $P = \varepsilon$, and using log-law characteristics (u_τ is the friction velocity),

$$\partial\tilde{U}_1/\partial x_2 = u_\tau/(\kappa x_2), \qquad k = u_\tau^2/C_\mu^{1/2}, \qquad \varepsilon = u_\tau^3/(\kappa x_2). \tag{9}$$

The latter relations imply further log-law relations,

$$L = \kappa x_2/C_\mu^{3/4}, \qquad \tau = \kappa x_2/(C_\mu^{1/2}u_\tau), \qquad \nu_t = \kappa x_2 u_\tau. \tag{10}$$

The parameters applied imply a relatively high value $\kappa = 0.43$ for the von Kármán constant [162,163].

Alternatively, the $k-\omega$ model can be applied in RANS, which implies for the turbulence frequency $\omega = \tau^{-1}$ the equation

$$\frac{D\omega}{Dt} = C_{\omega_1}\omega^2\left(\frac{P}{\varepsilon} - \beta\right) + D_\omega, \quad D_\omega = \frac{\partial}{\partial x_j}\left[\left(\nu + \frac{\nu_t}{\sigma_\omega}\right)\frac{\partial\omega}{\partial x_j}\right], \tag{11}$$

where $\beta = C_{\omega_2}/(C_\mu C_{\omega_1})$. For wall-bounded flows, $D_{\omega c} = C_\omega k^{-1}(\nu+\nu_t)[\partial k/\partial x_j][\partial\omega/\partial x_j]$ is often added to D_ω. The cross diffusion term $D_{\omega c}$ affects the model behavior near boundaries (it acts like a damping function). The constants involved have the values $(C_{\omega 1}, C_{\omega 2}, C_\mu, C_\omega, \sigma_\omega) = (0.49, 0.072, 0.09, 1.1, 1.8)$ [164]. The derivation of the ω equation from k and ε equations enables to establish relationships between model parameters, we find $C_{\omega 1} = C_{\varepsilon 1} - 1$ and $C_{\omega 2}/C_\mu = C_{\varepsilon 2} - 1$. In correspondence to $\kappa^2 = C_\mu^{1/2}\sigma_\varepsilon(C_{\varepsilon_2} - C_{\varepsilon_1})$, the log-law applicability condition for the $k-\omega$ model reads $\kappa^2 = C_\mu^{1/2}\sigma_\omega(C_{\omega 2}/C_\mu - C_{\omega 1})$ (the cross diffusion term $D_{\omega c}$ does not contribute to this equation). The $k-\omega$ model parameter values applied imply that $\kappa = 0.41$.

An interesting rewriting of Eqs. (7), (8) and (11) reads [165].

$$\frac{Dk}{Dt} - D_k = -\frac{k - k_{eq}}{\tau}, \qquad \frac{D\varepsilon}{Dt} - D_\varepsilon = -\frac{\varepsilon - \varepsilon_{eq}}{\tau_\varepsilon} - S_\varepsilon, \qquad \frac{D\omega}{Dt} - D_\omega = -\frac{\omega - \omega_{eq}}{\tau_\omega} - S_\omega. \tag{12}$$

The equilibrium values involved are given by $k_{eq} = kP/\varepsilon$, $\varepsilon_{eq} = P$, $\omega_{eq} = \omega P/\varepsilon$, the source rates read $S_\varepsilon = (1-\alpha^{-1})\,\varepsilon_{eq}/\tau_\varepsilon$ and $S_\omega = (1-\beta^{-1})\,\omega_{eq}/\tau_\omega$, and we introduced characteristic time scales $\tau_\varepsilon = \tau/C_{\varepsilon_2}$ and $\tau_\omega = \tau\,C_k/C_{\omega_2}$. These equations show that k, ε, and ω relax according to the structure of the Bhatnagar-Gross-Krook (BGK) approximation [166] to the Boltzmann equation [165]. The source terms S_ε and S_ω recover corresponding terms in the Boltzmann equation [165]. S_ε and S_ω are sink

terms, i.e., they reduce ε and ω. Correspondingly, these source terms imply an increase of the modeled viscosity which scales with ε and ω via $\nu_t = C_\mu k^2/\varepsilon = C_\mu k/\omega$. Such a relatively high modeled viscosity (compared with LES) is typical for RANS.

LES equations have the same problem as RANS equations: the closure of Eq. (6) and (7) requires scale information to close $\nu_t = C_\mu k^{1/2} L$ and $\varepsilon = k^{3/2}/L$. This means, regardless the type of averaging or filtering applied, we have the same equations in RANS and LES approaches (the definition of variables solved for in simulations does not affect simulations). The only difference between RANS and LES equations is the way to provide scale information to these equations: RANS equations apply modeled length or time scales that are relatively large compared with corresponding variables used in LES. The usual way to provide length scale information to LES equations is to make assumptions on the modeled length scale L. One possibility to provide such length scale information is described in Appx. C. For sufficiently small $\Delta_+ = \Delta/L_{tot}$, Δ is the filter width and L_{tot} is the total length scale (see Sect. 2.4), this approach implies $L = C_+\Delta$. The constant involved is given by $C_+ = (3C_K/2)^{3/2}/\pi$, where C_k is the Kolmogorov constant. Values $C_k = (1.3, 1.43, 1.5)$, e.g., result in $C_+ = (0.876, 1.0, 1.074)$. Hence, the setting $L = \Delta$ is very reasonable. In contrast to RANS, the underlying idea of this length scale setting is a proper definition of a small length scale (which obviously depends on the grid).

2.4. Mode relationships

The discussions of hybrid methods in Sect. 3 take reference to RANS-LES relationships for several variables, in particular the representation of RANS variables by modeled and resolved contributions. In preparation to these discussions, these relationships will be presented here.

A RANS-LES relationship for stresses can be obtained by considering the ensemble-averaged LES Eq. (3),

$$\frac{\partial\langle\tilde{U}_i\rangle}{\partial t}+\frac{\partial\langle\tilde{U}_i\rangle\langle\tilde{U}_k\rangle}{\partial x_k}+\frac{\partial\left(R_{ik}^{res}+\langle D_{ik}\rangle\right)}{\partial x_k}=-\frac{1}{\rho}\frac{\partial\langle\tilde{p}\rangle}{\partial x_i}+2\nu\frac{\partial\langle\tilde{S}_{ik}\rangle}{\partial x_k}. \tag{13}$$

Here, the brackets refer to an ensemble average, $\langle D_{ik}\rangle = \langle\widetilde{u_i u_k}\rangle$ is the mean modeled stress, and the mean resolved stress $R_{ik}^{res} = \langle\tilde{U}_i\tilde{U}_k\rangle - \langle\tilde{U}_i\rangle\langle\tilde{U}_k\rangle$ is introduced, which can be obtained via the known resolved velocity field. The sum of the mean resolved and modeled stress can be expected then to be equal to the RANS stress $R_{ij} = \langle U_i U_k\rangle - \langle U_i\rangle\langle U_k\rangle$ [1,85],

$$R_{ij} = R_{ij}^{res} + \langle D_{ij}\rangle. \tag{14}$$

This relation (the subscripts *tot* and *res* refer to total and resolved variables) implies

$$k_{tot} = k_{res} + k, \tag{15}$$

$k_{tot} = R_{nn}/2$, $k_{res} = R_{nn}^{res}/2$, and $k = \langle D_{nn}\rangle/2$ are the total (RANS) kinetic energy, resolved kinetic energy, and mean modeled energy, respectively, see also the discussion in Ref. [167].

According to Eq. (15), there is a corresponding superposition of resolved (ε_{res}) and modeled (ε) contributions to the dissipation rate of turbulent kinetic energy,

$$\varepsilon_{tot} = \varepsilon_{res} + \varepsilon, \tag{16}$$

where ε is an ensemble-averaged variable like k. The thermodynamically correct RANS dissipation rate is given by $\varepsilon_{tot} = \varepsilon_{TD}$ [1,3,168–172], where

$$\varepsilon_{TD} = 2\nu\langle s_{ij}s_{ji}\rangle = \nu\langle\frac{\partial u_i}{\partial x_j}\frac{\partial u_i}{\partial x_j}\rangle + \nu\frac{\partial^2\langle u_i u_j\rangle}{\partial x_i\,\partial x_j}. \tag{17}$$

Here, $s_{ij} = (\partial u_i/\partial x_j + \partial u_j/\partial x_i)/2$, and the last two terms represent an identical rewriting of the previous expression. However, in contrast to using ε_{TD}, it is usual practice to identify ε_{tot} by the first term of the last two expressions because its exact transport equation is simpler than for ε_{TD}. Justification for this approach arises from the fact that the relevance of the last term is rather low (with a maximum of about 2% [171]). Thus, in line with the standard modeling approach, ε_{tot} and ε_{res} are given by the expressions

$$\varepsilon_{tot} = \nu\left(\left\langle\frac{\partial U_i}{\partial x_j}\frac{\partial U_i}{\partial x_j}\right\rangle - \frac{\partial\langle U_i\rangle}{\partial x_j}\frac{\partial\langle U_i\rangle}{\partial x_j}\right),\quad \varepsilon_{res} = \nu\left(\left\langle\frac{\partial\tilde{U}_i}{\partial x_j}\frac{\partial\tilde{U}_i}{\partial x_j}\right\rangle - \frac{\partial\langle\tilde{U}_i\rangle}{\partial x_j}\frac{\partial\langle\tilde{U}_i\rangle}{\partial x_j}\right). \tag{18}$$

The latter expressions justify the calculation of $\varepsilon_{tot} = \varepsilon_{res} + \varepsilon$ in hybrid methods via ε_{res} according to Eq. (18) and ε given by the model applied.

By assuming an eddy viscosity structure, the stresses in Eq. (14) can be written

$$R_{ij} = 2k_{tot}\delta_{ij}/3 - 2\nu_{t,tot}\langle\tilde{S}_{ij}\rangle,\ R_{ij}^{res} = 2k_{res}\delta_{ij}/3 - 2\nu_{t,res}\langle\tilde{S}_{ij}\rangle,\ D_{ij} = 2k\delta_{ij}/3 - 2\nu_t\tilde{S}_{ij}. \tag{19}$$

In R_{ij}, $\langle\tilde{S}_{ij}\rangle = \langle S_{ij}\rangle$ is assumed [1,85], and $\nu_{t,tot}$ refers to the RANS viscosity. The resolved viscosity can be obtained by considering $R_{ij}^{res}\langle\tilde{S}_{ji}\rangle = -2\nu_{t,res}\langle\tilde{S}_{nk}\rangle\langle\tilde{S}_{kn}\rangle$, which defines $\nu_{t,res}$. The modeled viscosity ν_t is available via the model applied. The combination of Eqs. (14), (15) and (19) implies ($\langle\tilde{S}\rangle^{-1}$ refers to the inverse matrix $\langle\tilde{S}\rangle$)

$$\nu_{t,tot} = \nu_{t,res} + \langle\nu_t\tilde{S}_{nj}\rangle\langle\tilde{S}\rangle_{jn}^{-1}/3. \tag{20}$$

Corresponding relationships for turbulence length and time scales are also helpful. By using k and ε, modeled length and time scales are given by $L = k^{3/2}/\varepsilon$ and $\tau = k/\varepsilon$, respectively. By using the corresponding total variables, k_{tot} and ε_{tot}, total length and time scales read $L_{tot} = k_{tot}^{3/2}/\varepsilon_{tot}$ and $\tau_{tot} = k_{tot}/\varepsilon_{tot}$. In further discussion below, only modeled length and time scales (L and τ) and total length and time scales (L_{tot} and τ_{tot}) appear (there is, therefore, no need to take reference to resolved length or time scales).

3. Hybrid methods

The development of hybrid RANS-LES methods was significantly influenced by the introduction of DES by Spalart et al. [49], which seemed to offer a simple workable solution, and Speziale's suggestion of a model that can be used continuously to perform RANS, LES, and DNS [38], which originated the discussion of a number of questions. Speziale suggested $D_{ij} = [1 - exp(-\eta\Delta/\mu)]^n R_{ij}$, which relates the stress D_{ij} used in hybrid simulations to the RANS stress R_{ij} (μ is the Kolmogorov length scale, $n = 1$ and $\eta = 0.001$ are constants, see the discussion in Refs. [173–177]). A closer look at this expression for D_{ij} reveals questions, for example, about how the RANS stress R_{ij} is actually provided (RANS expressions used in hybrid models tend to be much smaller than in RANS mode). The exponential involved can be rewritten as $exp(-\Delta_+\eta L_{tot}/\mu)$, where $\Delta_+ = \Delta/L_{tot}$. The factor L_{tot}/μ reflects a *Re* dependence. For huge *Re*, the exponential will tend to be very small. Does this mean the use of a RANS model is our best option to simulate high Re flows? Another concern is that the model response to grid and *Re* induced resolution changes is imposed without taking reference to the actual resolution. A variety of approaches to deal with such questions were presented in the past two decades. They will be described in the following by focusing on common strategies based on theoretical concepts for hybridizing RANS and LES. Apart from offering a potential solution for the hybridizing, all of these hybrid methods have to deal with characteristic issues. In Sects. 3.1, 3.2, approaches will be described that face either computational cost questions or inconsistency questions. Then, methods are described in Sects. 3.3, 3.4 which face questions about either their completeness or their generality.

3.1. Wall-modeled LES

Comprehensive reviews of the WM-LES concept were recently presented by Larsson et al. [32] and Bose and Park [33] (the concept and basic strategies of wall-modeled LES are also very well described in Refs. [178–181]). The main thrust of WM-LES is on providing appropriate boundary conditions for LES performed on relatively coarse grids. The set-up of this problem may give the impression that the problem of designing hybrid methods is moved in this way to a modeling ingredient that does not strongly affect simulation results. The latter is clearly not the case [70], boundary condition can strongly affect LES results (see, e.g., the explicit demonstration in Ref. [182]).

In particular, boundary conditions to LES for wall-bounded flow can be provided via the setting of $(\nu+\nu_t)\tilde{S}_{ik}$ in the diffusion term of the momentum Eq. (6). The modeled viscosity is zero at the wall, and non-zero elements of the wall-shear stress are only given by $\tilde{\tau}_{w,i2}=\nu\tilde{S}_{i2}$ for $i=1$ and $i=3$. Here, $i=2$ refers to the wall-normal direction. The symbol $\tilde{\tau}_w=(\tilde{\tau}_{w,12}^2+\tilde{\tau}_{w,32}^2)^{1/2}$ is used to refer to the wall-shear stress magnitude. In wall-resolved LES, the correct values of the wall-shear stress can be obtained on a sufficiently fine grid by applying the no-slip condition to filtered velocities. In wall-modeled LES, the grid is too coarse to properly calculate the wall-normal velocity gradient. Thus, the basic goal of WM-LES is to obtain an accurate estimate for the wall-shear stress under the condition that a relatively coarse grid is used. It is usual practice (and applied by the methods described below) to neglect fluctuations of $\tilde{\tau}_w$ (which can clearly matter [178]) and to prescribe appropriate mean values for $\tilde{\tau}_{w,12}$ and $\tilde{\tau}_{w,32}$ based on a given mean of $\tilde{\tau}_w$.

Algebraic methods to provide the wall-shear stress depend on the applicability of nonlinear algebraic relationships between the distance to the wall, the corresponding velocity, and the wall-shear stress, which can be used to solve for the wall-shear stress [32,33,64–66,71–75]. Such an algebraic relationship is given by log-law type expressions for the mean velocity of wall flows [162,163]. A typical assumption of such algebraic approaches is to assume that such relationships are locally and instantaneously applicable [33,67] (the validity of the locality assumption depends on the size of grid cells, it becomes more accurate as the grid size increases and the large scale velocity approaches the mean velocity [67]). There are concepts aiming at the incorporation of the pressure gradient in such relationships in order to make algebraic models applicable to a wider range of flows [183,184]. However, these concepts are currently not broadly tested.

A significantly more flexible approach is the use of turbulent boundary layer equations for the calculation of the wall-shear stress. This approach is based on the momentum Eq. (6)

$$2\frac{\partial(\nu+\nu_t)\tilde{S}_{i2}}{\partial x_2}=\frac{D\tilde{U}_i}{Dt}+\frac{\partial(\tilde{p}/\rho+2k/3)}{\partial x_i}=F_i, \tag{21}$$

where the abbreviation F_i is used to refer to the previous expression. The difference to Eq. (6) is the reduction of gradients in the diffusion term to gradients along the wall-normal direction. The modeled viscosity ν_t in Eq. (21) is provided via a RANS model. Equation (21) is solved on a three-dimensional grid applied in addition to the coarse LES grid between the wall and a certain wall distance h. One option is to use the LES velocity at h as boundary condition for Eq. (21), which results in the need to solve Eq. (21) as a partial differential equation (PDE). Another option, leading to a simplified model, is to use the LES solution for the calculation of the force F_i, which implies that Eq. (21) turns into an ordinary differential equation (ODE). Further simplifications are applied via assumptions on F_i. The setting $F_i=0$ implies an equilibrium model providing the velocity as a steady RANS solution (which corresponds to using a law of the wall). The difficulty of this approach arises from the fact that LES fluctuations enter the region covered by the turbulent boundary layer equations. These fluctuations produce a resolved viscosity $\nu_{t,res}$. Park and Moin [73] suggest to account for $\nu_{t,res}$ via modifying the modeled viscosity based on the simplified version $\nu_t=\nu_{t,tot}-\nu_{t,res}$ of Eq. (20), where $\nu_{t,tot}$ refers to the prescribed RANS viscosity. Technically, this approach corresponds to a variant of RSC-LES: see the discussion of conceptual questions in Sect. 3.3.

The concept of WM-LES certainly faces questions [32,33]. For example, an adequate resolution of the boundary-layer thickness (which makes WM-LES orders of magnitude more expensive than original DES [32]) as expected in WM-LES will not be feasible under many conditions, for example, in thin, laminar boundary layers. In addition, the performance of WM-LES in simulations is known to depend on several design parameters, which need settings for a particular flow considered.

1. The off-wall location where the LES is coupled to the wall model needs to be prescribed as a fraction of the local boundary-layer thickness. However, the boundary-layer thickness is unknown a priori for complex geometries [32,33].
2. For the same number of grid points, WM-LES results can be significantly affected by different computational mesh distributions, see Ref. [185] and the discussion of periodic hill flow results in Fig. 6b.
3. The calculation of the modeled viscosity $\nu_t=\nu_{t,tot}-\nu_{t,res}$ as difference of RANS and resolved viscosities implies under partially resolving conditions the need to prescribe $\nu_{t,tot}$ so that $\nu_{t,tot}$ and $\nu_{t,res}$ can properly interact for the flow considered. This will not be the case if an eddy viscosity model or the RANS expression applied for $\nu_{t,tot}$ are inappropriate.

3.2. Source term methods

The use of source term methods (STM), which may be seen to represent a reformulation of methods focusing on providing appropriate boundary conditions, represents an alternative to the application of WM-LES methods.

Germano [39,186] Sagaut and Germano [187] proposed a hybrid approach based on considering hybrid variables as superposition of LES and RANS contributions, which are blended by using a blending function. This leads to equations for hybrid variables that contain additional source terms (contributions due to related RANS and LES variables). The advantage of this approach is the correct mathematical formulation of hybrid equations. The disadvantage is the need to provide RANS and LES variables. While RANS variables can be obtained from the simulation via averaging, reconstruction of LES variables based on the hybrid simulation is an ill-posed deconvolution problem and is an inherently noisy process (and thus, numerically intractable [39,188–190]). In addition, the need to involve LES variables results in computational cost that are higher than LES cost.

A consistent match of RANS and LES equations (which are applied simultaneously) was suggested recently [60–63]. The basic idea is to (i) use output of LES equations to approximate total variables (via an exponentially weighted time averaging of variables involved in LES), and (ii) to add source terms to both LES and RANS equations that enforce consistency between RANS variables and total variables obtained as output of LES equations (via a relaxation requirement between the two sorts of variables considered). This concept allows it to provide proper boundary conditions for well-resolved LES regions. However, this approach, too, results in computational cost that are higher than the cost of LES (although it seems to be possible to slightly relax resolution requirements for resolved LES).

Woodruff [191–195] proposed the concept of model-invariant hybrid simulations, which follows the idea of the continuous modeling concept proposed by Speziale [38]. The key idea is that there are physical quantities that do not depend on the LES-RANS mixture of the model (such quantities are called model invariants, as, e.g., the total kinetic energy) [192,193]. The technical approach applied to derive hybrid equations is (i) to assume that there exists a certain parameter that controls the amount of modeled motions, (ii) to derive hybrid

equations that involve explicit source terms which characterize the sensitivity of model parameters (like k and ω) to variations of the RANS-LES control parameter, and (iii) to approximate the additional source terms in hybrid equations (so that this approach may be seen as a variant of source-term methods described in the preceding paragraph). In particular, approximations are applied to provide these source terms: the modeled dissipation rates in k and ω equations are considered to be model invariants (equal to the corresponding total dissipation rates), which enables the derivation of relations applied to close the unknown source rates. This approach is very attractive because of its mathematical basis. Questions arise, however, regarding the generality of source rate estimates applied, and the influence of prescribing the RANS-LES transition and the RANS-LES blending parameter independent of the actual resolution supported by the grid.

3.3. RANS-bound methods: DES, UNI-LES, and RSC-LES

An alternative to the methods discussed before is the use of methods that apply a bounding of LES variables by taking reference to RANS variables: examples for such methods are given by DES [2,42,43,49–56,77], RSC-LES [85–96], and UNI-LES [10,29,30,97–107]. The basic idea of these methods is to address the problem of LES on coarse grids, in particular for wall bounded turbulent flows. Close to the wall where the characteristic LES length scale $L = \Delta$ is much larger than characteristic turbulence length scales, the modeled turbulent viscosity $\nu_t = C_\mu k^{1/2}\Delta$ and, therefore, the production of turbulence become large and the dissipation rate $\varepsilon = k^{3/2}/\Delta$ becomes small, which often implies significant over-predictions of turbulent kinetic energy (see, for example, Ref. [102]). To address the latter issue, RANS length or time scales are calculated during the simulation as part of one consistent system of equations. These RANS scales are used then for the bounding of LES length or time scales.

Based on its original simplicity, the most popular bounding method is DES [2,42,43,49–56,77,196]. Thorough reviews of DES were provided by Spalart [56] and Mockett et al. [43]. DES-type equations can be applied to many turbulence models in different versions. The DES concept is presented here with respect to the modeled energy Eq. (7) for k,

$$\frac{Dk}{Dt} = P - \psi_{DES}\varepsilon + D_k, \qquad \psi_{DES} = max\left(1, \frac{k^{3/2}}{C_{DES}\Delta\ \varepsilon}\right). \tag{22}$$

In contrast to Eq. (7), the k equation is modified here via introducing ψ_{DES}, where C_{DES} is a constant which is often considered to be $C_{DES} = 0.65$. The DES concept has two significant characteristics. First, no attempt is made to reflect the amount of resolved motions (see the discussion below after the paragraph on UNI-LES methods): according to Eq. (22), the model switches between model length scales, in particular, the RANS and LES length scales ($L = k^{3/2}/\varepsilon$ and Δ, respectively). Second, the switch of scales is usually applied in dissipation terms (the same applies to DES versions that modify terms in ε or ω equations; there are, however, exceptions as given by the derivation of corresponding hybrid methods in the framework of $k-\varepsilon$ models on the basis of a renormalization group (RG) approach [197–200], or the switch of LES and RANS length scales in all terms involving the modeled viscosity [201]). The idea behind such modifications of dissipation terms in k, ε, or ω equations is to have one control term that enables the simulation of resolved motions in RANS equations. With respect to Eq. (22), this is accomplished via increasing the dissipation of k, leading to lower k values and a reduced modeled viscosity. The DES concept is attractive due to its relative simplicity and focus on the practical implementation of a resolved motion capability in RANS equations. There arise, however, questions on its foundations, in particular, on the realizability of such computational methods (see next paragraph).

UNI-LES methods were developed in response to the latter realizability question [10,29,30,97–107]. The motivation for this development was to derive realizable turbulence models for both RANS and LES from an underlying stochastic turbulence model [10]. One advantage of this approach is the development of a systematic hierarchy of RANS and LES models ranging from stress tensor equations to simple algebraic stress models. Another advantage is given by evidence for the fact that RANS and LES apply the same equations for the velocity: the difference between RANS and LES is given by the use of different time scales. By introducing a unified time scale τ_u, the unification of RANS and LES can accomplished then by a switch of RANS and LES time scales ($\Delta k^{-1/2}$ and $\tau = k/\varepsilon$, respectively),

$$\frac{Dk}{Dt} = P - \varepsilon + D_k, \qquad \tau_u = min\left(\Delta k^{-1/2}, \tau\right). \tag{23}$$

The latter relation is symbolic: it refers to the replacement of the RANS turbulence time scale τ by τ_u in all terms in the k equation and mean momentum equation. More sophisticated transitions between RANS and LES scales than given by τ_u can be applied [10], but they were found to have insignificant effects [102]. Equation (23) involves a switch of dissipation rates as applied in DES methods determined by Eq. (22) (a minor difference is that no parameter C_{DES} is currently applied in UNI-LES). The much more relevant difference between DES and UNI-LES methods is the consistent RANS-LES switch in UNI-LES via a change of scales in all affected terms (not only in the dissipation term, but also in production and turbulent transport terms). This is highly beneficial, for example, with respect to the development of fluctuations in RANS-LES transition regions [105].

A characteristic property of both DES and UNI-LES methods is the focus on bounding LES scales by corresponding RANS scales without accounting for the amount of resolved motions. This concept is simple, valid (LES scales need to be bounded by RANS scales), and attractive, but it also faces questions. RANS variables are calculated in this way as output of RANS equations, but this does not mean that these variables are representative for total variables consisting of modeled and resolved variables (see Sect. 2.4). Conceptually, RANS variables provided in this way represent modeled motions. For under-resolving conditions (close to a wall), such RANS variables do approximate total variables (total variables may be slightly under-represented because resolved motions are still present). For resolving conditions (away from a wall), such RANS variables can be small compared with total variables. This does not need to pose a significant problem because the equations considered still apply relatively small length or time scales. This concept is much better than pure LES because scale variables in pure LES are usually not bounded. On the other hand, such methods are often rather sensitive to grid variations. For example, such bounding methods have an unclear standard if grids are applied that imply extended flow regions where RANS variables do not approximate total variables and simultaneously LES scale variables do not well characterize small-scale turbulence structures.

In contrast to DES and UNI-LES methods, RSC-LES methods do involve information about resolved motions. RSC-LES methods are based on Eq. (14), $R_{ij} = R_{ij}^{res} + \langle D_{ij}\rangle$, combined with a prescribed RANS model for R_{ij}. Because R_{ij}^{res} is known, the problem to provide the modeled stress is reduced then to the need to provide fluctuations $\tilde{D}_{ij} = D_{ij} - \langle D_{ij}\rangle$ of D_{ij} (via a model for D_{ij}). The latter can involve a dynamic calculation of model parameters because of the existence of resolved motions in all over the domain [85]. This concept looks to be more appropriate than DES and UNI-LES methods, but (on top of the question of how well the RANS stress actually reflects the total stress) it also faces conceptual questions because of the combination of different RANS and LES elements. Under resolving conditions, the mean modeled stress is provided by $\langle D_{ij}\rangle = R_{ij} - R_{ij}^{res}$. This means the mean modeled stress can be unphysical (leading to a spurious source term in the momentum equation) if the (anisotropy) structure of the Reynolds stress does not agree with the structure of the resolved stress: there is no guarantee that the Reynolds stress and resolved stress balance each other. The RSC-LES

concept excludes this case by working with an interface that separates resolved and non-resolved regions: in resolved regions dynamic LES is applied. The drawback of this concept is the introduction of an artificial interface that may affect simulation results. Under non-resolving conditions (close to the wall), the mean modeled stress may be considered to be the difference of the RANS stress and a noise source given by the resolved stress. This set-up is not ideal because the RANS stress is designed to provide a modeled viscosity under conditions where fluctuations are absent. A modification of the RSC-LES approach described here was suggested by Bhushan and Walters [202], Walters et al. [203]: the design of hybrid models based on a modeled hybrid stress that represents the linear weighted superposition of modeled LES and RANS stresses, where the weighting parameter can be dynamically calculated. A critical aspect of this approach is how the RANS stress can be properly provided [203].

3.4. RANS coefficient methods: PANS, PITM, and SAS

A strategy for the hybridization of RANS and LES that is very different from the approaches described before will be considered next: coefficient methods, which focus on the modification of model coefficients in RANS equations so that resolving modes can be generated. In particular, this section focuses on well established methods: SAS [42, 127–132], PANS [108–118], and PITM [25–27,119–126] methods.

The basic idea of PANS methods [108–118] can be explained in the following way. Variations between complete (RANS) and partial modeling can be accomplished by changes of the modeled viscosity $\nu_t = C_\mu k^2/\varepsilon = C_\mu k/\omega$: by keeping the calculation of k unchanged and increasing ε or ω via an appropriate modification of ε or ω equations, one can expect the generation of resolved motions. In particular, ε or ω equations should change in response to the ratio $k_+ = k/k_{tot}$ of modeled-to-total kinetic energy and the ratio $\varepsilon_+ = \varepsilon/\varepsilon_{tot}$ of modeled-to-total dissipation rate. Both, k_+ and ε_+ are considered to be constant and given. Based on $Dk/Dt = k_+ Dk_{tot}/Dt$ and the RANS Eq. (7) for k we have then

$$\frac{Dk}{Dt} = P - \varepsilon + D_k = k_+[P_{tot} - \varepsilon_{tot} + D_{k,tot}], \tag{24}$$

where the subscript *tot* is used to refer to total (RANS) variables. It is worth noting that $Dk/Dt = P - \varepsilon + D_k$ for the change of modeled energy reflects the assumption that the k calculation is not modified. An appropriate modification of the modeled ε equation can be derived on the basis of $D\varepsilon/Dt = \varepsilon_+ D\varepsilon_{tot}/Dt$ combined with the RANS Eq. (8) for ε_{tot},

$$\frac{D\varepsilon}{Dt} = \varepsilon_+\left[C_{\varepsilon_1}\frac{\varepsilon_{tot}}{k_{tot}}(P_{tot} - \alpha\,\varepsilon_{tot}) + D_{\varepsilon,tot}\right] = C_{\varepsilon_1}\frac{\varepsilon}{k}(k_+ P_{tot} - \alpha\varepsilon k_+/\varepsilon_+) + \varepsilon_+ D_{\varepsilon,tot}. \tag{25}$$

By replacing $k_+ P_{tot}$ in the parenthesis term according to Eq. (24) and introducing $\alpha_{PANS} = 1 + (\alpha - 1)k_+/\varepsilon_+$, we obtain the $k-\varepsilon$ model

$$\frac{Dk}{Dt} = P - \varepsilon + D_k, \qquad \frac{D\varepsilon}{Dt} = C_{\varepsilon_1}\frac{\varepsilon}{k}[P - \alpha_{PANS}\,\varepsilon + D_k - k_+ D_{k,tot}] + \varepsilon_+ D_{\varepsilon,tot}. \tag{26}$$

A corresponding ω equation is obtained on the basis of $D\omega/Dt = k_+^{-1}\varepsilon_+ D\omega_{tot}/Dt$ combined with the RANS Eq. (11) for ω_{tot} (the cross diffusion term $D_{\omega c}$ is not involved for simplicity),

$$\frac{D\omega}{Dt} = k_+^{-1}\varepsilon_+\left[C_{\omega_1}\frac{\omega_{tot}^2}{\varepsilon_{tot}}(P_{tot} - \beta\,\varepsilon_{tot}) + D_{\omega,tot}\right] = C_{\omega_1}\frac{\omega^2}{\varepsilon}(k_+ P_{tot} - \beta\varepsilon k_+/\varepsilon_+) + \frac{\varepsilon_+}{k_+}D_{\omega,tot}. \tag{27}$$

By using again the relation for $k_+ P_{tot}$ according to Eq. (24) in the parenthesis term and introducing $\beta_{PANS} = 1 + (\beta - 1)k_+/\varepsilon_+$, we obtain the $k-\omega$ model

$$\frac{Dk}{Dt} = P - \varepsilon + D_k, \qquad \frac{D\omega}{Dt} = C_{\omega_1}\frac{\omega^2}{\varepsilon}(P - \beta_{PANS}\varepsilon + D_k - k_+ D_{k,tot}) + \frac{\varepsilon_+}{k_+}D_{\omega,tot}. \tag{28}$$

It looks like the $k-\varepsilon$ Eq. (26) and $k-\omega$ Eq. (28) meet expectations: for small k_+, e.g., α_{PANS} and β_{PANS} become relatively small, leading to a relatively small dissipation of ε and ω, i.e. larger ε and ω, i.e. smaller modeled viscosities $\nu_t = C_\mu k^2/\varepsilon = C_\mu k/\omega$. However, the turbulent diffusion terms in these equations need another look. Regarding the latter we have

$$D_k - k_+ D_{k,tot} = \frac{\partial}{\partial x_j}\left[(\nu + \nu_t)\frac{\partial k}{\partial x_j}\right] - \frac{\partial}{\partial x_j}\left[(\nu + \nu_{t,tot})\frac{\partial k}{\partial x_j}\right] = \frac{\partial}{\partial x_j}\left[\left(1 - \frac{\varepsilon_+}{k_+^2}\right)\nu_t\frac{\partial k}{\partial x_j}\right], \tag{29}$$

$$\varepsilon_+ D_{\varepsilon,tot} = \frac{\partial}{\partial x_j}\left[\left(\nu + \frac{\varepsilon_+}{k_+^2}\frac{\nu_t}{\sigma_\varepsilon}\right)\frac{\partial\varepsilon}{\partial x_j}\right], \qquad \frac{\varepsilon_+}{k_+}D_{\omega,tot} = \frac{\partial}{\partial x_j}\left[\left(\nu + \frac{\varepsilon_+}{k_+^2}\frac{\nu_t}{\sigma_\omega}\right)\frac{\partial\omega}{\partial x_j}\right], \tag{30}$$

where $\nu_{t,tot} = \nu_t\varepsilon_+/k_+^2$ is used. These expressions reveal conceptual questions, for example, why we see a stronger effect of turbulent diffusion on the dynamics of ε and ω if the grid becomes finer (a finer grid has to imply smaller k_+ in $D_k - k_+ D_{k,tot}$), or why the total viscosity $\nu_{t,tot} = \nu_t\varepsilon_+/k_+^2$ controls the diffusivity in modeled ε and ω equations.

In applications of PANS methods, the term $D_k - k_+ D_{k,tot}$ is neglected, and (regarding the ε equation) the use of the Prandtl number $\sigma_\varepsilon k_+^2/\varepsilon_+$ is considered to be one out of two possibilities (the so called zero-transport (ZT) model in contrast to the maximum transport (MT) model, which considers σ_ε as Prandtl number) [110]. In simulations, the ZT model was found to be most appropriate in high Reynolds number flows, whereas the MT model was found to be better for low Reynolds number flows [110]. In particular the neglect of $D_k - k_+ D_{k,tot}$ represents a significant assumption that is, strictly speaking, only applicable to homogeneous turbulent flows (see the further analysis below). Arguably, the biggest concern about PANS methods is the concept to prescribe fixed values of k_+ and ε_+ independent of corresponding values supported by the grid (actual k_+ and ε_+ can be calculated during the simulation). Usually, PANS simulations are performed by setting $\varepsilon_+ = 1$ [108,110,111].

PITM methods [25–27,119–126,204] are based on very different assumptions than PANS methods (they are derived by spectral space analysis, see the recent review of Chaouat [42]), but the equations are, basically, equal to PANS equations. The term $D_k - k_+ D_{k,tot}$ is also neglected in PITM methods, $\varepsilon_+ = 1$ is immediately assumed, and the MT model is used for the Prandtl number in the turbulent diffusion term. The most noticeable difference between PANS and PITM methods is that k_+ is not prescribed but dynamically calculated via Eq. (58), $L_+ = \Delta_{C+}/(1 + \Delta_{C+}^3)^{1/3}$ (which is supported by spectral space analysis, see the discussion related to Eq. (58)): for the assumed $\varepsilon_+ = 1$ we find $k_+ = L_+^{2/3}$. However, given that this approach also is only strictly applicable to homogeneous turbulent flows like PANS, there is again the question of whether k_+ prescribed in this way agrees with the actual k_+.

In PANS and PITM methods, the modeled kinetic energy equation was presented in combination with equations for the dissipation rate ε and turbulence frequency $\omega = 1/\tau$. Another option would be the use of an equation for the turbulence length scale $L = k^{3/2}/\varepsilon = k^{1/2}\tau$ or kL instead of ε or ω. Differences between such equations are related to the physical characteristics of variables considered. Both ε and ω, which reflect the kinetic energy transfer from large to small scales, are directly influenced by small-scale processes. It is possible to derive exact equations for such variables, but such equations are hardly helpful for turbulence modeling because of the appearance of very complex correlations. An interesting fact in this regard is that kL reflects large-scale turbulence properties, as observed by Rotta [205,206].

This observation provides the basis for SAS methods: see Menter and

Egorov [130,131]. Based on a correction of Rotta's kL equation, it is possible to obtain an equation for the modeled viscosity $\nu_t = C_\mu k^{1/2} L$, C_μ is a constant [130,131]. By following Ref. [130,131], this equation is shown here for the high Re case (the contribution of ν to ν_t/σ_Φ is neglected),

$$\frac{D\nu_t}{Dt} = a^2 k(\zeta_1 - \zeta_2 R_{SAS}^2) - C_\mu^{1/4}\zeta_3 k + \frac{\partial}{\partial x_j}\left[\frac{\nu_t}{\sigma_\Phi}\frac{\partial \nu_t}{\partial x_j}\right]. \tag{31}$$

Here, $a = -\widetilde{u_1 u_2}/k = \nu_t \tilde{S}/k$ and $R_{SAS} = C_\mu^{3/4} L/L_{vK}$ are non-dimensional variables. The turbulence length scale L and von Kármán length scale L_{vK} involved in R_{SAS} and their ingredient S' are given by (as before, $S = (2\tilde{S}_{mn}\tilde{S}_{nm})^{1/2}$)

$$L = \nu_t \Big/ \left[C_\mu k^{1/2}\right], L_{vK} = \kappa |S/S'|, \quad S' = \left[\partial^2 \tilde{U}_i \Big/ \partial x_k^2 \times \partial^2 \tilde{U}_i \Big/ \partial x_j^2\right]^{1/2}. \tag{32}$$

In the logarithmic flow region we find $C_\mu^{3/4} L = L_{vK} = \kappa x_2$, this means $R_{SAS} = 1$. Similar to such relations reported before, we find the log-law consistency condition

$$\sigma_\Phi C_\mu^{1/2}\left(\zeta_2 - \zeta_1 + C_\mu^{-3/4}\zeta_3\right) = \kappa^2. \tag{33}$$

The standard SAS settings $(\zeta_1, \zeta_2, \zeta_3, \sigma_\Phi) = (0.8, 1.47, 0.0288, 2/3)$ combined with $C_\mu = 0.09$ then imply $\kappa = 0.41$. In contrast to other suggestions to postulate modeled viscosity equations [207,208], Eq. (31) is closed so that no other scale information (like an ε or ω equation [207]) is required. Combined with the k equation, Eq. (31) can be used to derive an ε and ω equation, respectively [130,131].

$$\frac{D\varepsilon}{Dt} = C_{\varepsilon_1}\frac{\varepsilon^2}{k}\left[\left(1 + \frac{\zeta_2}{C_{\varepsilon_1}}R_{SAS}^2\right)\frac{P}{\varepsilon} - \alpha\right] + \frac{\partial}{\partial x_j}\left[\frac{\nu_t}{\sigma_\Phi}\frac{\partial \varepsilon}{\partial x_j}\right] - \frac{2C_\mu}{\sigma_\Phi}k^2\tau^2\frac{\partial \omega}{\partial x_j}\frac{\partial \omega}{\partial x_j}, \tag{34}$$

$$\frac{D\omega}{Dt} = C_{\omega_1}\omega^2\left[\left(1 + \frac{\zeta_2}{C_{\omega_1}}R_{SAS}^2\right)\frac{P}{\varepsilon} - \beta\right] + \frac{\partial}{\partial x_j}\left[\frac{\nu_t}{\sigma_\Phi}\frac{\partial \omega}{\partial x_j}\right] + \frac{2C_\mu}{\sigma_\Phi}\frac{\partial k\tau}{\partial x_j}\frac{\partial \omega}{\partial x_j}. \tag{35}$$

The log-law consistency conditions read

$$\sigma_\Phi C_\mu^{1/2}(\zeta_2 + C_{\varepsilon_1} - C_{\varepsilon_2}) = \kappa^2, \qquad \sigma_\Phi C_\mu^{1/2}(\zeta_2 + C_{\omega_1} - C_{\omega_2}/C_\mu) = \kappa^2 \tag{36}$$

for the $k-\varepsilon$ and $k-\omega$ models, respectively. The model parameters are given by

$$C_{\omega_1} = C_{\varepsilon_1} - 1 = 1 - \zeta_1, \qquad C_{\omega_2}/C_\mu = C_{\varepsilon_2} - 1 = 1 - \zeta_3 C_\mu^{-3/4}. \tag{37}$$

The standard SAS settings $(\zeta_1, \zeta_3) = (0.8, 0.0288)$ then imply $C_{\varepsilon_1} = 1.2$, $C_{\varepsilon_2} = 1.82$, $C_{\omega_1} = 0.2$, and $C_{\omega_2}/C_\mu = 0.82$.

The functioning of SAS equations as hybrid RANS-LES models can be seen in the following way, where the modeled viscosity Eq. (31) is considered. An interesting property of this equation is that velocity gradients enter this equation first of all via the von Kármán length scale $L_{vK} = \kappa|S/S'|$ (if the modeled $a = -\widetilde{u_1 u_2}/k$ represents an appropriate model for the anisotropy factor $-\widetilde{u_1 u_2}/k$). On sufficiently fine grids that support the simulation of resolved motions, RANS equations may develop fluctuating solutions. The appearance of such velocity fluctuations can significantly reduce the von Kármán length scale L_{vK}: see the detailed analyses in Refs. [130, 209–212]]. Thus, R_{SAS} becomes larger than unity, which implies the simulation of resolved motions via a reduction of modeled viscosity.

4. Hybrid model concept validation by theory

After considering well known hybrid methods, let us ask which hybridization strategy should be preferred. Challenges for hybrid RANS-LES methods and related open questions will be described in Sect. 4.1. Ways to find answers to these questions are described in Sects. 4.2 and 4.3. Related implications of this analysis with respect to existing methods are pointed out in Sect. 4.4.

4.1. Beyond combinations of equations: challenges

An optimal hybrid RANS-LES method may be expected to be characterized by the following properties:

- The method can be well applied to turbulent flows at Re ranging from moderate to extreme Re using a wide variety of reasonable grids. Increasing Re and coarser grids imply continuous variations of the distribution of modeled and resolved motions.
- The method can be applied in conjunction with a variety of turbulence models. The turbulence models can be designed to have for the same grid a comparable resolution.
- There is a known relationship between the flow resolution and the grid. The resolution implied by this relationship agrees with the actual resolution seen in simulations.

Among the hybridization strategies described in Sect. 3, which concept offers the best chance to successfully address these challenges? WM-LES, STM, and bounding methods do not recognize and respond to the amount of resolved motions (on top of that, WM-LES and STM suffer either from the computational cost problem or involve several design parameters leading to conceptual questions, see the discussion at the end of Sect. 3.1). On the other hand, the basic constraint of optimal hybrid methods (continuous variations of the distribution of modeled and resolved motions in response to Re and grid variations), can be addressed on the basis of coefficient methods: the incorporation of coefficients offers a chance to derive relations that explain how a model has to respond (via variations of model coefficients) to a particular resolution (implied by the grid). Therefore, the design of optimal hybrid methods will be explored in the following of this Sect. 4 in the framework of coefficient methods.

In particular, the design of optimal hybrid methods that meet the three expectations described in the beginning of this Sect. 4.1 require answers to specific theoretical questions (which represent more specific versions of bullet point questions posed at the end of Sect. 1):

Q1. Is there a way to generally determine an appropriate response of a model to grid-implied resolution changes by avoiding restrictive assumptions (which needs an explanation of how the amount of resolved and modeled motion has to be measured in a model)?
Q2. Is there mathematical proof that many RANS equations can produce resolved motions, in particular, how can we design various hybrid models having for the same grid a comparable resolution?
Q3. What controls resolved motion (is resolved motion controlled by the grid, this means the filter width Δ)?

With respect to Q1, the difficulty of finding generally applicable relationships between model parameters and flow resolution indicators (like k_+) was already addressed in Sect. 3.4 related to the set-up of PANS and PITM methods. By looking for criteria for the equivalence of various hybrid methods, Friess et al. [77] recently derived relations between model coefficients of RANS equations and flow resolution indicators, but these relationships were obtained under rather restrictive conditions, and they change depending on the assumptions made [213]. Therefore, problem Q1 has to be seen to be unsolved so far. A closely related question, which is debated over decades, is how the amount of resolution actually can be evaluated [214].

With respect to Q2, both applications and theoretical arguments [215] indicate that RANS equations can produce resolved motions under certain conditions. But exact mathematical proof that RANS equations can produce resolved motions is currently missing. The latter requires a general explanation of how at least several RANS models depend on flow resolution indicators that can reflect certain amounts of resolution. A

closely related question is how different turbulence models can be designed that have the same resolution [77].

With respect to Q3, the question of how the grid affects the resolution is relevant to assess the resolution implied by a certain grid (and to see whether the resolution imposed in this way is equal to the actual resolution that can be calculated during the simulation). A potential solution to this problem, $L_+ = \Delta_{C+}/(1+\Delta_{C+}^3)^{1/3}$, which was derived from spectral theory by Chaouat and Schiestel [122], can be supported by using probabilistic arguments (in particular the realizability and statistically most-likely (SML) structure of the related PDF $f = dL_+^2/d\Delta_{C+}$), see Ref. [213] and Appx. C. By using $L_+ = \Delta_{C+}/(1+\Delta_{C+}^3)^{1/3}$ it is possible to assess the resolution that is imposed by a certain grid. Regarding the scaling of LES, it is worth noting that $L = C_+\Delta/(1+\Delta_{C+}^3)^{1/3}$ explains the scaling of the LES length scale L with Δ (which represents a non-trivial question, see the discussion in Sect. 2.3).

It appears that the approach described in the preceding paragraph with respect to question Q3 provides an appropriate solution to this problem. On the other hand, questions Q1 (resolution control mechanism) and Q2 (resolution control in several turbulence model frameworks) represent open research questions. Ways to find solutions to these questions will be described in Sects. 4.2 and 4.3 by following a recent publication of the author [213].

4.2. Mode control mechanism

Let us address the question Q1 described above by considering first the $k-\varepsilon$ model (other turbulence models will be considered below),

$$\frac{Dk}{Dt} = P - \varepsilon + D_k, \qquad \frac{D\varepsilon}{Dt} = C_{\varepsilon_1}\frac{\varepsilon^2}{k}\left(\frac{P}{\varepsilon} - \alpha^*\right) + D_\varepsilon, \tag{38}$$

where a variable α^* is considered instead of the constant α considered in Eq. (8). The most appropriate way to find an answer to question Q1 is to apply variational analysis [77]. This means, we consider variations of model parameters (like α^*) and related variations of model variables (like k and ε): the question is which model coefficients obey variation equations implied by the turbulence model considered. The approach applied below follows Ref. [213]. The technical framework applied to derive these results was provided by an analysis of Friess et al. [77]. The significant difference to the findings reported by Friess et al. [77] is that Friess et al. focused on a different question: for given PANS-type relations between model coefficients and resolution indicators (see Sect. 3.4), Friess et al. [77] determined equivalence criteria for hybrid methods based on other turbulence models.

By replacing P in the ε Eq. (38) according to $Dk/Dt = P - \varepsilon + D_k$ and taking the variation (denoted by δ) of this ε equation we obtain the exact relation

$$\delta\alpha^* = Q + \frac{D_k}{\varepsilon}\left[\frac{\delta D_\varepsilon}{D_\varepsilon} - \frac{\delta D_k}{D_k} + \frac{\delta k}{k} - \frac{\delta\varepsilon}{\varepsilon}\right] + (\alpha^* - 1)\left[\frac{\delta D_\varepsilon}{D_\varepsilon} + \frac{\delta k}{k} - 2\frac{\delta\varepsilon}{\varepsilon}\right], \tag{39}$$

where the ε Eq. (38) is applied to replace D_ε. Here, we introduced the abbreviation

$$Q = \frac{1}{\varepsilon}\frac{Dk}{Dt}\left[\frac{\delta\varepsilon}{\varepsilon} - \frac{\delta k}{k} - \frac{\delta D_\varepsilon}{D_\varepsilon}\right] + \frac{1}{\varepsilon}\delta\left(\frac{Dk}{Dt}\right) + \frac{k}{C_{\varepsilon 1}\varepsilon^2}\left[\frac{\delta D_\varepsilon}{D_\varepsilon}\frac{D\varepsilon}{Dt} - \delta\left(\frac{D\varepsilon}{Dt}\right)\right]. \tag{40}$$

A very important question is about the assumptions applied for this analysis. The coefficient α^* calculated via Eq. (39) should not depend on Dk/Dt or $D\varepsilon/Dt$. This corresponds to the neglect of Q, i.e. $Q = 0$. The coefficient α^* should not be proportional to the turbulent transport term D_k, which does not reflect a systematic influence on the relationship between α^* and variables characterizing the flow resolution. Thus, the second term in Eq. (39) should be equal to zero. It turns out that this is the case if we follow Friess et al. [77], Manceau et al. [216]: we assume that variations of $\delta k/k$ and $\delta\varepsilon/\varepsilon$ in space can be neglected, which means we look for model coefficient variations that produce an uniform relative variation of the energy partition over the domain. The assumed proportionality between δk (which measures the variation of the energy partition among resolved and modeled motions) and k means that there is a minimal [maximal] tendency for changes of the resolution status in highly resolved [highly under-resolved] flow regions where we have very low [very high] values of k, see also the justification provided by Friess et al. [77], Manceau et al. [216]. It is worth noting that the neglect of spatial variations of $\delta k/k$ and $\delta\varepsilon/\varepsilon$ is very different from the PANS assumption of constant k_+ and ε_+. For example, for wall-bounded turbulent flows, k_+ and ε_+ should not be constant in general (as indicators of the amount of modeled motion, they should increase with a decreasing distance to the wall). On the other hand, the assumption of spatially homogeneous $\delta k/k$ and $\delta\varepsilon/\varepsilon$ allows variations of k_+ and ε_+.

By using the assumption of spatially constant $\delta k/k$ and $\delta\varepsilon/\varepsilon$, we find the variations of diffusion terms to be $\delta D_k/D_k = \alpha_k^3/\alpha_\varepsilon - 1$ and $\delta D_\varepsilon/D_\varepsilon = \alpha_k^2 - 1$. In the first order of approximation, we find for $\delta D_k/D_k = \alpha_k^3/\alpha_\varepsilon - 1$ and $\delta D_\varepsilon/D_\varepsilon = \alpha_k^2 - 1$ the expressions

$$\frac{\delta D_k}{D_k} = N_k\frac{\delta k}{k} - N_{k\varepsilon}\frac{\delta\varepsilon}{\varepsilon}, \qquad \frac{\delta D_\varepsilon}{D_\varepsilon} = N_\varepsilon\frac{\delta k}{k}, \tag{41}$$

where $N_k = 3$, $N_{k\varepsilon} = 1$, and $N_\varepsilon = 2$. In contrast to corresponding relations reported by Friess et al. [77], these expressions include ε variations. These findings imply that the second term in Eq. (39) disappears. We find then

$$\delta\alpha^* = (\alpha^* - 1)\left[3\frac{\delta k}{k} - 2\frac{\delta\varepsilon}{\varepsilon}\right]. \tag{42}$$

This relation is equivalent to

$$\frac{\delta\alpha^*}{\alpha^* - 1} = 2\frac{\delta L}{L}, \tag{43}$$

which involves $L = k^{3/2}/\varepsilon$. This equation can be integrated from the RANS state to a state with a certain level of resolved motion, $\int_\alpha^{\alpha^*} dx/(x-1) = 2\int_{L_{tot}}^{L} dy/y$. By introducing $R = L_+^2$ we obtain

$$\alpha^* = 1 + R(\alpha - 1). \tag{44}$$

Such a result cannot trivially be expected as a result of the variational analysis applied: instead of Eq. (44), a reasonable expectation would be a result like $\alpha^* = \alpha - \int_{RANS}^{LES} f(z)dz$, where the subscript *RANS* and superscript *LES* refer to RANS and LES states of the antiderivative of a certain function $f(z)$, respectively. Such a result $\alpha^* = \alpha - \int_{RANS}^{LES} f(z)dz$ would not identify a resolution measure, and it would not explain how model coefficients depend on a resolution indicator, i.e. a flow variable given as ratio of modeled to total variable (like X/X_{tot}, X and X_{tot} refer to the modeled and total values of any flow variable).

However, it turns out that the clarity of the conclusion Eq. (44) enables to give an answer to the question Q1 (an explanation of how the amount of resolved and modeled motion has to be measured, and an explanation of how it is possible to generally determine a model's response to a changing resolution implied by grids). First, one significant advantage of the analysis presented here is the mathematical identification of L_+^2 as resolution measure regarding the model considered (it is worth noting that L_+^2 is also found as the appropriate resolution measure for several $k-\varepsilon$ and $k-\omega$ turbulence models and for different PANS-PITM-type and DES-type approaches to realize the hybridization: see Sect. 4.3). This result matters regarding the non-trivial question of how the flow resolution can be measured (because of the lack of theory, it was addressed so far on an empirical basis by considering the suitability of several appropriate criteria [214]). Second, another significant advantage of the analysis presented here is the explanation of how model parameters have to adjust to a particular flow resolution. In

particular, the estimation of L_+^2 (being a ratio of modeled to corresponding total variable) as driver for model coefficient variations via Eq. (44) provides the desired explanation.

4.3. Generality of concept

Let us address next question Q2 described in Sect. 4.1. The same approach as applied in Sect. 4.2 can be applied to other types of two-equation models, for example, the DES concept applied in conjunction with the $k-\varepsilon$ Eq. (22),

$$\frac{Dk}{Dt}=P-\psi_\alpha\varepsilon+D_k,\qquad \frac{D\varepsilon}{Dt}=C_{\varepsilon_1}\frac{\varepsilon^2}{k}\left(\frac{P}{\varepsilon}-\alpha\right)+D_\varepsilon. \tag{45}$$

Variations of the energy partition between resolved and modeled motions can be accomplished via the function ψ_α. As done before, we neglect the LHS of both equations and use $P=\psi_\alpha\varepsilon-D_k$ in the ε equation, leading to $0=C_{\varepsilon_1}k^{-1}\varepsilon^2(\psi_\alpha-D_k/\varepsilon-\alpha)+D_\varepsilon$. The comparison with the relation $0=C_{\varepsilon_1}k^{-1}\varepsilon^2(1-D_k/\varepsilon-\alpha^*)+D_\varepsilon$ obtained in Sect. 4.2 shows the equivalence of both models under the condition

$$\alpha^*=1+\alpha-\psi_\alpha. \tag{46}$$

The hybridization of $k-\omega$ models can be accomplished in correspondence to the $k-\varepsilon$ Eq. (38). By neglecting the cross diffusion term $D_{\omega c}$ for simplicity we consider

$$\frac{Dk}{Dt}=P-\varepsilon+D_k,\qquad \frac{D\omega}{Dt}=C_{\omega_1}\omega^2\left(\frac{P}{\varepsilon}-\beta^*\right)+D_\omega, \tag{47}$$

where the unknown function β^* replaces β used in Eq. (11). We neglect again both LHS's in Eq. (47) and use $P=\varepsilon-D_k$ in the ω equation, which implies $0=C_{\omega_1}\omega^2(1-D_k/\varepsilon-\beta^*)+D_\omega$. The variational analysis of this equation is equivalent to the corresponding analysis of $k-\varepsilon$ models [213]. We find $\delta D_\omega/D_\omega=\alpha_k-1$. In the first order of approximation we find $\delta D_\omega/D_\omega=N_\omega\delta k/k$, where $N_\omega=1$. The resulting variational equation reads

$$\delta\beta^*=(\beta^*-1)\left[(2+N_\omega)\frac{\delta k}{k}-2\frac{\delta\varepsilon}{\varepsilon}\right]-T_\beta, \tag{48}$$

where $T_\beta=\varepsilon^{-1}D_k[(1-N_{k\varepsilon})\delta\varepsilon/\varepsilon+(N_k-2-N_\omega)\delta k/k]$. In combination with $N_k=3$, $N_{k\varepsilon}=1$, and $N_\omega=1$, Eq. (48) implies

$$\beta^*=1+R(\beta-1), \tag{49}$$

which identifies again R to be $R=L_+^2$.

Like with respect to the $k-\varepsilon$ model, the same approach can be applied to design a DES version of the $k-\omega$ model. By involving the unknown function ψ_β we consider the equation

$$\frac{Dk}{Dt}=P-\psi_\beta\varepsilon+D_k,\qquad \frac{D\omega}{Dt}=C_{\omega_1}\omega^2\left(\frac{P}{\varepsilon}-\beta\right)+D_\omega. \tag{50}$$

We neglect both LHS's and use $P=\psi_\beta\varepsilon-D_k$ in the ω equation, which results in $0=C_{\omega_1}\omega^2(\psi_\beta-D_k/\varepsilon-\beta)+D_\omega$. The comparison with the corresponding $k-\omega$ equation $0=C_{\omega_1}\omega^2(1-D_k/\varepsilon-\beta^*)+D_\omega$ reveals the consistency of models under the condition

$$\beta^*=1+\beta-\psi_\beta. \tag{51}$$

What are corresponding consequences for question Q2 (the question of whether there is mathematical proof that many RANS equations can produce resolved motions, and how we can design several turbulence models that have a comparable resolution for the same grid)? The reported results show that at least several well-known RANS equations can generate resolved motions if $L_+\le 1$. It may be expected that resolving modes can be implemented in most RANS equations provided they involve model coefficients that can be chosen in agreement with the flow resolution reflected by L_+^2. The reported results do also show that several turbulence models can have at least a comparable resolution: independent of the model type, the resolution enters the turbulence models considered via the same resolution indicator: L_+^2. With respect to question Q1 discussed above, the results reported here confirm that L_+^2 is the appropriate resolution measure for several ($k-\varepsilon$ and $k-\omega$) turbulence models and for different (PANS-PITM-type and DES-type) hybridization approaches.

An illustration of the functioning of hybrid methods presented here (in particular the interaction of resolved and modeled motions) is given in Fig. 3. The model Eqs. ((38), (45), (47) and (50) combined with the corresponding settings of model parameters as function of $R=L_+^2$ will be referred to below as CES-KES, CES-KEK, CES-KOS, CES-KOK models, respectively. Here, CES refers to continuous eddy simulation, CES-KE and CES-KO refer to CES performed with the $k-\varepsilon$ model and $k-\omega$ model, respectively. The last character (S and K) refers to a hybridization within the scale equation and k equation, respectively.

4.4. Hybrid model concept validation by theory

The results reported above provide a basis for the generalization (or improvement) of other hybrid RANS-LES. WM-LES and STM methods are generalized in the following (general) sense. The simulation performance of WM-LES and STM methods is known to depend on several design parameters [32,33], which need settings for a particular flow considered (see the discussion at the end of Sect. 3.1). The modeling approach presented here is independent of such design requirements. No off-wall switch location has to be specified, there is no need to meet pure LES resolution requirements, and there are no discrepancies regarding the balance of total and resolved viscosities (or RANS and LES equations applied in the WM-LES approach). Implications of results presented here for coefficient methods and bounding methods will be considered in the following.

With respect to other coefficient methods discussed in Sect. 3.4, what are the consequences of results reported here? We consider PANS (and PITM) methods: SAS models have a different RANS structure, which does not allow meaningful comparisons with the equations considered here. To see the consequences of the PANS assumption $\alpha^*=1+k_+(\alpha-1)$ used in the $k-\varepsilon$ model, we use $\alpha^*=1+k_+(\alpha-1)$ in the variation Eq. (42),

$$\frac{\delta k}{k}[N_\varepsilon-\gamma(N_k-1-N_\varepsilon)]=\frac{\delta\varepsilon}{\varepsilon}[2+\gamma(1-N_{k\varepsilon})], \tag{52}$$

where $\gamma=D_k/[(\alpha-1)k_+\varepsilon]$. The variations $\delta k/k$ and $\delta\varepsilon/\varepsilon$ are independent, and the RHS cannot be made equal to zero. Therefore, ε variations have to be neglected, which implies $N_\varepsilon=0$. The requirement of a zero LHS can only be satisfied by setting $\gamma=0$, which corresponds to $D_k=0$. Thus, fully in line with the analysis results in Sect. 3.4, we see that PANS methods are applicable to homogeneous turbulence, and they require the neglect of ε variations. The same conclusion can be obtained regarding the consequences of the PANS assumption $\beta^*=1+k_+(\beta-1)$ used in the context of the $k-\omega$ model. A consequence of using the PANS set-up for nonhomogeneous flows is, for example, the usual appearance of imbalances regarding the imposed and actual resolution [216], this means a desired resolution that is imposed cannot be accomplished in such simulations [217]. It is worth noting that the differences between PANS methods and the methods described here also imply significant consequences with respect to the computational cost of hybrid methods applied. By assuming $\varepsilon_+=1$ for simplicity (which implies $k_+=L_+^{2/3}$), the PANS coefficient setting in the $k-\varepsilon$ model is $\alpha^*=1+L_+^{2/3}(\alpha-1)$, in contrast to $\alpha^*=1+L_+^2(\alpha-1)$ derived in Sect. 4.2. Because of $L_+^{2/3}\ge L_+^2$, PANS methods indicate a much lower resolution than the methods presented here. An analysis of the impact of such differences on the computational cost provided in Ref. [213] shows that PANS-PITM

methods require a much finer grid than the methods described here in order to ensure the same resolution. In particular, PANS-PITM approaches produce significant additional computational cost in the high-cost LES regime.

With respect to bounding methods discussed in Sect. 3.3, what are the consequences of results reported here? In general, the consistent inclusion of RANS variables in the methods reported here provides a natural bounding of LES variables instead of explicit bounds applied in DES, UNI-LES, and RSC-LES. A specific comparison with the popular DES concept reveals the following. By equating the dissipation rates in the k equation used in DES (see Eq. (22)) and the k equation in the $k-\varepsilon$ model of the approach presented here (see Eq. (45) combined with $\alpha^* = 1 + \alpha - \psi_\alpha = 1 + L_+^2(\alpha - 1)$) we obtain

$$\alpha - L_+^2(\alpha - 1) = max(1, L / [C_{DES}\Delta]) = max(1, L_+ / [C_{DES}\Delta_+]). \tag{53}$$

The latter relation represents a quadratic equation in L_+ which is solved by

$$L_+ = min\left(\frac{\sqrt{1 + 4\alpha(\alpha-1)C_{DES}^2\Delta_+^2} - 1}{2(\alpha-1)C_{DES}\Delta_+}, 1\right). \tag{54}$$

For small Δ_+, Eq. (54) provides $L_+ = \alpha C_{DES}\Delta_+$. The same comparison using the k equation in the $k-\omega$ model of the approach presented here implies Eq. (54) with α replaced by β,

$$L_+ = min\left(\frac{\sqrt{1 + 4\beta(\beta-1)C_{DES}^2\Delta_+^2} - 1}{2(\beta-1)C_{DES}\Delta_+}, 1\right). \tag{55}$$

For small Δ_+, Eq. (55) provides $L_+ = \beta C_{DES}\Delta_+$. An L_+ plot implied by Eq. (54), Eq. (55) is given in Fig. 5 by using $\alpha C_{DES} = C_+$ combined with $\alpha = 1.33$, and $\beta C_{DES} = C_+$ combined with $\beta = 1.63$, respectively. By using $C_+ = 1$, this implies $C_{DES} = 0.75$ and $C_{DES} = 0.61$ in $k-\varepsilon$ and $k-\omega$ models, respectively, which is not far from the standard value $C_{DES} = 0.65$. An L_+ plot according to Eq. (58) is also shown in Fig. 5 for a comparison. The following observations can be made with respect to the CES-DES equivalence conditions (54), (55):

1. Support: There is a good agreement between Eqs. (54) and (55) and between them and Eq. (58) (which is based on a very different reasoning) regarding the $L_+ - \Delta_+$ relation.
2. Relevance: In correspondence to Eq. (58), the computational realization of Eqs. (54) and (55) in simulations is expected to ensure a stable model performance under grid variations.
3. Use in DES: The technical solution to adjust Δ_+ to L_+ is absurd. Thus, the framework of DES is too narrow to ensure Eqs. (54) and (55). Because of that, DES is unstable with regard to grid variations (in particular on coarse grids), which is the known DES drawback [218].

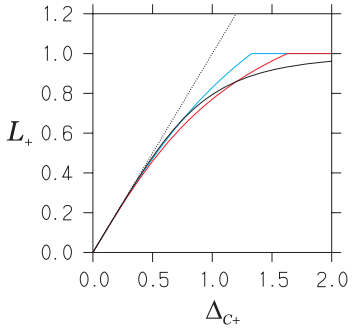

Fig. 5. The black line shows L_+ given by Eq. (58). The dashed line shows Δ_{C+}. The blue and red lines show L_+ according to Eq. (54) and Eq. (55), respectively. (For interpretation of the references to colour in this figure legend, the reader is referred to the Web version of this article.)

4. Use in CES: An implementation of Eqs. (54) and (55) in CES is possible. It occurs to be valid. It is controllable via the actual $L_+ - \Delta_+$ relationship seen in simulations. A corresponding computational method generalizes DES by enabling a proper response to grid variations.

5. Hybrid model concept validation by separated flow simulations

Let us consider applications of the hybrid methods described in Sect. 3 to several types of separated flows. Simulations of hill-type flows with increasing complexity will be considered in Sects. 5.1–5.3, respectively. Compared with airfoil flow simulations, which are affected by a variety of factors (airfoil shape, angle of attack, inflow, Re), such hill-type flow simulations directly focus on the core question, the ability of hybrid models to deal with complex separation patterns. Airfoil flow simulations will be considered finally in Sect. 5.4.

The discussions in Sects. 5.2–5.4 apply, basically, to the use of WM-LES and DES methods; other hybrid methods were hardly applied to these flows. Essential conceptual problems of WM-LES and DES were addressed before: see the discussion of design parameters at the end of Sect. 3.1 and the discussion of resolution questions at the end of Sect. 4.4, respectively. As it can be expected, these WM-LES and DES characteristics imply typical hybrid model problems (prediction uncertainty, resolution deficiencies, and inconsistent improvements).

5.1. Periodic hill flows: variability of methods and mode distributions

The flow over two-dimensional hills considered [12] is illustrated in Fig. 1. This flow involves several relevant flow regimes, for example, separation, recirculation, and natural reattachment. The flow configuration corresponds to an experimental set-up of Mellen et al. [14] who modified the geometry applied by Almeida et al. [13] in experimental studies to provide a better reference for the evaluation of numerical simulation studies. In particular, Mellen et al. [14] kept the hill shapes but reduced the channel height by a factor of two to decrease the computational cost, and the distance between succeeding hills was doubled to allow for natural reattachment. Periodicity was ensured in streamwise direction and statistical homogeneity was ensured in spanwise directions, which enabled numerical simulation studies at lower computational cost and the use of periodic boundary conditions in streamwise and spanwise directions. A usual set-up for numerical studies is to consider a computational domain size of $L_x = 9h$, $L_y = 3.035h$, and $L_z = 4.5h$ in streamwise (x), wall normal (y), and spanwise (z) directions, respectively, h being the height of the hill. The hill crest is located at $(x,y)/h = (0,1)$. The channel is constrained by solid walls at the bottom and top. No-slip and impermeability boundary conditions are applied at these walls.

Experimental results for the evaluation of computational simulations are available for a range of Reynolds numbers $Re = U_b h/\nu$ (based on h and the bulk velocity U_b above the hill crest at $x = 0$), for example, $Re = (5,600, 10,600, 19,000, 37,000)$ [24]. Using the relationship between bulk Reynolds numbers and friction Reynolds numbers Re_τ for channel flow [1], rough estimates for corresponding channel flow Re_τ would be $Re_\tau = (470, 830, 1,400, 2,500)$, respectively. A comprehensive study of Re effects focused on the shape of the recirculation zone was presented by Kähler et al. [223]. In particular, these authors studied the mean points of separation and reattachment obtained by many studies in dependence on Re. It is evident that there is a large scatter of data depending on the experimental or numerical method applied. There are, however, indications that the recirculation region becomes smaller with increasing Re for the range of Re considered (the separation point becomes larger, the reattachment point becomes smaller). This applies, in particular, to the reattachment point which follows a trend given by $0.49\,(Re/10^4)^{-1.4} + 3.71$ [223]. Although strict evidence is currently missing, this analysis of Re effects provides support for the view that there can be

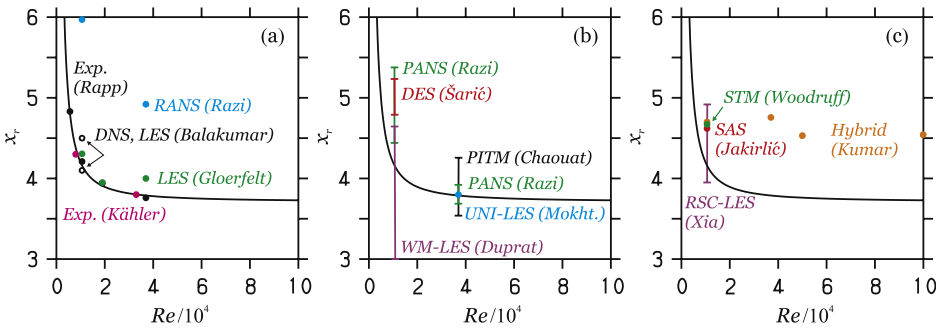

Fig. 6. Periodic hill flow reattachment points x_r depending on the Reynolds number reported by different sources. The name of the first author is used to refer to the source. The references are the following ones: (a) Exp. (Rapp) [24], Exp. (Kähler) [223], LES (Gloerfelt) [232], RANS (Razi) [226], DNS, LES (Balakumar) [28], (b) PANS (Razi) [226], DES (Šarić) [221], UNI-LES (Mokht.) [29], PITM (Chaouat) [27], WM-LES (Duprat) [185], (c) RSC-LES (Xia) [222], SAS (Jakirlić) [18], STM (Woodruff) [192], Hybrid (Kumar) [231]. The fit $0.49(Re/10^4)^{-1.4}+3.71$ to experimental data [223] (solid black line) is shown in all plots.

an asymptotic shape of the recirculation zone at extreme Re (the reattachment point seems to level off at 3.71). These results also support the view that results at $Re = 37K$ are not too far from the asymptotic recirculation pattern. An overview of experimental and numerical simulation studies is presented in Table 1. Differences between such numerical and experimental studies, which will be discussed in following paragraphs, are illustrated in Fig. 6 with respect to the reattachment point prediction depending on Re. The separation point prediction is not involved here. Fig. 11a in Kähler et al. [223] shows that previous experimental studies do not reveal clear conclusions about its dependence on Re, i.e., there is an insufficient basis to evaluate the large scatter of separation point predictions made on the basis of different numerical studies.

Comparisons of RANS, DNS and LES results with experimental data are shown in Fig. 6a. The inability of RANS to properly describe the main flow structure can be clearly seen in Fig. 1. A thorough study of the performance of many RANS models confirms that the correct capturing of the flow configuration considered is beyond the reach of the conventional, inherently steady RANS models, almost independent of the modeling level [17]. DNS and LES results are found to be in relatively good agreement with experimental results as long as the LES resolution is sufficiently high. It is of interest that there is a significant deviation for $Re = 10,600$ with respect to DNS and LES and experimental results on the other hand [28]. For $Re = 37K$, despite the 33.6 M grid points applied [232], there is a noticeable deviation between the LES result and experimental results at this Re.

PANS, PITM, WM-LES, DES, and RSC-LES results shown in Fig. 6b–c are reported to have a large variability of predictions. The PANS variability of results can be attributed to the unknown modeled-to-total kinetic energy ratio f_k (equal to k_+ considered above). An illustration of the influence of f_k settings on calculated separation and reattachment points for $Re = 10,600$, which was reported by Ma et al. [233], is given in Fig. 7. It is worth noting that this $x_r - f_k$ relation is different from the corresponding $x_r - f_k$ relation reported by Razi et al. [226]: according to Razi et al., x_r always increases with f_k up to $f_k = 1$ (see Table 2 and Fig. 18 in Ref. [226]). For the same flow, it turns out that different conclusions can be drawn regarding the most appropriate f_k setting: $f_k = 0.4$ is recommended for simulations by Ma et al. [233], whereas Razi et al. [226] suggest $f_k = 0.15$. The PITM and WM-LES variability results from different computational mesh distributions using the same number of grid points, see Refs. [27,185], respectively. The DES variability results from the use of different DES versions and codes [221], and the RSC-LES variability results from the use of different RANS models representing the RANS ingredient of this approach [222].

Other hybrid results also shown in Fig. 6b–c are reported without an uncertainty range. SAS [18] and STM [192] results obtained for $Re = 10,600$ agree relatively well with measured data. Kumar et al. [231] reported results up to $Re = 100K$, which show a clear disagreement with experimental data for high Re (and there is no obvious Re trend, which has to be expected). The fact that the predictions of Kumar et al. [231] at

Table 1
Periodic hill flow experimental and numerical studies. Lower Re studies are shown in the upper part, higher Re studies are shown in the lower part.

$10^{-3}Re$	References	RANS	WM-LES	STM	DES	UNI-LES	RSC-LES	PANS	PITM	SAS	LES	DNS	Exp.
0.1 – 10.6	Mellen et al. [14], Breuer et al. [21]										x		x
0.7 – 10.6	Breuer et al. [21], Krank et al. [219]											x	
10.6	Balakumar [28]		x								x	x	
10.6	Fröhlich [20], Temmerman, Jang et al. [15,16,19]										x		
10.6	Friess et al [77].				x			x	x				
10.6	He et al. [220], Šarić et al [221].				x								
10.6	Xia et al. [222]						x						
10.6	Duprat et al [185].		x										
10.6	Jakirlić and Maduta [132]									x			
2.8 – 10.6	Xiao et al. [60–63], Woodruff [192]			x									
5.6 – 37	Rapp [22–24], Kähler, Schröder [223,224] et al.												x
37	Murman [225]	x											
10.6 – 37	Jakirlić et al. [17,18]	x			x			x		x			
10.6 – 37	Razi et al [226].	x						x	x				
10.6 – 19	Krank et al. [227–230]	x	x		x								
10.6 – 100	Kumar et al [231].	x			x								
10.6 – 37	Gloerfelt et al. [232]										x		
10.6 – 37	Ma et al [233].							x			x		
10.6 – 37	Chaouat and Schiestel [26,27,124]								x				
10.6 – 37	Mokhtarpoor et al. [29,30,106,107,217]					x					x		

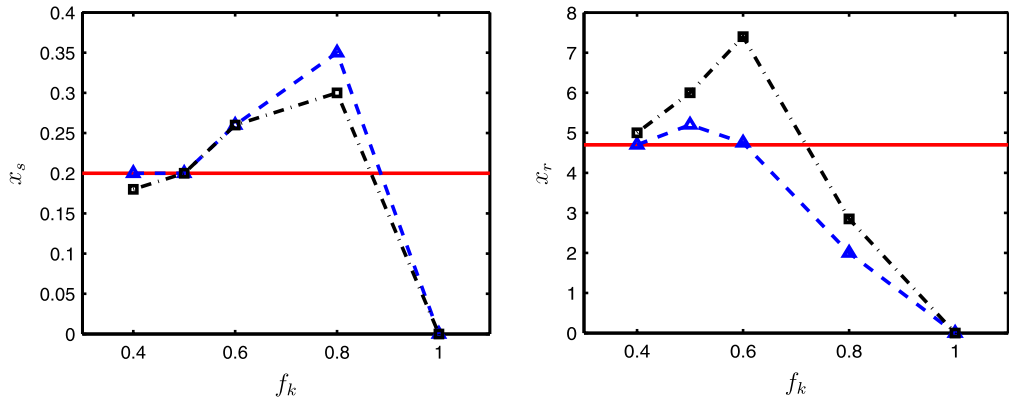

Fig. 7. Periodic hill flow separation (x_s) and reattachment (x_r) points obtained by PANS simulations for $Re = 10,600$ depending on the modeled-to-total kinetic energy ratio f_k [from Ma et al. [233] with permission]. The red lines at $x_s = 0.2$ and $x_r = 4.7$ refer to LES, □: standard PANS, △: low-Reynolds number PANS. (For interpretation of the references to colour in this figure legend, the reader is referred to the Web version of this article.)

Table 2
2D NASA hump flow simulations according to experiments of Greenblatt et al. [253–255].

References	RANS	WM-LES	DES	STM	other hy.	LES
Evans et al. [236], Lardeau and Billard [237], Han et al [238].	x					
Avdis et al [239].						x
Kiris et al [240].	x		x			x
Mockett et al. [241], Probst et al [242].	x		x			
Yin [243], Garbaruk et al. [244], Siggeirsson and Andersson [245]			x			
Dilip [246], Park [247]		x				
Uzun and Malik [234,248], Iyer and Malik [249]		x				
Woodruff [193, 195]				x		
Koklu [250, 251], Haering et al [252].					x	

$Re = 10,600$ basically agree with the predictions of SAS [18] and STM [192] results underlines the need for the evaluation of hybrid methods at relatively high Re. Results of UNI-LES (used without adjustable parameters) at $Re = 37K$ agree very well with the experimental results [29].

The dominant feature of this comparison is the adaptability of various hybrid methods (PANS, PITM, WM-LES, DES, RSC-LES) via design parameter variations. Given this uncertainty, it appears to be not possible to conclude that these hybrid RANS-LES significantly reduce the error of RANS. On the other hand, other hybrid methods (SAS, STM, UNI-LES) apparently reduce the RANS error significantly, although their application range is limited.

A very essential expectation for hybrid RANS-LES methods concerns their mode variability, their proper functioning under grid and Re variations. A minimal expectation is that hybrid methods increase the contribution of modeled motions if (using the same grid) Re increases or the grid becomes coarser (if the grid Reynolds number $\Delta/\mu = u_\mu \Delta/\nu$ increases, u_μ is the Kolmogorov velocity scale: instead of Δ/μ, $Re_\Delta = \Delta^2 S/\nu$ is also applied, which is always available in simulations [235]). This is not a characteristic property of usually applied hybrid methods. Within PANS, being based on the consideration of a constant k_+, it is impossible to correctly reflect an increased amount of modeled motion due to a grid coarsening or higher Re. Within PITM, using a $L_+ - \Delta_+$ relationship like Eq. (58), $L_+ = \Delta_{C+}/(1 + \Delta_{C+}^3)^{1/3}$, the reflection of the expected Re trend of hybrid methods is unclear. For example, for a higher Re it is realistic to expect a higher L_{tot}, which would imply (using the same grid) a lower (instead of an expected higher) amount of modeled motion calculated via the RHS of Eq. (58) (by considering relatively small Δ_{C+} for simplicity). Equation (58) gives the impression that PITM can deal correctly with the expected grid variation trend of hybrid methods. Figure 8, which shows PITM k_+ plots for periodic hill flows obtained on four grids, shows that this is not necessarily the case. Overall, a coarser grid implies higher k_+ values, but there are obvious deviations from this trend, in particular, in the relevant near wall regions. It is also of interest to see that PITM simulations using approximately the same number of grid points (PITM2 and PITM3) can imply rather different k_+, which illustrates the grid sensitivity of PITM results.

Although thorough studies of grid and Re effects on the mode distribution of hybrid RANS-LES based on existing methods were not presented so far, there are, however, indications that existing methods do not behave stably in this regard. It is worth mentioning that the PANS and PITM based arguments presented here are in line with the behavior of DES [43] and UNI-LES (not shown), for which similar observations were made.

5.2. NASA hump flow: resolution deficiencies

Compared with simulations of periodic hill flows discussed in Sect. 5.1, the 2D wall-mounted NASA hump flow configuration [253] as illustrated in Fig. 9 represents a bigger challenge for hybrid RANS-LES and other methods. This flow configuration creates several relevant regimes: separation of the boundary layer from the hump, reattachment of the separated shear layer, and relaxation of the reattached boundary layer. The hump cord length $c = 0.42m$, and the crest height is $0.0537m$. The hump, which is mounted on a splitter plate of thickness $0.0127m$, is placed in a wind tunnel of $0.771m$ width and $0.508m$ height. The nominal test section height (between the splitter plate and the top wall) is $0.382m$ and the nominal hump width (between the two end plates) is $0.584m$. The characteristic Reynolds number based on freestream velocity and chord length has a value of $Re_c \approx 936,000$. The Mach number is 0.1, which allows both incompressible and compressible simulations. This flow configuration has been investigated by experiments and a variety of computational simulation methods: see the overview provided in Table 2.

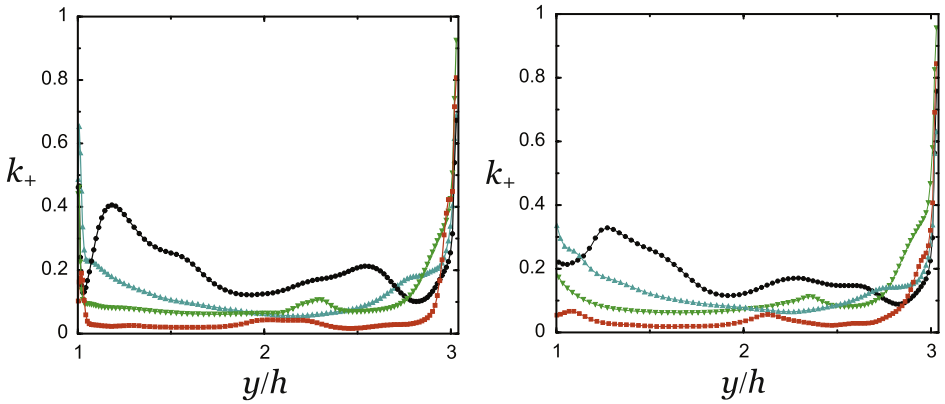

Fig. 8. PITM periodic hill flow simulations ($Re = 37K$): k_+ on four grids, $x/h = 0.05$ (left) and $x/h = 0.5$ (right) [from Ref. [27] with permission]. Black symbols: PITM1 grid ($80 \times 30 \times 100 \approx 1/4$ M), blue symbols: PITM2 grid ($160 \times 30 \times 100 \approx 1/2$ M), green symbols: PITM3 grid ($80 \times 60 \times 100 \approx 1/2$ M), red symbols: PITM4 grid ($160 \times 60 \times 100 \approx 1$ M). (For interpretation of the references to colour in this figure legend, the reader is referred to the Web version of this article.)

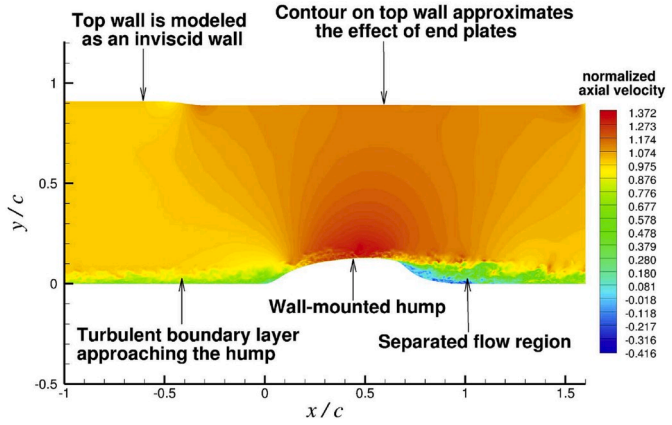

Fig. 9. 2D NASA hump flow illustration: instantaneous normalized axial velocity contours according to Uzun and Malik [234] with permission of the authors.

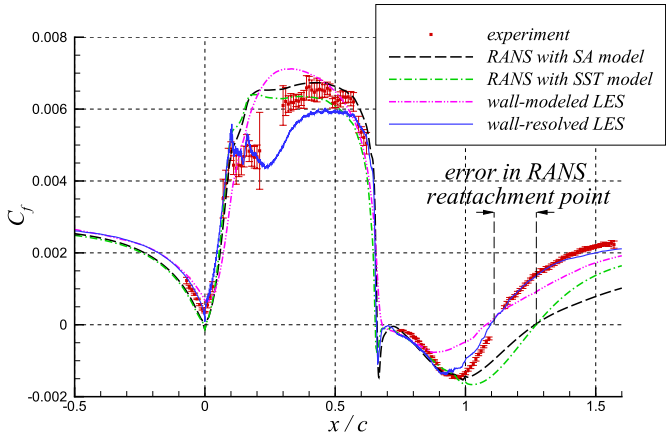

Fig. 10. 2D NASA hump flow – predictions of the skin friction coefficient C_f: experimental results [253], RANS, WM-LES and resolved LES results [from Uzun and Malik [234] with permission of the authors].

By following the comparison of methods with respect to periodic hill flow simulations in Sect. 5.1, an overview of reattachment point (x_r) predictions and related errors implied by different methods is provided in Table 3. There is an excellent agreement between LES and experimental results. The RANS variability [237] depends on the model applied. The DES variability [242] arises from the DES model applied and the spatial combination of RANS and DES simulations. The WM-LES variability [249] arises from the mesh distribution and the setting of the wall model/LES exchange location. The variability of STM [193] arises from the model parameter settings applied. It is obvious that the use of hybrid methods can reduce the error of RANS methods. However, given the limited range of methods applied so far and the variability range of results, it is not possible to derive specific conclusions about the capabilities of different hybrid methods on this basis.

A more specific picture of differences between RANS, LES, and hybrid results is provided in terms of predictions of the skin friction coefficient C_f shown in Fig. 10. The failure of RANS regarding the prediction of the separation-bubble length is obvious. Resolved LES results agree well with the experimental data. WM-LES results are better than RANS, although the double-peak structure of the skin friction profile and the recirculation region structure are inaccurately represented. Results of several DES models (two zonal approaches using different synthetic-turbulence generators at the RANS-LES interface, and a non-zonal approach based on a shear-layer-adapted subgrid length scale) [242]

Table 3
2D NASA hump flow: reattachment point (x_r) predictions of different methods and their errors e. An error illustration is given on the RHS. The red line refers to the idea of a reduced error because of flow resolution.

Studies	References	x_r	e/%
Exp.	Greenblatt et al [253].	1.10	±0.5
RANS	Lardeau and Billard [237]	1.188 – 1.305	8 – 18.6
LES	Uzun and Malik [234,248]	1.095	– 0.5
DES	Probst et al [242].	1.114 – 1.152	1.3 – 4.7
WM-LES	Iyer and Malik [249]	1.035 – 1.105	– 5.9 – 0.5
STM	Woodruff [193]	1.08 – 1.19	– 1.8 – 8.2

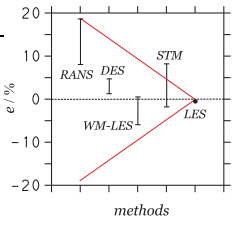

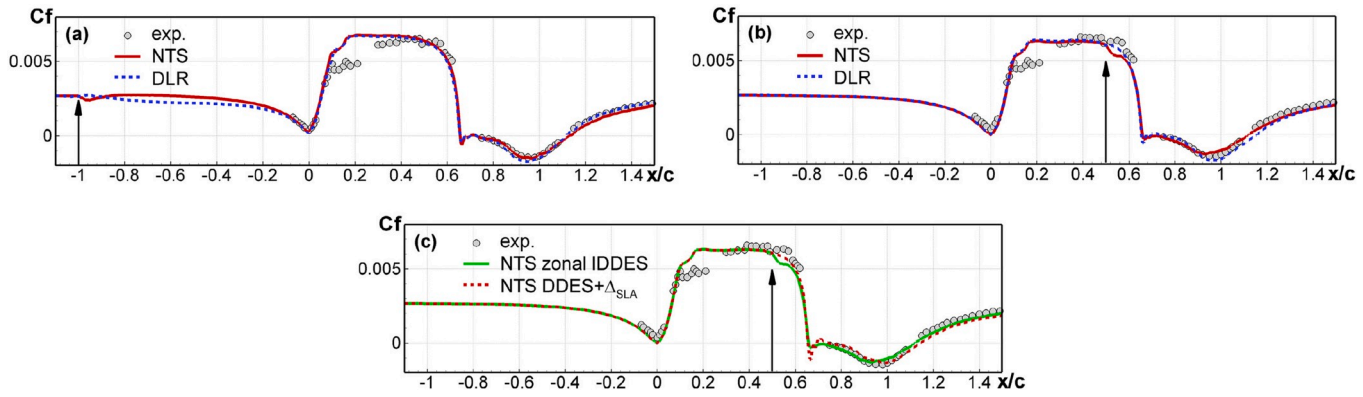

Fig. 11. 2D NASA hump flow – C_f predictions based on several DES methods, see the details in Ref. [242] [taken from Probst et al. [242] with permission]. Vertical arrows show RANS-DES interface locations.

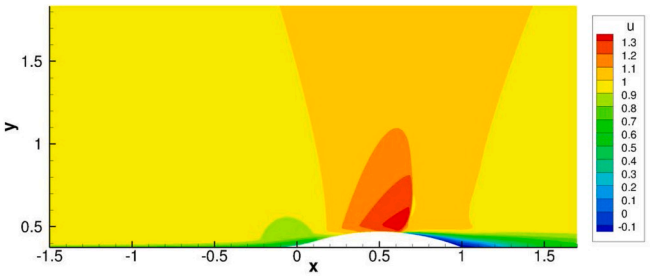

Fig. 12. Axisymmetric transonic bump flow illustration: mean velocity contours [256].

are shown in Fig. 11. It may be seen that a better representation of the recirculation region can be accomplished by appropriate model modifications. However, similar to WM-LES and in contrast to resolved LES, inaccuracies regarding the proper resolution of the double-peak C_f structure are still observed. The Reynolds shear stresses are reasonably well predicted by several DES methods.

5.3. NASA bump flow: inconsistent improvements

The 2D NASA hump configuration considered before is characterized by a nearly fixed separation, which makes it not very sensitive to the accurate resolution of the attached turbulent boundary layer prior to separation [242]. A more severe test case with non-fixed separation from a smooth body is given by the axisymmetric transonic bump configuration studied experimentally by Bachalo and Johnson [277], see Fig. 12. The experiments were conducted at the NASA Ames Research Center. The bump was placed over a cylindrical pipe, the geometry is axisymmetric. The oncoming freestream Mach number is $M_\infty = 0.875$ and Re based on the bump chord length is $Re_c = 2.763 \times 10^6$. The freestream Re based on the distance from the leading edge is $Re_x = u_\infty x/\nu_\infty \approx 5.53 \times 10^6$ at $x = c = -1$. The diameter of the cylindrical pipe was 15.24 cm and the bump chord length was 20.32 cm. The cylindrical pipe extended 61 cm upstream of the bump leading edge. The flow separation is induced by the combination of the shock effect and the adverse pressure gradient at this Mach number. This bump flow configuration has been investigated by experiments and several computational simulation methods: see the overview provided in Table 4.

In similarity to the corresponding discussions of periodic hill and

Table 4
Transonic bump flow simulations according to the experiments of Bachalo and Johnson [254,277]. The third RANS row refers to Reynolds stress RANS.

References	RANS	WM-LES	DES	DNS
Murman [257], Schaefer et al. [258,259], Elkhoury [260]	x			
Abdol-Hamid et al. [261,262], Mor-Yossef [263], Xu et al [264].	x			
Kim [265], Eisfeld [266], Cécora [267] et al., Souza and Radespiel [268]	x			
Witte et al. [269,270], Han et al. [238,271,272], Han and Agarwal [273]	x		x	
Belyaev et al. [274], Spalart et al [275].			x	x
Iyer et al [276].		x		

Table 5
NASA bump flow: reattachment point (x_r) predictions of different methods and their errors e in correspondence to Table 3.

Studies	References	x_r	e/%
Exp.	Bachalo, Johnson [277]	1.10	
DNS	Spalart et al [275].	1.18	7.3
LES	Spalart et al [275].	1.08	– 1.8
RANS	Abdol-Hamid [262]	1.069 – 1.280	– 2.8 – 16.4
$RANS^{RSM}$	Cécora et al [267].	1.092 – 1.194	– 0.7 – 8.5
DES	Han and Agarwal [273]	1.17 – 1.22	6.4 – 10.9
WM-LES	Iyer et al [276].	1.123 – 1.157	2.1 – 5.3

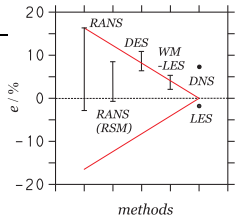

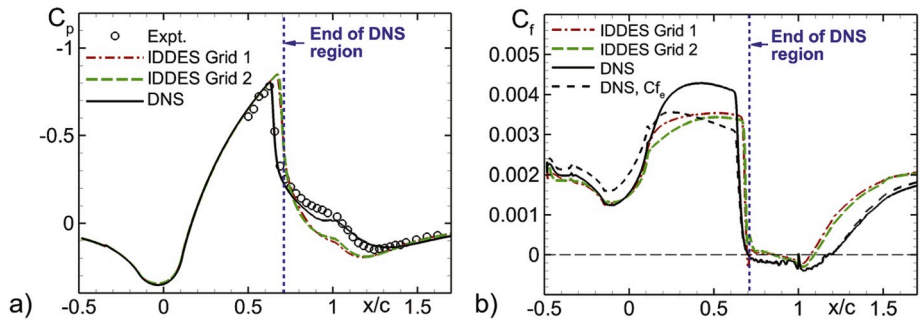

Fig. 13. Transonic bump flow: DES and DES with embedded DNS results for the mean pressure coefficient C_p and skin-friction coefficient C_f along x/c [from Spalart et al. [275] with permission].

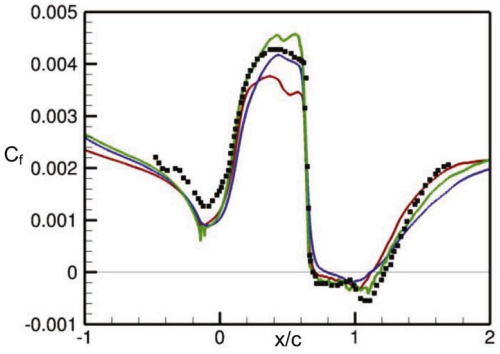

Fig. 14. Transonic bump flow – C_f predictions along x/c obtained from DES-DNS (black squares) [275] and WM-LES [276]: green, blue, red lines refer to NEQWM3, EQWM3, EQWM1, respectively. NEQWM (EQWM) refers to the use of a nonequilibrium (equilibrium) wall model, 1 and 3 refer to a wall model/LES exchange location at the first and third grid point [from Iyer et al. [276] with permission of the authors]. (For interpretation of the references to colour in this figure legend, the reader is referred to the Web version of this article.)

NASA hump flows, an overview of reattachment point (x_r) predictions and related errors implied by different methods is provided in Table 5. The variability of RANS [262] and RANS^{RSM} [267] [RANS^{RSM} refers to Reynolds stress model (RSM) based RANS] depends on the RANS model applied. It may be seen that the RANS^{RSM} variability is significantly smaller than the RANS variability. The variability of DES [273] arises from the DES model applied, and the variability of WM-LES [276] arises from the wall model applied and the setting of the wall model/LES exchange location. LES results agree very well with experimental results. It is surprising to see the performance of DNS, which is seen to be a consequence of a small domain both in the lateral and streamwise directions [275]. Similar to conclusions obtained for the NASA hump flow, the hybrid results are in line with the notion that the inclusion of flow resolution decreases the RANS error. More specific conclusions cannot be obtained on this basis.

DES on two grids (with 4.7×10^8 and 1.6×10^9 cells) and DES with embedded DNS (8×10^9 cells) were recently reported by Spalart et al. [275]. The mean pressure coefficient C_p and skin-friction coefficient C_f along the streamwise direction x/c are shown in Fig. 13. The DES results agree well with each other but they are seen to be disappointing: they fail to agree with the experimental results on the shock position and post-shock pressure. The inclusion of DNS is found to be beneficial, there is a much better agreement with experimental data regarding the pressure coefficient. However, with respect to the Reynolds shear stress, DES with embedded DNS (which suffers from a small domain both in the lateral and streamwise direction) is not successful, see Fig. 12 in Ref. [275]. This level of disagreement is considered to not be tolerable for turbulence-modeling studies. In particular, there is no clear trend for DNS to be closer to experiment than simpler methods [275].

The first WM-LES of this flow was recently reported by Iyer et al. [276]. Good agreement was observed with experiment for the wall-pressure distribution, separation and reattachment locations, and reasonable agreement was observed for the mean velocity and Reynolds stresses in the separation region [276]. The comparison with DES-DNS C_f results of Spalart et al. [275] shown in Fig. 14 reveals the difficulty of such WM-LES. A good agreement with DES-DNS results can be obtained by an appropriate choice of the wall model/LES exchange location. However, it is not possible in this way to accomplish both good agreement with the C_f maximum in the shock region and the C_f maximum in the reattachment region: a better agreement in the shock region deteriorates the agreement in the reattachment region (see EQWM1 and EQWM3 predictions). The EQWM1 simulation provides the best agreement with experimental separation and reattachment points (see Ref. [276], Fig. 7). The NEQWM3 simulation, which predicts a delayed reattachment location, offers the best overall prediction. Overall, consistent improvements compared with RANS are hard to accomplish in this way.

5.4. Airfoil flow: open questions

A particular challenge of separated flow simulations is often the significant variability of flow configurations, as given in airfoil flow simulations. Such simulations are affected by geometry factors (airfoil shape, angle of attack, domain considered) and inflow conditions (Re, level of inflow turbulence intensity). This complicates a comprehensive evaluation of simulation methods under conditions where often discrepancies are found between different experiments and different simulations, and between experiments and simulations [281]. Typical questions will be addressed here by focusing on simulations of flow around the NACA 4412 airfoil (a RANS study of flow around other

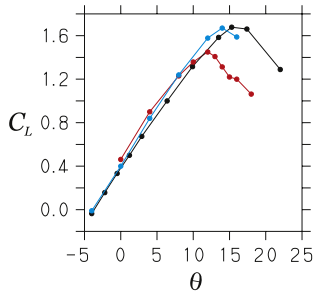

Fig. 15. Experimental NACA 4412 airfoil flow data: lift coefficient C_L versus angle of attack θ. Black: data of Pinkerton [278], red: data of Wadcock [279], blue: data of Coles and Wadcock [280]. (For interpretation of the references to colour in this figure legend, the reader is referred to the Web version of this article.)

airfoils was presented in Ref. [282]).

Most model evaluations were performed by using RANS equations [260,271,282–292]. A comprehensive evaluation of 13 RANS models was recently presented [291] by considering laminar and turbulent subsonic inflow conditions, a wide range of Re ($7 \times 10^5 \leq Re \leq 9 \times 10^6$) based on the chord length and free-stream velocity, and a wide range of angles of attack ($-10^\circ \leq \theta \leq 20^\circ$). Two-dimensional simulations were performed involving up to about $300K$ elements. Experimental data of Pinkerton [278], Abbott and von Doenhoff [293], and Loftin and Smith [294] were used for model validation. Common modeling shortcomings are related to the inadequate modeling of the laminar-to-turbulent flow transition [291,295]. It appears that there is currently no methodology that can provide accurate predictions for both lift and drag coefficients. One of the RSM's was identified as top-performer: for all Re it was able to predict lift forces in agreement with experimental results even under stall conditions, but simultaneously drag forces were found to be substantially over-predicted (as a consequence of the model's lacking ability to properly simulate the laminar-to-turbulent transition). Transition-based models have been developed to accurately determine the laminar-to-turbulent transition [296,297]. Such models are able to accurately predict drag forces but they tend to over-predict lift forces [291]. The worst performance had turbulence models based on the eddy viscosity hypothesis, which were unable to reflect an Re effect on both lift and drag coefficients (see also Ref. [298]).

Usually, LES and hybrid RANS-LES simulations are compared with the experimental data of Wadcock [279] (which are seen to be more accurate [299] than data of Coles and Wadcock [280] and Pinkerton [278], see the differences in Fig. 15), performed at high angles of attack, $12 \leq \theta \leq 14^\circ$, and characterized by the lack of comparisons of lift and drag coefficients, which are considered to be challenging [300]. Instead, emphasis is placed on the pressure coefficient distribution (which can be reasonably obtained on relatively coarse grids [301]) and mean streamwise velocity profiles. Such LES calculations were presented by several groups [299,301–305]. Several WM-LES were also presented [33,72,75,303,304]. The impact of the span extent on such LES is not fully clear, but there are indications that WM-LES can be artificially close to the experiment if a narrow span extent is considered due to computational restrictions [303,304]. DES calculations are reported in Refs. [271,289,290]. The results are different from corresponding RANS studies, but consistent improvements of RANS results are not found.

There are, however, hybrid simulations that addressed the RANS problem related to the prediction of lift and drag coefficients, where experimental data of Wadcock [279] were applied for model validation. DES were reported by Beyhaghi and Amano [306]. Depending on the model considered, drag coefficients are under-predicted by more than 34%. Comparisons of pressure coefficients and velocity profiles with measurements show obvious discrepancies with experimental results. Hybrid RANS-LES using a RSM combined with the PITM approach for hybridization and $3M$ grid points are reported in Refs. [307–309]. The results improve corresponding RANS calculations. Very good agreement with experimental results was found with respect to mean streamwise velocities. Corresponding normal stress results were found to not agree well with experimental data. The error $(+14\%, -54\%)$ of RANS with regard to lift and drag coefficients, respectively, is reduced to $(+7\%, -39\%)$. It is of interest to note that drag coefficients obtained by the hybrid methods described in this paragraph under-predict measured drag coefficients, whereas the top-performing RSM identified in Ref. [291] over-predicts drag coefficients (see above).

Therefore, the accurate prediction of both lift and drag coefficients at affordable computational cost, and a clearer demonstration of advantages of hybrid RANS-LES over RANS and resolved LES still remain a challenge. It is obviously difficult to address these questions as long as the validity of the experimental data of Wadcock [279], Coles and Wadcock [280], Pinkerton [278], Abbott and von Doenhoff [293], and Loftin and Smith [294], which are often used for model validation (see Fig. 15 with respect to the data of Wadcock [279], Coles and Wadcock [280] and Pinkerton [278]), is still debated [290,299].

6. Conclusions

Let us summarize observations made here regarding the status of hybrid RANS-LES methods and chances for significant further methodological improvements.

The applications of hybrid RANS-LES methods considered here support several conclusions about the current status of their development:

1. There is broad support for the view that the basic limitations of RANS and LES methods need to be addressed by the development of hybrid RANS-LES. Many promising new methods were developed over the last 15 years, which complement classical hybrid methods as DES and WM-LES. There is, however, considerable restraint regarding the use of hybrid methods different from DES or WM-LES (see the discussions in Sects. 5.2–5.4).
2. From a rather general viewpoint, hybrid RANS-LES keep their promise. Their predictions are often found to be better than RANS because of the inclusion of resolved motion and significantly more efficient than resolved LES for wall-bounded turbulent flows. In particular, a basic expectation for hybrid models is their capability to simulate separated flows more accurately than RANS. This is often the case (see Sect. 5.1).
3. A typical property of hybrid methods is uncertainty of their predictions. Classical methods as WM-LES and DES are known to be sensitive to different mesh distributions (using the same total number of grid points), parameter settings (wall model/LES exchange location) or various models: see Sect. 5.1. In addition, predictions of alternative hybrid methods can be significantly affected by model parameter assumptions.
4. On the one hand, the grid-sensitivity of hybrid model predictions may cause resolution deficiencies as described in Sect. 5.2: the dependence on suitable grids can hamper the study of grid refinements. On the other hand, room for prediction variations opens the way for inconsistent improvements: the improvement of certain model behaviors can deteriorate other model behaviors: see the discussions in Sect. 5.3.
5. The derivation of conclusions about capabilities of hybrid methods under conditions of significant test case variability and an uncertain model validation basis (airfoil flow simulations, see Sect. 5.4) is even much more difficult. Typical RANS problems (the prediction of lift and drag coefficients) are often not completely addressed, or there can be unclear evidence for the advantages of hybrid methods compared with RANS.
6. A basic expectation for hybrid models is their proper applicability to flows at Re ranging from moderate to extreme Re using a variety of grids: increasing Re and coarser grids should imply continuous variations of modeled and resolved motions. The capabilities of hybrid models are hardly investigated in this regard. There are indications that existing hybrid concepts do not allow to meet this challenge (see the end of Sect. 5.1).

From a theoretical viewpoint, there are the following characteristic features of existing hybrid RANS-LES methods:

1. The classical hybridization concept is to combine equations known to have a RANS and LES structure. This is often done by involving several design settings. With respect to WM-LES and DES, e.g., the performance of models depends on the wall model/LES exchange location, the models applied, and the mesh distribution. The dependence on these design settings complicates significantly the evaluation of hybridization concepts.
2. A relevant aspect of such classical (WM-LES and DES type) hybridization strategies is that no information about resolved motion

produced by such models on a certain grid enters the model. This concept can imply massive imbalances between resolved and modeled motions under significant *Re* and grid variations (for example, for huge *Re* the model does not receive information that it needs to increase its contribution).
3. Only PANS and PITM concepts make an attempt to transfer information about the resolution to the model. Within PANS (based on a constant $k_+ = k/k_{tot}$) it is impossible to correctly reflect an increased amount of modeled motion due to a grid coarsening or higher *Re*. With respect to PITM, there are well-founded questions about the validity of resolution-related relations for nonhomogeneous flows (and the reflection of *Re* effects).

It is likely to expect an ongoing significant interest in further developments of hybrid RANS-LES as indicated by Fig. 2. Their development opens the path to study high *Re* wall-bounded turbulent flows that cannot be investigated by LES or experimentally [310]. Their development also enables a much improved understanding of flow separation mechanisms [311–315]. The discussion in Sect. 4 (which presents new CES concepts and addresses the conceptual questions posed in Sect. 1) shows that it is possible to overcome limitations of existing hybrid methods via generalizations of existing hybrid methods. We may expect a competition of classical hybrid methods (preferred because of the simplicity of the underlying concept) versus mathematics-based hybrid methods in the future (which are not more difficult to apply). The CES methods described here offer advantages in this regard:

1. From a rather general viewpoint, given the problems of classical hybrid methods presenting a mix of RANS and LES elements, it is reasonable to expect that it requires exactly one equation framework to avoid inconsistencies and implied imbalances.
2. On top of being theory-based, the CES methods discussed here offer advantages through the general applicability of the hybridization concept to many RANS model structures (i.e., the potential systematic improvement of many RANS models, including RSM's).
3. LES, seen as basic tool to uncover the structure of high *Re* flows, suffers from a serious problem: the dependence on an artificial parameter, the filter width Δ (and usually the need for small Δ) [316]. The CES methods described here are not affected by this problem.

The discussion in Sect. 2.1 revealed that the use of physical and mathematical realizability concepts enables substantial practical improvements of simulations (computationally stable RANS and dynamic LES). Correspondingly, the use of additional mathematical realizability constraints described here (with respect to mode variations) will result in additional computational advantages (stable RANS-LES mode variations).

Declaration of competing interest

The authors declare that they have no known competing financial interests or personal relationships that could have appeared to influence the work reported in this paper.

Acknowledgments

The author would like to acknowledge support through NASA's NRA research opportunities in aeronautics program (Grant No. NNX12AJ71A monitored by Dr. P. Balakumar), the National Science Foundation (DMS-CDS&E-MSS, Grant No. 1622488 monitored by Dr. Y. Zeng), and the Hanse-Wissenschaftskolleg (Delmenhorst, Germany, monitor W. Stenzel). I am thankful to Prof. M. Stoellinger, Dr. R. Mokhtarpoor, Dr. H. Gopalan, G. Ahmadi, Dr. B. Stoevesandt, Dr. H. Kassem, and Prof. J. Peinke for common work and helpful discussions. I would like to thank Dr. P. S. Iyer, Dr. M. R. Malik, and Dr. A. Uzun for their support regarding the reproduction of their figures.

Appendix A. LB Methods

LB methods are not based on a Fokker-Planck equation for the velocity PDF but on the Bhatnagar-Gross-Krook (BGK) approximation to the Boltzmann equation [166]: the name Lattice Boltzmann methods reflects the numerical solution of such equations. An interesting and attractive feature of this equation is that the fluctuations involved refer to both molecular and turbulent fluctuations. In particular, the velocity PDF transport equation considered is given by Refs. [78–84,317–319]

$$\frac{\partial f}{\partial t}+\frac{\partial w_k f}{\partial x_k}=-\frac{f-g}{\tau_{BGK}}. \tag{56}$$

Here τ_{BGK} is a reference time scale and g refers to the equilibrium PDF given by an isotropic normal PDF with variance $2k_{BGK}/3$ (k_{BGK} being a reference kinetic energy),

$$g(\mathbf{w},\mathbf{x},t)=\frac{1}{(4\pi k_{BGK}/3)^{3/2}}exp\left\{-\frac{(w_i-\tilde{U}_i)(w_i-\tilde{U}_i)}{4k_{BGK}/3}\right\}. \tag{57}$$

Equation (56) implies $\partial\tilde{U}_i/\partial x_i = 0$. Consistency with the momentum and stress equations implies $\tau_{BGK} = 3(\nu+\nu_t)/[2(e+k)]$ and $k_{BGK} = e+k$ [320]: $\nu = 2\tau_{BGK}e/3$ and $\nu_t = 2\tau_{BGK}k/3$ refer to the kinematic and modeled viscosity, and e and k refer to the molecular and modeled turbulent kinetic energy. Depending on how τ_{BGK} is provided as a function of the modeled viscosity ν_t, LB methods can be applied as RANS, LES, or hybrid RANS-LES methods [78–84,317,318]. These methods are not seen as modeling alternative to the corresponding RANS, LES, and hybrid RANS-LES methods: the expectation is that these methods enable more accurate and more efficient numerical solutions of turbulence equations [79,81,82].

Appendix B. PDF and FDF Definitions

The velocity PDF is defined by $f(\mathbf{w},\mathbf{x},t) = \langle\delta(\mathbf{w}-\mathbf{U}(\mathbf{x},t))\rangle$. Here, $\mathbf{U} = (U_1, U_2, U_3)$ is the instantaneous three-dimensional velocity field, $\mathbf{w} = (w_1, w_2, w_3)$ is the corresponding sample space velocity, $\delta(\mathbf{w}-\mathbf{U})$ is the three-dimensional delta function [133], t it time, and the brackets refer to ensemble averaging. LES methods differ from RANS methods by the consideration of spatial or temporal filtered variables [1,6–9,74,97,321]. Instead of using the RANS PDF we apply (by restricting attention to filtering in space) the FDF $f(\mathbf{w},\ \mathbf{x},\ t) = \langle\delta(\mathbf{w}-\ \mathbf{U}(\mathbf{x},\ t))\rangle_s$, where $\langle\delta(\mathbf{w}-\mathbf{U}(\mathbf{x},t))\rangle_s = \int G(\mathbf{r})\,\delta[\mathbf{w}-\mathbf{U}(\mathbf{x}+\mathbf{r},t)]\,d\mathbf{r}$ [1,97,143]. The filter function G is assumed to be homogeneous, i.e., independent of $\mathbf{x}$. We assume $\int G(\mathbf{r})\,d\mathbf{r} = 1$ and $G(\mathbf{r}) = G(-\mathbf{r})$. Only positive filter functions are considered for which all the moments $\int r^m G(\mathbf{r})\,d\mathbf{r}$ exist for $m \geq 0$ [143]. Thus, G has the properties of a PDF.

Appendix C. LES Length Scale

The problem to explain the modeled LES length scale L is considered over decades. There are several strategies: the search for relationships between L and the filter width Δ (which scales the FDF width), or the search for explaining L as a fraction of an integral length scale, see Refs. [25,42,119,122,215,322–324]. The issue with $L-\Delta$ relationships is that such expressions usually do only apply to small Δ. The issue with the second strategy is that the reasoning for such relations depends on arguable assumptions. Only a few suggestions for solving this problem were presented as being supported by spectral theory [25,119,122]. The recent version of this development reads [122].

$$L_+ = \Delta_{C+} \Big/ \left(1+\Delta_{C+}^p\right)^{1/p}. \tag{58}$$

Here, $L_+ = L/L_{tot}$ and $\Delta_{C+} = C_+\Delta_+$ with $\Delta_+ = \Delta/L_{tot}$. The constant C_+ was determined to be $C_+ = (3C_K/2)^{3/2}/\pi$, where C_k is the Kolmogorov constant (see also the discussion of Girimaji and Abdol-Hamid's suggestion [109] in Ref. [213]). Values $C_k = (1.3, 1.43, 1.5)$, e.g., imply $C_+ = (0.876, 1.0, 1.074)$. In practice, $p=3$ is applied [42]. Justification for $p=3$ was provided in Ref. [213]. Equation (58) explains L as fraction of the integral length scale L_{tot} in dependence on Δ. For sufficiently small Δ_+, Eq. (58) implies $L_+ = \Delta_{C+}$, this means $L = C_+\Delta$. For large Δ_+, L approaches the integral length scale L_{tot}.

A rewriting of Eq. (58) reads $L_+^{-p} = 1+\Delta_{C+}^{-p}$, which is simply an interpolation between the limits of small and large Δ_+ values (Δ_{C+} and unity). Evidence for the suitability of Eq. (58) for inhomogeneous flows can be obtained by the following probabilistic arguments. L_+^2 controls the resolution features of equations [213]. In particular, $0 \le L_+^2 \le 1$ represents a cumulative distribution function (CDF). Its PDF reads $f(t) = dL_+^2/\, d\Delta_{C+} = 2t^{1/p}(1-t)^{1+1/p}$. Here, $0 \le t \le 1$ is defined via $1-t = (1+\Delta_{C+}^p)^{-1}$. This PDF has the structure of a beta PDF in the variable t (the normalized $f(t)/[2B(1+1/p, 2+1/p)]$ is a beta PDF). The use of a beta PDF is a very reasonable choice: a beta PDF is almost exclusively applied under conditions where an analytical PDF has to be specified on the bounded probability space between zero and unity. It is of interest that the beta PDF has theoretical support: it represents a statistically most-likely (SML) PDF on the unit interval. In general, this PDF can be written as $f(t) = exp[-\lambda_0 - \lambda_1 ln(t) - \lambda_2 ln(1-t)]$, where $\lambda_0, \lambda_1, \lambda_2$ are Lagrangian multipliers. The latter PDF maximizes the entropy $E = -\int ln[f(t)]f(t)dt$ subject to the moment conditions $\int_0^1 ln(t)f(t)dt = \mu_1$ and $\int_0^1 ln(1-t)f(t)dt = \mu_2$, where μ_1 and μ_2 are assumed to be given [325]. The maximum entropy reads $E = \lambda_0 + \lambda_1\mu_1 + \lambda_2\mu_2$. A characteristic feature of Eq. (58) is that it does not imply a two-parameter but a one-parameter beta PDF. The latter is implied by the need to cover the limits of small and large Δ_+ values.

References

[1] S.B. Pope, Turbulent Flows, Cambridge University Press, Cambridge, 2000.
[2] P.R. Spalart, Strategies for turbulence modelling and simulations, Int. J. Heat Fluid Flow 21 (3) (2000) 252–263.
[3] D.C. Wilcox, Turbulence Modeling for CFD, second ed., DCW Industries, Canada, 1998.
[4] P.A. Durbin, B.A. Petterson, Statistical Theory and Modeling for Turbulent Flows, John Wiley and Sons, Chichester, New York, Weinheim, Brisbane, Singapore, Toronto, 2001.
[5] K. Hanjalić, Advanced turbulence closure models: a view of current status and future prospects, Int. J. Heat Fluid Flow 15 (3) (1994) 178–203.
[6] P. Sagaut, Large Eddy Simulation for Incompressible Flows: an Introduction, Springer, Berlin, 2002.
[7] M. Lesieur, O. Metais, P. Comte, Large-Eddy Simulations of Turbulence, Cambridge University Press, Cambridge, 2005.
[8] U. Piomelli, Large-eddy simulation: achievements and challenges, Prog. Aerosp. Sci. 35 (4) (1999) 335–362.
[9] C. Meneveau, J. Katz, Scale-invariance and turbulence models for large-eddy simulation, Annu. Rev. Fluid Mech. 32 (1) (2000) 1–32.
[10] S. Heinz, Unified turbulence models for LES and RANS, FDF and PDF simulations, Theor. Comput. Fluid Dyn. 21 (2) (2007) 99–118.
[11] D.A. von Terzi, J. Fröhlich, W. Rodi, Hybrid techniques for large-eddy simulations of complex turbulent flows, in: W.E. Nagel, D.B. Kröner, M.M. Resch (Eds.), High Performance Computing in Science and Engineering '08, Transactions of the High Performance Computing Center Stuttgart (HLRS) 2008, Springer, Berlin, 2009, pp. 317–332.
[12] http://qnet-ercoftac.cfms.org.uk/w/index.php/ufr_ 3-30_ test_ case, 2018.
[13] G.P. Almeida, D.F.G. Durao, M.V. Heitor, Wake flows behind two dimensional model hills, Exp. Therm. Fluid Sci. 7 (1993) 87–101.
[14] C.P. Mellen, J. Fröhlich, W. Rodi, Large-eddy simulation of the flow over periodic hills, in: Proceedings of 16th IMACS World Congress, 2000, pp. 1–6. Lausanne, Switzerland.
[15] L. Temmerman, M.A. Leschziner, Large eddy simulation of separated flow in a streamwise periodic channel constriction, in: Proceedings of 2nd International Symposium of Turbulence and Shear Flow Phenomena, KTH, Stockholm, 2001, pp. 399–404.
[16] L. Temmerman, M.A. Leschziner, C.P. Mellen, J. Fröhlich, Investigation of wall-function approximations and subgrid-scale models in large eddy simulation of separated flow in a channel with streamwise periodic constrictions, Int. J. Heat Fluid Flow 24 (2) (2005) 157–180.
[17] S. Jakirlić, Extended Excerpt Related to the Test Case: "Flow over a Periodical Arrangement of 2D Hills", Technical report, TU Darmstadt, 2012. Final report on "Assessment of the RSM, URANS and hybrid models with respect to the different roadmaps including the industrial application challenges", ACP8-GA-2009-233710-ATAAC.
[18] S. Jakirlić, S. Šarić, G. Kadavelil, E. Sirbubalo, B. Basara, B. Chaouat, SGS modelling in LES of wall-bounded flows using transport RANS models: from a zonal to a seamless hybrid LES/RANS method, in: Proceeding of the 6th Symposium on Turbulent Shear Flow Phenomena, vol. 3, 2009, pp. 1057–1062. Seoul, Korea.
[19] Y.J. Jang, M.A. Leschziner, K. Abe, L. Temmerman, Investigation of anisotropy-resolving turbulence models by reference to highly-resolved LES data for separated flow, Flow, Turbul. Combust. 69 (2) (2002) 161–203.
[20] J. Fröhlich, C.P. Mellen, W. Rodi, L. Temmerman, M.A. Leschziner, Highly resolved large-eddy simulation of separated flow in a channel with streamwise periodic constrictions, J. Fluid Mech. 526 (2005) 19–66.
[21] M. Breuer, N. Peller, C. Rapp, M. Manhart, Flow over periodic hills - numerical and experimental study in a wide range of Reynolds numbers, Comput. Fluids 38 (2) (2009) 433–457.
[22] C. Rapp, M. Manhart, Experimental investigations on the turbulent flow over a periodic hill geometry, in: 5th International Symposium Turbulence and Shear Flow Phenomena, vol. 2, 2007, pp. 649–654. Garching, Germany.
[23] C. Rapp, F. Pfleger, M. Manhart, New experimental results for a LES benchmark case, in: Proceedings of the Seventh International ERCOFTAC Workshop on Direct and Large-Eddy Simulation, 2008, pp. 69–74. Trieste, Italy.
[24] C. Rapp, M. Manhart, Flow over periodic hills – an experimental study, Exp. Fluid 51 (2011) 247–269.
[25] B. Chaouat, R. Schiestel, A new partially integrated transport model for subgrid-scale stresses and dissipation rate for turbulent developing flows, Phys. Fluids 17 (6) (2005), 065106/1–065106/19.
[26] B. Chaouat, Subfilter-scale transport model for hybrid RANS/LES simulations applied to a complex bounded flow, J. Turbul. 11 (51) (2010) 1–30.
[27] B. Chaouat, R. Schiestel, Hybrid RANS-LES simulations of the turbulent flow over periodic hills at high Reynolds number using the PITM method, Comput. Fluids 84 (8) (2013) 279–300.
[28] P. Balakumar, G.I. Park, B. Pierce, DNS, LES and wall-modeled LES of separating flow over periodic hills, in: Center for Turbulence Research Proceedings of the Summer Program 2014, 2014, pp. 407–415.
[29] R. Mokhtarpoor, S. Heinz, M. Stoellinger, Dynamic unified RANS-LES simulations of high Reynolds number separated flows, Phys. Fluids 28 (9) (2016), 095101/1–095101/36.
[30] R. Mokhtarpoor, S. Heinz, Dynamic large eddy simulation: stability via realizability, Phys. Fluids 29 (10) (2017) 105104/1–105104/22.
[31] H. Choi, P. Moin, Grid-point requirements for large eddy simulation: chapman's estimates revisited, Phys. Fluids 24 (1) (2012), 011702/1–011702/5.
[32] J. Larsson, S. Kawai, J. Bodart, I. Bermejo-Moreno, Large eddy simulation with modeled wall-stress: recent progress and future directions, Mech. Eng. Rev. 3 (1) (2016), 15–00418/1-15–00418/23.
[33] S.T. Bose, G.I. Park, Wall-modeled large-eddy simulation for complex turbulent flows, Annu. Rev. Fluid Mech. 50 (2018), 535–61.
[34] P.R. Spalart, V. Venkatakrishnan, On the role and challenges of CFD in the aerospace industry, Aeronaut. J. 120 (1223) (2016) 209–232.

[35] J. Slotnick, A. Khodadoust, J. Alonso, D. Darmofal, W. Gropp, E. Lurie, D. Mavriplis, CFD vision 2030 study: a path to revolutionary computational aerosciences, NASA/CR-2014-218178, https://ntrs.nasa.gov/search.jsp?R= 20140003093, 2014.

[36] Future CFD Technologies Workshop, Bridging Mathematics and Computer Science for Advanced Aerospace Simulation Tools. Kissimmee, FL, USA, Jan. 6-7, 2018, 2018. https://scientific-sims.com/cfdlab/WORKSHOP/workshop.html.

[37] C.L. Rumsey, J.P. Slotnick, A.J. Sclafani, Overview and summary of the third AIAA high lift prediction workshop, in: 2018 AIAA Aerospace Sciences Meeting, AIAA SciTech Forum, AIAA Paper 18-1258, 2018, pp. 1–33. Kissimmee, FL.

[38] C.G. Speziale, Turbulence modeling for time-dependent RANS and VLES: a review, AIAA J. 36 (2) (1998) 173–184.

[39] M. Germano, Properties of the hybrid RANS/LES filter, Theor. Comput. Fluid Dyn. 17 (4) (2004) 225–231.

[40] K. Hanjalić, Will RANS survive LES?: a view of perspectives, ASME J. Fluids Eng. 127 (5) (2005) 831–839.

[41] J. Fröhlich, D.V. Terzi, Hybrid LES/RANS methods for the simulation of turbulent flows, Prog. Aerosp. Sci. 44 (5) (2008) 349–377.

[42] B. Chaouat, The state of the art of hybrid RANS/LES modeling for the simulation of turbulent flows, Flow, Turbul. Combust. 99 (2) (2017) 279–327.

[43] C. Mockett, M. Fuchs, F. Thiele, Progress in DES for wall-modelled LES of complex internal flows, Comput. Fluids 65 (7) (2012) 44–55.

[44] N.V. Nikitin, F. Nicoud, B. Wasistho, K.D. Squires, P.R. Spalart, An approach to wall modeling in large-eddy simulations, Phys. Fluids 12 (7) (2000) 1629–1632.

[45] J.G. Brasseur, T. Wei, Designing large-eddy simulation of the turbulent boundary layer to capture law-of-the-wall scaling, Phys. Fluids 22 (2) (2010), 021303/1–021303/22.

[46] P. Wu, J. Meyer, A constraint for the subgrid-scale stresses in the logarithmic region of high Reynolds number turbulent boundary layers: a solution to the log-layer mismatch problem, Phys. Fluids 25 (1) (2013), 015104/1– 015104/17.

[47] T. Chatterjee, Y.T. Peet, Effect of artificial length scales in large eddy simulation of a neutral atmospheric boundary layer flow: a simple solution to log-layer mismatch, Phys. Fluids 29 (7) (2017), 075105/1–075105/21.

[48] X.I.A. Yang, G.I. Park, P. Moin, Log-layer mismatch and modeling of the fluctuating wall stress in wall-modeled large-eddy simulations, Phys. Rev. Fluids 2 (2017) 104601/1–104601/13.

[49] P.R. Spalart, W.H. Jou, M. Strelets, S.R. Allmaras, Comments on the feasibility of LES for wings, and on a hybrid RANS/LES approach, in: C. Liu, Z. Liu (Eds.), Advances in DNS/LES, Greyden Press, Columbus, 1997, pp. 137–147.

[50] A. Travin, M.L. Shur, M. Strelets, P. Spalart, Detached-eddy simulations past a circular cylinder, Flow, Turbul. Combust. 63 (1–4) (1999) 113–138.

[51] M. Strelets, Detached eddy simulation of massively separated flows, in: 39th AIAA Aerospace Sciences Meeting and Exhibit, AIAA Paper 01-0879, 2001, pp. 1–18. Reno, NV.

[52] A. Travin, M.L. Shur, Physical and numerical upgrades in the detached-eddy simulation of complex turbulent flows, in: R. Friedrich, W. Rodi (Eds.), Advances in LES of Complex Flows, Kluwer Academic Publishers, 2002, pp. 239–254.

[53] F.R. Menter, M. Kuntz, R. Langtry, Ten years of industrial experience with SST turbulence model, Turb. Heat Mass Transf. 4 (6) (2003) 625–632.

[54] P.R. Spalart, S. Deck, M.L. Shur, K.D. Squires, M.K. Strelets, A. Travin, A new version of detached-eddy simulation, resistant to ambiguous grid densities, Theor. Comput. Fluid Dyn. 20 (3) (2006) 181–195.

[55] M.L. Shur, P.R. Spalart, M.K. Strelets, A. Travin, A hybrid RANS-LES approach with delayed-DES and wall-modelled LES capabilities, Int. J. Heat Fluid Flow 29 (6) (2008) 1638–1649.

[56] P.R. Spalart, Detached-eddy simulation, Annu. Rev. Fluid Mech. 41 (2009) 181–202.

[57] U. Piomelli, E. Balaras, H. Pasinato, K.D. Squires, P. Spalart, The inner-outer layer interface in large-eddy simulations with wall-layer models, Int. J. Heat Fluid Flow 24 (4) (2003) 538–550.

[58] L. Davidson, Hybrid LES-RANS: an approach to make LES applicable at high Reynolds numbers, Int. J. Comput. Fluid Dyn. 19 (6) (2005) 415–427.

[59] L. Davidson, Hybrid LES-RANS: back scatter from a scale-similarity model used as forcing, Phil. Trans. R. Soc. A 367 (2009) 2905–2915.

[60] H. Xiao, P. Jenny, A consistent dual-mesh framework for hybrid LES/RANS modeling, J. Comput. Phys. 231 (4) (2012) 1848–1865.

[61] H. Xiao, Y. Sakai, R. Henniger, M. Wild, P. Jenny, Coupling of solvers with non-conforming computational domains in a dual-mesh hybrid LES/RANS framework, Comput. Fluids 88 (12) (2013) 653–662.

[62] H. Xiao, J.X. Wang, P. Jenny, Dynamic evaluation of mesh resolution and its application in hybrid LES/RANS methods, Flow, Turbul. Combust. 93 (1) (2014) 141–170.

[63] H. Xiao, J.X. Wang, P. Jenny, An implicitly consistent formulation of a dual-mesh hybrid LES/RANS method, Commun. Comput. Phys. 21 (2) (2017) 570–599.

[64] J.W. Deardorff, A numerical study of three-dimensional turbulent channel flow at large Reynolds numbers, J. Fluid Mech. 41 (1970) 453–480.

[65] U. Schumann, Subgrid scale model for finite difference simulations of turbulent flows in plane channels and annuli, J. Comput. Phys. 18 (4) (1975) 376–404.

[66] G. Grötzbach, Direct numerical and large eddy simulation of turbulent channel flow, in: Encyclopedia of Fluid Mechanics, 1987, pp. 1337–1391. Houston: Gulf.

[67] U. Piomelli, J. Ferziger, P. Moin, New approximate boundary conditions for large eddy simulations of wall-bounded flows, Phys. Fluids 6 (1) (1989) 1061–1068.

[68] W. Cabot, P. Moin, Approximate wall boundary conditions in the large-eddy simulation of high Reynolds number flow, Flow, Turbul. Combust. 63 (1–4) (1999) 269–291.

[69] U. Piomelli, E. Balaras, Wall-layer models for large-eddy simulations, Annu. Rev. Fluid Mech. 34 (2002) 349–374.

[70] U. Piomelli, Wall-layer models for large-eddy simulations, Prog. Aerosp. Sci. 44 (2008) 437–446.

[71] S. Kawai, J. Larsson, Wall-modeling in large eddy simulation: length scales, grid resolution, and accuracy, Phys. Fluids 24 (1) (2012), 015105/1–015105/10.

[72] S.T. Bose, P. Moin, A dynamic slip boundary condition for wall-modeled large-eddy simulation, Phys. Fluids 26 (1) (2014), 015104/1–015104/18.

[73] G.I. Park, P. Moin, An improved dynamic non-equilibrium wall-model for large eddy simulation, Phys. Fluids 26 (1) (2014), 015108/1–015108/21.

[74] U. Piomelli, Large eddy simulations in 2030 and beyond, Phil. Trans. R. Soc. A 372 (2022) (2014), 20130320/1–20130320/23.

[75] P. Moin, J. Bodart, S. Bose, G.I. Park, Wall-modeling in complex turbulent flows, in: M. Braza, A. Bottaro, M. Thompson (Eds.), Advances in Fluid-Structure Interaction, Notes on Numerical Fluid Mechanics and Multidisciplinary Design 133, Springer International Publishing Switzerland, 2016, pp. 207–219.

[76] X.I.A. Yang, J. Sadique, R. Mittal, C. Meneveau, Integral wall model for large eddy simulations of wall-bounded turbulent flows, Phys. Fluids 27 (2) (2015), 025112/1–025112/32.

[77] C. Friess, R. Manceau, T.B. Gatski, Toward an equivalence criterion for hybrid RANS/LES methods, Comput. Fluids 122 (11) (2015) 233–246.

[78] Z. Guo, C. Shu, Lattice Boltzmann Method and its Applications in Engineering, Volume 3 of Advances in Computational Fluid Dynamics, World Scientific Publishing Co. Pte. Ltd., New Jersey, Londond, Singapre, Beijing, Shanghai, Hong Kong, Taipei, Chennai, 2004.

[79] P. Sagaut, Toward advanced subgrid models for Lattice-Boltzmann-based large-eddy simulation: theoretical formulations, Comput. Math. Appl. 59 (7) (2010) 2194–2199.

[80] L. Jahanshaloo, E. Pouryazdanpanah, N.A.C. Sidik, A review on the application of the lattice Boltzmann method for turbulent flow simulation, Num. Heat Tr. A-Appl 64 (11) (2013) 938–953.

[81] M. Righi, A modified gas-kinetic scheme for turbulent flow, Commun. Comput. Phys. 16 (1) (2014) 239–263.

[82] M. Righi, A gas-kinetic scheme for turbulent flow, Flow, Turbul. Combust. 97 (1) (2016) 121–139.

[83] J. Li, C. Zhong, D. Pan, C. Zhuo, A gas-kinetic scheme coupled with SST model for turbulent flows, Comput. Math. Appl. 78 (4) (2019) 1227–1242.

[84] H. Sajjadi, M. Salmanzadeh, G. Ahmadi, S. Jafari, Turbulent indoor airflow simulation using hybrid LES/RANS model utilizing Lattice Boltzmann method, Comput. Fluids 150 (6) (2017) 66–73.

[85] S. Chen, Z. Xia, S. Pei, J. Wang, Y. Yang, Z. Xiao, Y. Shi, Reynolds-stress-constrained large-eddy simulation of wall-bounded turbulent flows, J. Fluid Mech. 703 (2012) 1–28.

[86] S. Chen, Y. Chen, Z. Xia, K. Qu, Y. Shi, Z. Xiao, Q. Liu, Q. Cai, F. Liu, C. Lee, R. Zhang, J. Cai, Constrained large-eddy simulation and detached eddy simulation of flow past a commercial aircraft at 14 degrees angle of attack, Sci. China Phys. Mech. Astron. 56 (2) (2013) 270–276.

[87] Z. Xia, Y. Shi, R. Hong, Z. Xiao, S. Chen, Constrained large-eddy simulation of separated flow in a channel with streamwise-periodic constrictions, J. Turbul. 14 (1) (2013) 1–21.

[88] Z. Jiang, Z. Xiao, Y. Shi, S. Chen, Constrained large-eddy simulation of wall-bounded compressible turbulent flows, Phys. Fluids 25 (10) (2013), 106102/1–106102/28.

[89] R. Hong, Z. Xia, Y. Shi, Z. Xiao, S. Chen, Constrained large-eddy simulation of compressible flow past a circular cylinder, Commun. Comput. Phys. 15 (2) (2014) 388–421.

[90] Y. Zhao, Z. Xia, Y. Shi, Z. Xiao, S. Chen, Constrained large-eddy simulation of laminar-turbulent transition in channel flow, Phys. Fluids 26 (9) (2014), 095103/1–095103/14.

[91] Q. Xua, Y. Yang, Reynolds stress constrained large eddy simulation of separation flows in a U-duct, J. Propul. Power Res. 3 (2) (2014) 49–58.

[92] Z. Xia, Z. Xiao, Y. Shi, S. Chen, Constrained large-eddy simulation for aerodynamics, in: S. Girimaji, W. Haase, S.-H. Peng, D. Schwamborn (Eds.), Progress in Hybrid RANS-LES Modelling, Notes on Numerical Fluid Mechanics and Multidisciplinary Design 130, Springer International Publishing Switzerland, 2015, pp. 239–254.

[93] Z. Jiang, Z. Xiao, Y. Shi, S. Chen, Constrained large-eddy simulation of turbulent flow and heat transfer in a stationary ribbed duct, Int. J. Numer. Method. H. 26 (3–4) (2016) 1069–1091.

[94] A. Verma, N. Park, K. Mahesh, A hybrid subgrid-scale model constrained by Reynolds stress, Phys. Fluids 25 (11) (2013), 110805/1–110805/20.

[95] Z. Xiao, Y. Shi, Z. Xia, S. Chen, Comment on 'A hybrid subgrid-scale model constrained by Reynolds stress' [Phys. Fluids 25, 110805 (2013)], Phys. Fluids 26 (5) (2014), 059101/1–059101/3.

[96] A. Verma, N. Park, K. Mahesh, Response to 'Comment on 'A hybrid subgrid-scale model constrained by Reynolds stress [Phys. Fluids 26, 059101 (2014)], Phys. Fluids 26 (5) (2014), 059102/1–059102/1.

[97] S. Heinz, Statistical Mechanics of Turbulent Flows, Springer, Berlin, 2003.

[98] S. Heinz, On Fokker–Planck equations for turbulent reacting flows. Part 1. Probability density function for Reynolds-averaged Navier–Stokes equations, Flow, Turbul. Combust. 70 (1) (2003) 115–152.

[99] S. Heinz, On Fokker–Planck equations for turbulent reacting flows. Part 2. Filter density function for large eddy simulation, Flow, Turbul. Combust. 70 (1) (2003) 153–181.

[100] S. Heinz, Realizability of dynamic subgrid-scale stress models via stochastic analysis, Monte Carlo Methods Applic 14 (4) (2008) 311–329.

[101] S. Heinz, H. Gopalan, Realizable versus non-realizable dynamic subgrid-scale stress models, Phys. Fluids 24 (11) (2012), 115105/1–115105/23.
[102] H. Gopalan, S. Heinz, M. Stöllinger, A unified RANS-LES model: computational development, accuracy and cost, J. Comput. Phys. 249 (2013) 249–279.
[103] S. Heinz, M. Stöllinger, H. Gopalan, Unified RANS-LES simulations of turbulent swirling jets and channel flows, in: Progress in Hybrid RANS-LES Modelling (Notes on Numerical Fluid Mechanics and Multidisciplinary Design 130, Springer, Cham, 2015, pp. 265–275.
[104] E. Kazemi, S. Heinz, Dynamic large eddy simulations of the Ekman layer based on stochastic analysis, Int. J. Nonlinear Sci. Numer. Stimul. 17 (2) (2016) 77–98.
[105] M. Stöllinger, S. Heinz, C. Zemtsop, H. Gopalan, R. Mokhtarpoor, Stochastic-based RANS-LES simulations of swirling turbulent jet flows, Int. J. Nonlinear Sci. Numer. Stimul. 18 (5) (2017) 351–369.
[106] R. Mokhtarpoor, S. Heinz, M. Stöllinger, Realizable dynamic large eddy simulation, in: Direct and Large-Eddy Simulation XI (ERCOFTAC Series), Springer, Cham, 2019, pp. 119–126.
[107] R. Mokhtarpoor, S. Heinz, M. Stöllinger, Dynamic unified RANS-LES simulations of periodic hill flow, in: Direct and Large-Eddy Simulation XI (ERCOFTAC Series), Springer, Cham, 2019, pp. 489–496.
[108] S.S. Girimaji, R. Srinivasan, E. Jeong, PANS turbulence for seamless transition between RANS and LES: fixed-point analysis and preliminary results, in: Proc. ASME FEDSM03, ASME Paper FEDSM2003-45336, Honolulu, Hawaii, 2003, pp. 1–9.
[109] S.S. Girimaji, K. Abdol-Hamid, Partially averaged Navier Stokes model for turbulence: implemantation and validation, in: 43rd AIAA Aerospace Sciences Meeting and Exhibit, AIAA Paper 05-0502, Reno, NV, 2005, pp. 1–14.
[110] S.S. Girimaji, Partially-averaged Navier-Stokes method for turbulence: a Reynolds-averaged Navier-Stokes to direct numerical simulation bridging method, ASME J. Appl. Mech. 73 (3) (2006) 413–421.
[111] S.S. Girimaji, E. Jeong, R. Srinivasan, Partially averaged Navier-Stokes method for turbulence: fixed point analysis and comparisons with unsteady partially averaged Navier-Stokes, ASME J. Appl. Mech. 73 (3) (2006) 422–429.
[112] S. Lakshmipathy, S.S. Girimaji, Extension of Boussinesq turbulence constitutive relation for bridging methods, J. Turbul. 8 (31) (2007) 1–20.
[113] A. Frendi, A. Tosh, S. Girimaji, Flow past a backward-facing step: comparison of PANS, DES and URANS results with experiments, Int. J. Comput. Methods Eng. Sci. Mech. 8 (1) (2007) 23–38.
[114] S. Lakshmipathy, S.S. Girimaji, Partially averaged Navier-Stokes (PANS) method for turbulence simulations: flow past a circular cylinder, ASME J. Fluids Eng. 132 (12) (2010) 121202/1–121202/9.
[115] E. Jeong, S.S. Girimaji, Partially averaged Navier–Stokes (PANS) method for turbulence simulations: flow past a square cylinder, ASME J. Fluids Eng. 132 (12) (2010), 121203/1–121203/11.
[116] B. Basara, S. Krajnovic, S.S. Girimaji, Z. Pavlovic, Near-wall formulation of the partially averaged Navier-Stokes turbulence model, AIAA J. 42 (12) (2011) 2627–2636.
[117] S. Krajnovic, R. Lárusson, B. Basara, Superiority of PANS compared to LES in predicting a rudimentary landing gear flow with affordable meshes, Int. J. Heat Fluid Flow 37 (10) (2012) 109–122.
[118] H. Foroutan, S. Yavuzkurt, A partially averaged Navier Stokes model for the simulation of turbulent swirling flow with vortex breakdown, Int. J. Heat Fluid Flow 50 (12) (2014) 402–416.
[119] R. Schiestel, A. Dejoan, Towards a new partially integrated transport model for coarse grid and unsteady turbulent flow simulations, Theor. Comput. Fluid Dyn. 18 (6) (2005) 443–468.
[120] B. Chaouat, R. Schiestel, From single-scale turbulence models to multiple-scale and subgrid-scale models by Fourier transform, Theor. Comput. Fluid Dyn. 21 (3) (2007) 201–229.
[121] I. Befeno, R. Schiestel, Non-equilibrium mixing of turbulence scales using a continuous hybrid RANS/LES approach: application to the shearless mixing layer, Flow, Turbul. Combust. 78 (2) (2007) 129–151.
[122] B. Chaouat, R. Schiestel, Progress in subgrid-scale transport modelling for continuous hybrid nonzonal RANS/LES simulations, Int. J. Heat Fluid Flow 30 (4) (2009) 602–616.
[123] B. Chaouat, Simulation of turbulent rotating flows using a subfilter scale stress model derived from the partially integrated transport modeling method, Phys. Fluids 24 (4) (2012), 045108/1–045108/35.
[124] B. Chaouat, R. Schiestel, Analytical insights into the partially integrated transport modeling method for hybrid Reynolds averaged Navier-Stokes equations-large eddy simulations of turbulent flows, Phys. Fluids 24 (8) (2012), 085106/1–085106/34.
[125] B. Chaouat, R. Schiestel, Partially integrated transport modeling method for turbulence simulation with variable filters, Phys. Fluids 25 (12) (2013), 125102/1–125102/39.
[126] B. Chaouat, Application of the PITM method using inlet synthetic turbulence generation for the simulation of the turbulent flow in a small axisymmetric contraction, Flow, Turbul. Combust. 98 (4) (2017) 987–1024.
[127] F.R. Menter, M. Kuntz, R. Bender, A scale-adaptive simulation model for turbulent flow predictions, in: 41st AIAA Aerospace Sciences Meeting and Exhibit, AIAA Paper 03-0767, Reno, NV, 2003, pp. 1–12.
[128] F.R. Menter, Y. Egorov, A scale-adaptive simulation model using two-equation models, in: 43rd AIAA Aerospace Sciences Meeting and Exhibit, AIAA Paper 05-1095, Reno, NV, 2005, pp. 1–13.
[129] F.R. Menter, Y. Egorov, Revisiting the turbulent scale equation, in: G.E.A. Meier, K.R. Sreenivasan (Eds.), IUTAM Symposium on One Hundred Years of Boundary Layer Research, Springer, Netherlands, 2006, pp. 279–290.
[130] F.R. Menter, Y. Egorov, The scale-adaptive simulation method for unsteady turbulent flow prediction: Part 1: theory and model description, Flow, Turbul. Combust. 78 (1) (2010) 113–138.
[131] F.R. Menter, Y. Egorov, The scale-adaptive simulation method for unsteady turbulent flow prediction: Part 2: application to complex flows, Flow, Turbul. Combust. 78 (1) (2010) 139–165.
[132] S. Jakirlić, R. Maduta, Extending the bounds of "steady" RANS closures: toward an instability-sensitive Reynolds stress model, Int. J. Heat Fluid Flow 51 (2) (2015) 175–194.
[133] S. Heinz, Mathematical Modeling, Springer, Heidelberg, 2011.
[134] U. Schumann, Realizability of Reynolds stress turbulence models, Phys. Fluids 20 (5) (1977) 721–725.
[135] R. Du Vachat, Realizability inequalities in turbulent flows, Phys. Fluids 20 (4) (1977) 551–556.
[136] J.L. Lumley, Computational modelling of turbulent flows, Adv. Appl. Mech. 18 (1978) 126–176.
[137] S.B. Pope, PDF methods for turbulent reactive flows, Prog. Energy Combust. Sci. 11 (2) (1985) 119–192.
[138] S.B. Pope, On the relationship between stochastic Lagrangian models of turbulence and second-moment closures, Phys. Fluids 6 (2) (1994) 973–985.
[139] C.G. Speziale, R. Abid, P.A. Durbin, New results on the realizability of Reynolds stress turbulence closures, ICASE Report 93–76 (1993) 1–47.
[140] P.A. Durbin, C.G. Speziale, Realizability of second-moment closure via stochastic analysis, J. Fluid Mech. 280 (1994) 395–407.
[141] C.G. Speziale, R.M.C. So, Turbulence modeling and simulation, in: R.W. Johnson (Ed.), Handbook of Fluid Dynamics, CRC Press, Taylor & Francis Group, Boca Raton, FL, 2016, pp. 12/1–12/73.
[142] L.Y.M. Gicquel, P. Givi, F.A. Jaberi, S.B. Pope, Velocity filtered density function for large eddy simulation of turbulent flows, Phys. Fluids 14 (3) (2002) 1196–1213.
[143] P. Givi, Filtered density function for subgrid scale modeling of turbulent combustion, AIAA J. 44 (1) (2006) 16–23.
[144] H. Pitsch, Large eddy simulation of turbulent combustion, Annu. Rev. Fluid Mech. 38 (2006) 453–482.
[145] V. Raman, H. Pitsch, R.O. Fox, Hybrid large eddy simulation/Lagrangian filtered-density-function approach for simulating turbulent combustion, Combust. Flame 143 (1–2) (2005) 56–78.
[146] M.R.H. Sheikhi, T.G. Drozda, P. Givi, F.A. Jaberi, S.B. Pope, Large eddy simulation of a turbulent nonpremixed piloted methane jet flame (Sandia Flame D), Proc. Combust. Inst. 30 (2005) 549–556.
[147] M.R.H. Sheikhi, T.G. Drozda, P. Givi, S.B. Pope, Velocity-scalar filtered density function for large eddy simulation of turbulent flows, Phys. Fluids 15 (8) (2003) 2321–2337.
[148] S.S. Girimaji, A new perspective on realizability of turbulence models, J. Fluid Mech. 512 (2004) 191–210.
[149] H.A. Wouters, T.W.J. Peeters, D. Roekaerts, On the existence of a generalized Langevin model representation for second-moment closures, Phys. Fluids 8 (7) (1996) 1702–1704.
[150] C. Fureby, G. Tabor, Mathematical and physical constraints on large-eddy simulations, Theor. Comput. Fluid Dyn. 9 (2) (1997) 85–102.
[151] S. Ghosal, Mathematical and physical constraints on large-eddy simulation of turbulence, AIAA J. 37 (4) (1999) 425–433.
[152] B. Vreman, B. Geurts, H. Kuerten, Realizability conditions for the turbulent stress tensor in large-eddy simulation, J. Fluid Mech. 278 (1994) 351–362.
[153] A.V. Johansson, M. Hallback, Modelling of rapid pressure-strain in Reynolds stress closures, J. Fluid Mech. 269 (1994) 143–168.
[154] B. Merci, C. De Langhe, J. Vierendeels, A quasi-realizable cubic low-Reynolds eddy-viscosity turbulence model with a new dissipation rate equation, Flow, Turbul. Combust. 66 (2) (2001) 133–157.
[155] J.R. Ristorcelli, J.L. Lumley, R. Abid, A rapid-pressure covariance representation consistent with the Taylor-Proudman theorem materially frame indifferent in the two-dimensional limit, J. Fluid Mech. 292 (1995) 111–152.
[156] T. Sjögren, A.V. Johansson, Development and calibration of algebraic nonlinear models for terms in the Reynolds stress transport equations, Phys. Fluids 12 (6) (2000) 1554–1572.
[157] M. Germano, U. Piomelli, P. Moin, W.H. Cabot, A dynamic subgrid-scale eddy viscosity model, Phys. Fluids 3 (7) (1991) 1760–1765.
[158] D.K. Lilly, A proposed modification of the Germano subgrid-scale closure method, Phys. Fluids 4 (3) (1992) 633–635.
[159] C. Meneveau, T.S. Lund, W.H. Cabot, A Lagrangian dynamic subgrid-scale model for turbulence, J. Fluid Mech. 319 (1996) 353–385.
[160] P.A. Davidson, Turbulence: an Introduction for Scientists and Engineers, Oxford University Press, Oxford, 2004.
[161] C. Bailly, G. Comte-Bellot, Turbulence, Springer, Cham, 2015.
[162] S. Heinz, On mean flow universality of turbulent wall flows. I. High Reynolds number flow analysis, J. Turbul. 19 (11–12) (2018) 929–958.
[163] S. Heinz, On mean flow universality of turbulent wall flows. II. Asymptotic flow analysis, J. Turbul. 20 (2) (2019) 174–193.
[164] J. Bredberg, S.H. Peng, L. Davidson, An improved k-ω turbulence model applied to recirculating flows, Int. J. Heat Fluid Flow 23 (6) (2002) 731–743.
[165] P. Asinari, M. Fasano, E. Chiavazzo, A kinetic perspective on k-ε turbulence model and corresponding entropy production, *Entropy* 18 (4) (2016), 121/1–121/14.
[166] P.L. Bhatnagar, E.P. Gross, M. Krook, A model for collision processes in gases. I. Small amplitude processes in charged and neutral one-component systems, Phys. Rev. 94 (3) (1954) 511–525.

[167] M. Klein, M. Germano, Decomposition of the Reynolds stress from filtered data, Phys. Rev. Fluids 3 (11) (2018) 114606/1–114606/13.
[168] S. Corrsin, Interpretation of viscous terms in the turbulent energy equation, J. Aeronaut. Sci. 30 (12) (1953) 853–854.
[169] A.A. Townsend, The Structure of Turbulent Shear Flow, first ed., Cambridge University Press, Cambridge, UK, 1956.
[170] J.O. Hinze, Turbulence, second ed., McGraw-Hill, New York, NY, 1975.
[171] P. Bradshaw, J.B. Perot, A note on turbulent energy dissipation in the viscous wall region, Phys. Fluids A5 (12) (1993) 3305–3306.
[172] P. Bradshaw, Addendum to "A note on turbulent energy dissipation in the viscous wall region" [Phys. Fluids A 5, 3305 (1993)], Phys. Fluids 7 (9) (1995), 2297–2297.
[173] S. Arunajatesan, N. Sinha, Unsteady RANS-LES simulations of cavity flowfields, in: 39th Aerospace Sciences Meeting and Exhibit, AIAA Paper 01-0516, Reno, NV, 2001, pp. 1–15.
[174] P. Batten, U. Goldberg, S. Chakravarthy, LNS-An approach towards embedded LES, in: 40th AIAA Aerospace Sciences Meeting & Exhibit, AIAA Paper 02-0427, Reno, NV, 2002, pp. 1–11.
[175] C. Kannepalli, J. Chenoweth, S. Arunajatesan, A. Hosangadi, A hybrid RANS/LES approach to modeling of swirling jet flows, in: 38th Fluid Dynamics Conference and Exhibit, AIAA Paper 08-3853, Seattle, WA, 2008, pp. 1–14.
[176] A. Gross, H. Fasel, Hybrid RANS/LES simulations of turbulent channel flow, in: 47th AIAA Aerospace Sciences Meeting Including the New Horizons Forum and Aerospace Exposition, AIAA Paper 09-1327, Orlando, FL, 2009, pp. 1–30.
[177] A. Gross, H. Fasel, Hybrid RANS/LES simulations of turbulent channel and diffuser flows, in: 48th AIAA Aerospace Sciences Meeting Including the New Horizons Forum and Aerospace Exposition, AIAA Paper 09-0919, Orlando, FL, 2010, pp. 1–19.
[178] T. Mukha, Modelling Techniques for Large-Eddy Simulation of Wall-Bounded Turbulent Flows, PhD Thesis, Uppsala University, 2018.
[179] T. Mukha, M. Johansson, M. Liefvendahl, Effect of wall-stress model and mesh-cell topology on the predictive accuracy of LES of turbulent boundary layer flows, in: R. Owen, R. de Borst, J. Reese, C. Pearce (Eds.), Proceedings of the 7th European Conference on Computational Fluid Dynamics (ECFD 7), International Center for Numerical Methods in Engineering (CIMNE) Barcelona, Spain, 2018, pp. 323–333. Glasgow, UK.
[180] S. Rezaeiravesh, T. Mukha, M. Liefvendahl, A-priori study of wall-modeling in large eddy simulation, in: R. Owen, R. de Borst, J. Reese, C. Pearce (Eds.), Proceedings of the 7th European Conference on Computational Fluid Dynamics (ECFD 7), International Center for Numerical Methods in Engineering (CIMNE) Barcelona, Glasgow, Uk, 2018, pp. 290–301. Spain.
[181] S. Rezaeiravesh, T. Mukha, M. Liefvendahl, Systematic study of accuracy of wall-modeled large eddy simulation using uncertainty quantification techniques, Comput. Fluids 185 (5) (2019) 34–58.
[182] J. Mirocha, G. Kirkil, E. Bou-Zeid, F.K. Chow, B. Kosović, Transition and equilibration of neutral atmospheric boundary layer flow in one-way nested large-eddy simulations using the weather research and forecasting model, Mon. Weather Rev. 141 (3) (2013) 918–940.
[183] T.-H. Shih, Generalized wall functions for complex turbulent flows, J. Turbul. 4 (2003), 15/37–15/41.
[184] C. Fureby, Large eddy simulation of ship hydrodynamics, in: Proceedings of the 27th Symposium on Naval Hydrodynamics, vols. 5–10, Seoul National University, Seoul, Korea, 2008.
[185] C. Duprat, G. Balarac, O. Métais, P.M. Congedo, O. Brugière, A wall-layer model for large-eddy simulations of turbulent flows with/out pressure gradient, Phys. Fluids 23 (1) (2011), 015101/1–015101/12.
[186] M. Germano, From RANS to DNS: toward a bridging model, in: P.R. Voke, N. D. Sandham, L. Kleiser (Eds.), Direct and Large-Eddy Simulation III, Springer, Dordrecht, 1999, pp. 225–236.
[187] P. Sagaut, M. Germano, On the filtering paradigm for LES of flows with discontinuities, J. Turbul. 6 (23) (2005) 1–9.
[188] B. Rajamani, J. Kim, A hybrid-filter approach to turbulence simulation, Flow, Turbul. Combust. 85 (3–4) (2010) 1–21.
[189] M. Sánchez-Rocha, S. Menon, The compressible hybrid RANS/LES formulation using an additive operator, J. Comput. Phys. 228 (6) (2009) 2037–2062.
[190] M. Sánchez-Rocha, S. Menon, An order-of-magnitude approximation for the hybrid terms in the compressible hybrid RANS/LES governing equations, J. Turbul. 12 (16) (2011) 1–22.
[191] S. Woodruff, A new formulation for hybrid LES-RANS computations, in: *21st* AIAA Computational Fluid Dynamics Conference, AIAA Paper 13-2722, San Diego, CA, 2013, pp. 1–19.
[192] S. Woodruff, Model-invariant hybrid LES-RANS computation of separated flow past periodic hills, in: Progress in Hybrid RANS-LES Modelling (Notes on Numerical Fluid Mechanics and Multidisciplinary Design 130, Springer, Cham, 2015, pp. 345–355.
[193] S. Woodruff, Model-invariant hybrid computations of separated flows for RCA standard test cases, in: 2016 AIAA SciTech Forum, AIAA Paper 16-1559, San Diego, CA, 2016, pp. 1–19.
[194] S. Ravindran, S. Woodruff, Model-invariant hybrid RANS-LES computations on unstructured meshes, in: 2018 Fluid Dynamics Conference, AIAA Paper 18-3408, Atlanta, GA, 2018, pp. 1–16.
[195] S. Woodruff, Adaptive embedded LES of the NASA hump, in: 2019 AIAA SciTech Forum, AIAA Paper 19-1649, San Diego, CA, 2019, pp. 1–23.
[196] Z. Yin, K.R. Reddy, P.A. Durbin, On the dynamic computation of the model constant in delayed detached eddy simulation, Phys. Fluids 27 (2) (2015), 025105/1–025105/15.
[197] C. De Langhe, B. Merci, E. Dick, Hybrid RANS/LES modelling with an approximate renormalization group. I: model development, J. Turbul. 6 (13) (2005) 1–18.
[198] C. De Langhe, B. Merci, K. Lodefier, E. Dick, Hybrid RANS/LES modelling with an approximate renormalization group. II: Applications, J. Turbul. 6 (14) (2005) 1–16.
[199] C. De Langhe, B. Merci, E. Dick, Application of a RG hybrid RANS/LES model to swirling confined turbulent jets, J. Turbul. 7 (56) (2006) 1–19.
[200] C. De Langhe, J. Bigda, K. Lodefier, E. Dick, One-equation RG hybrid RANS/LES computation of a turbulent impinging jet, J. Turbul. 9 (16) (2008) 1–19.
[201] R. Bush, M. Mani, A two-equation large eddy stress model for high sub-grid shear, in: 15th AIAA Computational Fluid Dynamics Conference, AIAA Paper 01-2561, Anaheim, CA, 2001, pp. 1–11.
[202] S. Bhushan, D.K. Walters, A dynamic hybrid Reynolds-averaged Navier Stokes–Large eddy simulation modeling framework, Phys. Fluids 24 (1) (2012), 015103/1–015103/7.
[203] D.K. Walters, S. Bhushan, M.F. Alam, D.S. Thompson, Investigation of a dynamic hybrid RANS/LES modelling methodology for finite-volume CFD simulations, Flow, Turbul. Combust. 91 (3) (2013) 643–667.
[204] S. Kenjereš, K. Hanjalić, LES, T-RANS and hybrid simulations of thermal convection at high Ra numbers, Int. J. Heat Fluid Flow 27 (5) (2006) 800–810.
[205] J.C. Rotta, Turbulente Strömumgen, BG Teubner, Stuttgart, 1972.
[206] J.C. Rotta, Über eine Methode zur Berechnung Turbulenter Scherströmungen, *Aerodynamische Versuchsanstalt Göttingen*, Rep. 69 (A14) (1968).
[207] A. Yoshizawa, H. Abe, Y. Matsuo, H. Fujiwara, Y. Mizobuchi, A Reynolds-averaged turbulence modeling approach using three transport equations for the turbulent viscosity, kinetic energy, and dissipation rate, Phys. Fluids 24 (7) (2012), 075109/1–075109/22.
[208] F. Hamba, Exact transport equation for local eddy viscosity in turbulent shear flow, Phys. Fluids 25 (8) (2013), 085102/1–085102/14.
[209] L. Davidson, Evaluation of the SST-SAS model: channel flow, asymmetric diffuser and axi-symmetric hill, in: P. Wesseling, E. Oñate, J. Périaux (Eds.), European Conference on Computational Fluid Dynamics, ECCOMAS CFD 2006, vols. 1–20, TU Delft, The Netherlands, 2006.
[210] L. Davidson, The SAS model: a turbulence model with controlled modelled dissipation, in: 20th Nordic Seminar on Computational Mechanics vols. 1–4, 2007. Gothenburg, Sweden.
[211] M. Shen, J.R. Edwards, Development of a new LES/RANS formulation, in: 46th AIAA Fluid Dynamics Conference, AIAA Paper 16-3638, Washington, D.C., 2016, pp. 1–16.
[212] M. Shen, A New Hybrid LES/RANS Model with Eddy Viscosity Transport (EVT) Based Outer-Layer Length Scale, PhD Thesis, North Carolina State University, 2017.
[213] S. Heinz, The large eddy simulation capability of Reynolds-averaged Navier-Stokes equations: analytical results, Phys. Fluids 31 (2) (2019), 021702/1–021702/6.
[214] L. Davidson, Large eddy simulations: how to evaluate resolution, Int. J. Heat Fluid Flow 30 (5) (2009) 1016–1025.
[215] J.B. Perot, J. Gadebusch, A self-adapting turbulence model for flow simulation at any mesh resolution, Phys. Fluids 19 (11) (2007), 115105/1–025112/11.
[216] R. Manceau, T.B. Gatski, C. Friess, Recent progress in hybrid temporal-LES/RANS Modeling, in: J.C.F. Pereira, A. Sequeira (Eds.), *V. European Conference on Computational Fluid Dynamics*, ECCOMAS CFD 2010, vols. 1–20, 2010. Lisbon, Portugal.
[217] S. Heinz, R. Mokhtarpoor, M. Stoellinger, Physics-based control of hybrid RANS-LES methods, in: 2019 AIAA Aerospace Sciences Meeting, AIAA SciTech Forum, AIAA Paper 19-0327, San Diego, CA, 2019, pp. 1–12.
[218] P.R. Spalart, Young-person's Guide Simulation Grids to Detached-Eddy, Seattle, WA, 2001. NASA/CR-2001-211032.
[219] B. Krank, M. Kronbichler, W.A. Wall, Direct numerical simulation of flow over periodic hills up to Re_H= 10,595, Flow, Turbul. Combust. 101 (2) (2018) 521–551.
[220] C. He, Y. Liu, S. Yavuzkurt, A dynamic delayed detached-eddy simulation model for turbulent flows, Comput. Fluids 146 (3) (2017) 174–189.
[221] S. Šarić, S. Jakirlić, M. Breuer, B. Jaffrézic, G. Deng, O. Chikhaoui, J. Fröhlich, D. Von Terzi, M. Manhart, N. Peller, Evaluation of detached eddy simulations for predicting the flow over periodic hills, in: ESAIM: Proceedings, 16, EDP Sciences, Marseille, France, 2007, pp. 133–145.
[222] Z. Xia, Y. Shi, R. Hong, Z. Xiao, S. Chen, Constrained large-eddy simulation of separated flow in a channel with streamwise-periodic constrictions, J. Turbul. 14 (1) (2013) 1–21.
[223] C.J. Kähler, S. Scharnowski, C. Cierpka, Highly resolved experimental results of the separated flow in a channel with streamwise periodic constrictions, J. Fluid Mech. 796 (2016) 257–284.
[224] A. Schröder, D. Schanz, D. Michaelis, C. Cierpka, S. Scharnowski, C.J. Kähler, Advances of PIV and 4D-PTV "Shake-The-Box" for turbulent flow analysis - the flow over periodic hills, Flow, Turbul. Combust. 95 (2–3) (2015) 193–209.
[225] S.M. Murman, A scalar anisotropy model for turbulent eddy viscosity, Int. J. Heat Fluid Flow 42 (8) (2013) 115–130.
[226] P. Razi, P. Tazraei, S. Girimaji, Partially-averaged Navier–Stokes (PANS) simulations of flow separation over smooth curved surfaces, Int. J. Heat Fluid Flow 66 (8) (2017) 157–171.
[227] B. Krank, W.A. Wall, A new approach to wall modeling in LES of incompressible flow via function enrichment, J. Comput. Phys. 316 (2016) 94–116.

[228] B. Krank, M. Kronbichler, W.A. Wall, Wall modeling via function enrichment within a high-order DG method for RANS simulations of incompressible flow, Int. J. Numer. Methods Fluids 86 (1) (2018) 107–129.
[229] B. Krank, M. Kronbichler, W.A. Wall, Wall modeling via function enrichment: extension to detached-eddy simulation, Comput. Fluids 179 (1) (2019).
[230] B. Krank, Wall Modeling via Function Enrichment for Computational Fluid Dynamics, PhD Thesis, Washington University, St. Louis), 2019.
[231] G. Kumar, S.K. Lakshmanan, H. Gopalan, A. De, Investigation of the sensitivity of turbulent closures and coupling of hybrid RANS-LES models for predicting flow fields with separation and reattachment, Int. J. Numer. Methods Fluids 83 (12) (2017) 917–939.
[232] X. Gloerfelt, P. Cinnella, Large eddy simulation requirements for the flow over periodic hills, Flow, Turbul. Combust. 103 (1) (2019) 55–91.
[233] J.M. Ma, S.-H. Peng, L. Davidson, F.J. Wang, A low Reynolds number variant of partially-averaged Navier–Stokes model for turbulence, Int. J. Heat Fluid Flow 32 (3) (2011) 652–669.
[234] A. Uzun, M.R. Malik, Large-Eddy Simulation of flow over a wall-mounted hump with separation and reattachment, AIAA J. 56 (2) (2018) 715–730.
[235] C. Meneveau, T.S. Lund, The dynamic Smagorinsky model and scale-dependent coefficients in the viscous range of turbulence, Phys. Fluids 9 (12) (1997) 3932–3934.
[236] S. Evans, S. Lardeau, C. Pettinelli, Validation of a turbulence methodology using the SST k-ω model for adjoint calculation, in: *2016* AIAA Aerospace Sciences Meeting, AIAA SciTech Forum, AIAA Paper 16-0585, San Diego, CA, 2016, pp. 1–11.
[237] S. Lardeau, C.F. Billard, Development of an elliptic-blending lag model for industrial applications, in: 2016 AIAA Aerospace Sciences Meeting, AIAA SciTech Forum, AIAA Paper 16-1600, San Diego, CA, 2016, pp. 1–17.
[238] X. Han, M.M. Rahman, R.K. Agarwal, Development and application of a wall distance free Wray-Agarwal turbulence model, WA2018, in: *2018* AIAA Aviation, AIAA Paper 18-0593, Kissimmee, FL, 2018, pp. 1–24.
[239] A. Avdis, S. Lardeau, M. Leschziner, Large eddy simulation of separated flow over a two-dimensional hump with and without control by means of a synthetic slot-jet, Flow, Turbul. Combust. 83 (3) (2009) 343–370.
[240] C.C. Kiris, D. Stich, J.A. Housman, J.G. Kocheemoolayil, M.F. Barad, F. Cadieux, Application of Lattice Boltzmann and Navier-Stokes methods to NASA's wall mounted hump, in: 2018 Fluid Dynamics Conference, AIAA Paper 18-3855, Atlanta, GA, 2018, pp. 1–31.
[241] C. Mockett, W. Haase, F. Thiele, Go4Hybrid: a European initiative for improved hybrid RANS-LES modelling, in: Progress in Hybrid RANS-LES Modelling (Notes on Numerical Fluid Mechanics and Multidisciplinary Design 130), Springer, Cham, 2015, pp. 299–303.
[242] A. Probst, D. Schwamborn, A. Garbaruk, E. Guseva, M. Shur, M. Strelets, A. Travin, Evaluation of grey area mitigation tools within zonal and non-zonal RANS-LES approaches in flows with pressure induced separation, Int. J. Heat Fluid Flow 68 (12) (2017) 237–247.
[243] Z. Yin, Adaptive Detached Eddy Simulation and Passive Scalar Transport Modeling for Hybrid RANS/LES, PhD Thesis, Iowa State University, 2017.
[244] A. Garbaruk, E. Guseva, M. Shur, M. Strelets, A. Travin, 2D wall-mounted hump, in: Go4Hybrid: Grey Area Mitigation for Hybrid RANS-LES Methods (Notes on Numerical Fluid Mechanics and Multidisciplinary Design 134), Springer, Cham, 2018, pp. 173–187.
[245] E.M. Siggeirsson, N. Andersson, The NASA 2D wall-mounted hump simulated using DDES-SA with the G3D: flow solver, in: 2019 AIAA Aerospace Sciences Meeting, AIAA SciTech Forum, AIAA Paper 19-0083, San Diego, CA, 2019, pp. 1–13.
[246] D. Dilip, Wall Modeled Large Eddy Simulation of Flow over a Wall Mounted Hump, M.S. Thesis, Virginia Polytechnic Institute and State University, 2014.
[247] G.I. Park, Wall-modeled large-eddy simulation of a high Reynolds number separating and reattaching flow, AIAA J. 55 (11) (2017) 3709–3721.
[248] A. Uzun, M.R. Malik, Wall-resolved Large-Eddy Simulation of flow separation over NASA wall-mounted hump, in: 2017 AIAA Aerospace Sciences Meeting, AIAA SciTech Forum, AIAA Paper 17-0538, Grapevine, TX, 2017, pp. 1–25.
[249] P.S. Iyer, M.R. Malik, Wall-modeled large eddy simulation of flow over a wall-mounted hump, in: 2016 AIAA Aerospace Sciences Meeting, AIAA SciTech Forum, AIAA Paper 16-3186, Washington, D.C., 2016, pp. 1–22.
[250] M. Koklu, Steady and unsteady excitation of separated flow over the NASA hump model, in: 2018 AIAA Flow Control Conference, AIAA Paper 18-4016, Atlanta, GA, 2018, pp. 1–24.
[251] M. Koklu, A numerical and experimental investigation of flow separation control over a wall-mounted hump model, in: 2018 AIAA Aerospace Sciences Meeting, AIAA SciTech Forum, AIAA Paper 18-1280, Kissimmee, FL, 2018, pp. 1–22.
[252] S. Haering, T.A. Oliver, R.D. Moser, Towards a predictive hybrid RANS/LES framework, in: 2019 AIAA Aerospace Sciences Meeting, AIAA SciTech Forum, AIAA Paper 19-0087, San Diego, CA, 2019, pp. 1–21.
[253] D. Greenblatt, K.B. Paschal, C.S. Yao, J. Harris, N.N.W. Schaeffler, A.E. Washburn, Experimental investigation of separation control - Part 1: baseline and steady suction, AIAA J. 44 (12) (2006) 2820–2830.
[254] J. DeBonis, C. Rumsey, M. Malik, Test cases for NASA's revolutionary computational aerosciences technical challenge, Kissimmee, FL, in: *53rd* AIAA Aerospace Sciences Meeting, 2015. Available, https://turbmodels.larc.nasa.gov./StandardTestCasesFinal5.pdf.
[255] C. Kiris, G. Stich, J. Housman, M. Barad, J. Kocheemoolayil, F. Cadieux, Wall modeled lattice Boltzmann and Navier-Stokes approaches for selected RCA cases, Kissimmee, FL, in: 2018 *AIAA SciTech Forum*, 2018. Available, https://ntrs.nasa.gov/archive/nasa/casi.ntrs. nasa.gov/20180001907.pdf.
[256] https://turbmodels.larc.nasa.gov/other_les_data/transbump_uzun_2018.html, 2019.
[257] S.M. Murman, Evaluating modified diffusion coefficients for the SST turbulence model using benchmark tests, in: 41st AIAA Fluid Dynamics Conference and Exhibit, AIAA Paper 11-3571, Honolulu, HI, 2011, pp. 1–16.
[258] J. Schaefer, S. Hosder, T. West, C. Rumsey, J.-R. Carlson, W. Kleb, Uncertainty quantification of turbulence model closure coefficients for transonic wall-bounded flows, AIAA J. 55 (1) (2017) 195–213.
[259] J. Schaefer, A. Cary, M. Mani, J. Krakos, S. Hosder, Grid influence on turbulence model coefficient uncertainties in transonic wall-bounded flows, AIAA J. 56 (8) (2018) 3123–3137.
[260] M. Elkhoury, On eddy viscosity transport models with elliptic relaxation, J. Turbul. 18 (3) (2017) 240–259.
[261] K.S. Abdol-Hamid, J.-R. Carlson, C.L. Rumsey, Verification and validation of the k-kL turbulence model in FUN3D and CFL3D codes, in: 46th AIAA Fluid Dynamics Conference, AIAA Paper 16-3941, Washington, D.C., 2016, pp. 1–31.
[262] K.S. Abdol-Hamid, Development of kL-based linear, nonlinear, and full Reynolds stress turbulence models, in: 2019 AIAA Aerospace Sciences Meeting, AIAA SciTech Forum, AIAA Paper 19-1878, San Diego, CA, 2019, pp. 1–43.
[263] Y. Mor-Yossef, AUFSR+: low Mach number enhancement of the AUFSR scheme, Comput. Fluids 136 (9) (2016) 301–311.
[264] J. Xu, D. Chen, Y. Song, S. Ji, Y. Zhou, Mean flow compressibility effects in transonic turbulence modeling, Aero. Sci. Technol. 79 (2018) 492–499.
[265] K.-Y. Kim, J.-W. Son, C.-H. Cho, Assessment of Reynolds stress turbulence closures in the calculation of a transonic separated flow, KSME Int. J. 15 (7) (2001) 889–894.
[266] B. Eisfeld, C. Rumsey, V. Togiti, Verification and validation of a second-moment-closure model, AIAA J. 54 (5) (2016) 1524–1541.
[267] R.-D. Cécora, R. Radespiel, S. Jakirlić, Modeling of Reynolds-stress augmentation in shear layers with strongly curved velocity profiles, in: B. Eisfeld (Ed.), Differential Reynolds Stress Modeling for Separating Flows in Industrial Aerodynamics, Springer Tracts in Mechanical Engineering, Springer International Publishing Switzerland, 2015, pp. 85–101.
[268] A.C. Botelho e Souza, R. Radespiel, Second-moment-closure modeling for low-Reynolds-number regions of aeronautical applications, in: 2019 AIAA Aerospace Sciences Meeting, AIAA SciTech Forum, AIAA Paper 19-0585, San Diego, CA, 2019, pp. 1–20.
[269] I.R. Witte, Uncertainty Quantification of Turbulence Model Closure Coefficients on Openfoam and Fluent for Mildly Separated Flows, MS Thesis, Washington University, St. Louis), 2017.
[270] I. Witte, K. Stephanopoulos, T.J. Wray, R.K. Agarwal, Uncertainty quantification of turbulence model coefficients in OpenFOAM and Fluent for mildly separated flows, in: 2018 Fluid Dynamics Conference, AIAA Paper 18-3553, Atlanta, GA, 2018, pp. 1–28.
[271] X. Han, T.J. Wray, R.K. Agarwal, Application of a new DES model based on Wray-Agarwal turbulence model for simulation of wall-bounded flows with separation, in: 2017 AIAA AVIATION Forum, AIAA Paper 17-3966, Denver, CO, 2017, pp. 1–23.
[272] X. Han, T.J. Wray, R.K. Agarwal, A new DES model based on Wray-Agarwal turbulence model for simulation of wall-bounded flows, in: 2017 AIAA SciTech Forum, AIAA Paper 17-0979, Denver, CO, 2017, pp. 1–20.
[273] X. Han, R.K. Agarwal, Application of a new IDDES model based on Wray-Agarwal turbulence model for simulation of wall-bounded flows with separation, in: 2018 AIAA Aviation, AIAA Paper 18-1086, Kissimmee, FL, 2018, pp. 1–19.
[274] K.V. Belyaev, A.V. Garbaruk, M.L. Shur, M.K. Strelets, P. R Spalart, Experience of direct numerical simulation of turbulence on supercomputers, in: Russian Supercomputing Days, vols. 67–77, 2016.
[275] P.R. Spalart, K.V. Belyaev, A.V. Garbaruk, M.L. Shur, M. Kh Strelets, A.K. Travin, Large-eddy and direct numerical simulations of the bachalo-johnson flow with shock-induced separation, Flow, Turbul. Combust. 99 (3–4) (2017) 865–885.
[276] P.S. Iyer, G.I. Park, M.R. Malik, Wall-modeled Large Eddy Simulation of transonic flow over an axisymmetric bump with shock-induced separation, in: 2017 AIAA AVIATION Forum, AIAA Paper 17-3953, Denver, CO, 2017, pp. 1–19.
[277] W.D. Bachalo, D.A. Johnson, Transonic, turbulent boundary-layer separation generated on an axisymmetric flow model, AIAA J. 24 (3) (1986) 437–443.
[278] R.M. Pinkerton, The Variation with Reynolds Number of Pressure Distribution over an Airfoil Section. Technical Report, 1937. Technical Report, NACA Report 613.
[279] A.J. Wadcock, Investigation of low-speed turbulent separated flow around airfoils, NACA Contract Report 177450 (1987).
[280] D. Coles, A.J. Wadcock, Flying-hot-wire study of flow past an NACA 4412 airfoil at maximum lift, AIAA J. 17 (4) (1979) 321–329.
[281] J. Tank, L. Smith, G.R. Spedding, On the possibility (or lack thereof) of agreement between experiment and computation of flows over wings at moderate Reynolds number, Interface Focus 7 (1) (2017), 20160076/1–20160076/17.
[282] A.A. Matyushenko, E.V. Kotov, A.V. Garbaruk, Calculations of flow around airfoils using two-dimensional RANS: an analysis of the reduction in accuracy, St. Petersburg Polytech. Univ. J. Phys. Math. 3 (1) (2017) 15–21.
[283] T. Wray, R.K. Agarwal, Application of new one-equation turbulence model to computations of separated flows, AIAA J. 52 (6) (2014) 1325–1330.
[284] T.J. Wray, R.K. Agarwal, Low-Reynolds-number one-equation turbulence model based on k-ω closure, AIAA J. 53 (8) (2015) 2216–2227.
[285] M.M. Rahman, K. Keskinen, V. Vuorinen, M. Larmi, T. Siikonen, Consistently formulated eddy-viscosity coefficient for k-equation model, J. Turbul. 19 (11–12) (2018) 959–994.

[286] F.R. Menter, Two-equation eddy-viscosity turbulence models for engineering applications, AIAA J. 32 (8) (1994) 1598–1605.
[287] L. Jiang, G. Tabor, G. Gao, A new turbulence model for separated flows, Int. J. Comput. Fluid Dyn. 25 (8) (2011) 427–438.
[288] A. Garcia-Uceda Juarez, A. Raimo, E. Shapiro, B. Thornber, Steady turbulent flow computations using a low mach fully compressible scheme, AIAA J. 52 (11) (2014) 2559–2575.
[289] X. Han, Development and Application of Hybrid Wray-Agarwal Turbulence Model and Large-Eddy Simulation, PhD Thesis, Washington University, St. Louis), 2018.
[290] S. Jee, K. Shariff, Detached-eddy simulation based on the v2-f model, Int. J. Heat Fluid Flow 46 (4) (2014) 84–101.
[291] J.F. Herbert-Acero, O. Probst, C.I. Rivera-Solorio, K.K. Castillo-Villar, S. Méndez-Díaz, An extended assessment of fluid flow models for the prediction of two-dimensional steady-state airfoil aerodynamics, Math. Probl. Eng. (2015), 854308/1–854308/31, 2015.
[292] S. Jakirlic, B. Eisfeld, B. Basara, Performance assessment of some popular RANS models by relevance to high-lift aerodynamics, in: 47th AIAA Aerospace Sciences Meeting Including the New Horizons Forum and Aerospace Exposition, AIAA Paper 09-0049, 2009, pp. 1–16.
[293] I.H. Abbott, A.E. von Doenhoff, Theory of Wing Sections, Dover Publications, New York, NY, 1959.
[294] L.K. Loftin, H.A. Smith, Aerodynamic Characteristics of 15 NACA Airfoil Sections at Seven Reynolds Numbers from 0.7×10^6 to 9×10^6 Technical Report, National Advisory Committee for Aeronautics, Washington, DC, 1949. Technical Note 1945, NASA.
[295] E. Tangermann, M. Klein, Detached eddy simulation of an SD7003 airfoil, in: Progress in Hybrid RANS-LES Modelling (Notes on Numerical Fluid Mechanics and Multidisciplinary Design 137, Springer, Cham, 2018, pp. 301–311.
[296] P. Khayatzadeh, S. Nadarajah, Laminar-turbulent flow simulation for wind turbine profiles using the transition model, *Wind Energy* 17 (6) (2014) 901–918.
[297] D.D. Pasquale, A. Rona, S.J. Garrett, A selective review of CFD transition models, in: 39th Aerospace Sciences Meeting and Exhibit, AIAA Paper 09-3812, San Antonio, TX, 2009, pp. 1–10.
[298] C.-M. Hsiun, C.-K. Chen, Aerodynamic characteristics of a two-dimensional airfoil with ground effect, J. Aircraft 33 (2) (1996) 386–392.
[299] K. Jansen, Large-eddy Simulation of Flow Around a NACA 4412 Airfoil Using Unstructured Grids. Annual Research Briefs, Center for Turbulence Research, NASA Ames/Stanford University, 1996, pp. 225–232.
[300] W. Gao, W. Zhang, W. Cheng, R. Samtaney, Wall-modelled large-eddy simulation of turbulent flow past airfoils, J. Fluid Mech. 873 (2019) 174–210.
[301] H.-J. Kaltenbach, H. Choi, Large-eddy Simulation of Flow Around an Airfoil on a Structured Mesh. Annual Research Briefs, Center for Turbulence Research, NASA Ames/Stanford University, 1995, pp. 51–60.
[302] S. Schmidt, M. Franke, F. Thiele, Assessment of SGS models in LES applied to a NACA 4412 airfoil, in: 39th Aerospace Sciences Meeting and Exhibit, AIAA Paper 01-434, Reno, NV, 2001, pp. 1–9.
[303] A. Frère, K. Hillewaert, P. Chatelain, G. Winckelmans, High Reynolds number airfoil: from wall-resolved to wall-modeled LES, Flow, Turbul. Combust. 101 (2) (2018) 457–476.
[304] A. Frère, K. Hillewaert, P. Chatelain, G. Winckelmans, High Reynolds number airfoil: from wall-resolved to wall-modeled LES, in: Direct and Large-Eddy Simulation XI (ERCOFTAC Series), Springer, Cham, 2019, pp. 381–387.
[305] A. Islam, B. Thornber, A high-order hybrid turbulence model with implicit large-eddy simulation, Comput. Fluids 167 (5) (2018) 292–312.
[306] S. Beyhaghi, R.S. Amano, Investigation of flow over an airfoil using a hybrid detached eddy simulation–algebraic stress turbulence model, J. of Energy Resour.-ASME 139 (5) (2017), 051206.
[307] M. Stoellinger, S. Heinz, P. Saha, Reynolds stress closure in hybrid RANS-LES methods, in: Progress in Hybrid RANS-LES Modelling (Notes on Numerical Fluid Mechanics and Multidisciplinary Design 130, Springer, Cham, 2015, pp. 319–328.
[308] M.K. Stoellinger, R. Roy, N. Ashton, Application of an elliptic blending Reynolds stress model in attached and separated flows, in: *22nd* AIAA Computational Fluid Dynamics Conference, AIAA Paper-15-2926, Dallas, TX, 2015, pp. 1–12.
[309] R. Roy, M.K. Stoellinger, Potential of the elliptic blending Reynolds stress model for use in hybrid rans-les methods, in: 53rd AIAA Aerospace Sciences Meeting, AIAA Paper 15-1982, Kissimmee, FL, 2015, pp. 1–17.
[310] S. Heinz, R. Mokhtarpoor, M. Stöllinger, Hybrid RANS-LES methods with continuous mode variation, in: Direct and Large-Eddy Simulation XII (ERCOFTAC Series), vols. 1–6, Springer, Cham, 2020.
[311] G. Haller, Exact theory of unsteady separation for two-dimensional flows, J. Fluid Mech. 512 (2004) 257–311.
[312] A. Surana, O. Grunberg, G. Haller, Exact theory of three-dimensional flow separation. Part 1. Steady separation, J. Fluid Mech. 564 (2006) 57–103.
[313] A. Surana, G.B. Jacobs, O. Grunberg, G. Haller, An exact theory of three-dimensional fixed separation in unsteady flows, Phys. Fluids 20 (10) (2008), 107101.
[314] M. Weldon, T. Peacock, G.B. Jacobs, M. Helu, G. Haller, Experimental and numerical investigation of the kinematic theory of unsteady separation, J. Fluid Mech. 611 (1–11) (2008).
[315] M. Serra, J. Vétel, G. Haller, Exact theory of material spike formation in flow separation, J. Fluid Mech. 845 (2018) 51–92.
[316] S.B. Pope, Ten questions concerning the large-eddy simulation of turbulent flows, New J. Phys. 6 (1) (2004) 35/1–35/23.
[317] B. Perot, C. Chartrand, Modeling return to isotropy using kinetic equations, Phys. Fluids 17 (3) (2005), 035101/1–035101/18.
[318] S. Tan, Q. Li, Z. Xiao, S. Fu, Gas kinetic scheme for turbulence simulation, Aero. Sci. Technol. 78 (2018) 214–227.
[319] H. Chen, S.A. Orszag, I. Staroselsky, S. Succi, Expanded analogy between Boltzmann kinetic theory of fluids and turbulence, J. Fluid Mech. 519 (2004) 301–314.
[320] S. Heinz, Comment on gas kinetic scheme for turbulence simulation, Aero. Sci. Technol. 93 (2019), 105263/1–105263/2.
[321] M. Lesieur, O. Metais, New trends in large-eddy simulations of turbulence, Annu. Rev. Fluid Mech. 28 (1) (1996) 45–82.
[322] L. Davidson, Zonal PANS: evaluation of different treatments of the RANS-LES interface, J. Turbul. 17 (3) (2016) 274–307.
[323] B. Basara, Z. Pavlovic, S. Girimaji, A new approach for the calculation of the cut-off resolution parameter in bridging methods for turbulent flow simulation, Int. J. Heat Fluid Flow 74 (12) (2018) 76–88.
[324] U. Piomelli, A. Rouhi, B.J. Geurts, A grid-independent length scale for large-eddy simulations, J. Fluid Mech. 766 (2015) 499–527.
[325] A.M. Kagan, Y.V. Linik, C.R. Rao, Characterization Problems in Mathematical Statistics, Wiley, New York, 1973.